1-25-2016

Pristine Graphene as a Two-Dimensional Surfactant

Steven J. Woltornist
University of Connecticut - Storrs, steven.woltornist@gmail.com

Pristine Graphene as a Two-Dimensional Surfactant

Steven J. Woltornist, Ph.D.

University of Connecticut, 2016

Abstract

Graphene, with its outstanding electrical, mechanical, and thermal properties, has been the focus of much attention since it was the topic of the 2010 Nobel Prize. Current methods to produce graphene include chemical vapor deposition (CVD) and epitaxial growth, as well as micromechanical, oxidation-reduction, and solvent/surfactant aided exfoliation of graphite. All of these methods, however, have serious limitations. A common theme for all of these procedures is that the insolubility of graphene in virtually all solvents is an obstacle to be overcome. In this dissertation, we present a method for the production of pristine graphene (graphene that has not been chemically modified) that instead relies on the insolubility of graphene. In the interface trapping method, graphene is seen to act as a two dimensional surfactant, where it is trapped at the interface of oil and water, and lowers the interfacial energy of the system.

By utilizing this technique, we are able to produce conductive, transparent films of few layer graphene sheets on hydrophilic substrates. These can then be transferred to virtually any substrate and have the potential to be used in applications such as solar cells and flexible displays. Using the same approach, pristine graphene and graphite may be infused into fabrics to impart conductivity and increased strength for use in

smart textiles. By altering the initial method to produce films, graphene stabilized emulsions are formed. If a monomer is used in place of the original inert oil, the emulsions may be used to template the creation of strong, lightweight, conductive composite materials. Furthermore, by varying the monomer used, flexible composite materials may be formed that are conductive and chemically sensing. These may find potential applications in energy storage, filtration, sensing, and construction materials.

Pristine Graphene as a Two-Dimensional Surfactant

Steven J. Woltornist

B.S. Franciscan University of Steubenville, 2011

A Dissertation

Submitted in Partial Fulfillment of the

Requirements for the Degree of

Doctor of Philosophy

at the

University of Connecticut

2016

APPROVAL PAGE

Doctor of Philosophy Dissertation

Pristine Graphene as a Two-Dimensional Surfactant

Presented by

Steven J. Woltornist, B.S.

Major Advisor: _____

Prof. Douglas H. Adamson

Associate Advisor: _____

Prof. Andrey V. Dobrynin

Associate Advisor: _____

Prof. Gregory A. Sotzing

Associate Advisor: _____

Prof. Fotios Papadimitrakopoulos

Associate Advisor: _____

Prof. Edward J. Neth

University of Connecticut
2016

Dedication

This work is dedicated to my wife, Kathryn, whose love and support has been invaluable during my Ph.D. program, and to our baby girl.

Acknowledgements

I would first like to thank my Major Advisor, Dr. Douglas Adamson. When I first arrived at the University of Connecticut, I knew very little about polymers, and nothing about graphene. He has been the best of mentors, and is largely responsible for where I am today in my scientific career. Perhaps even more importantly, our several-hour long spontaneous conversations about new ideas have helped develop my scientific curiosity. I would also like to thank Dr. Andrey Dobrynin, who pushed me harder than most to be the best scientist I could, and to never settle for less. The other members of my committee have also have had very important roles in my time here at the University of Connecticut. Dr. Gregory Sotzing was both an excellent collaborator and teacher, Dr. Fotios Papadimitrakoupolos helped lay my initial foundation in graphene research, and Dr. Neth greatly developed my teaching skills. Dr. Montgomery Shaw is also deserving of thanks for helping me solve countless seemingly random questions.

There are also several staff members that I would like to thank. First, I would like to thank Dr. Laura Pinatti for the time she spent teaching me how to use countless instruments and patiently helping me analyze the results. Special thanks must also be given to the members of the machine shop and electronics shop, Robert Bouchard, Matthew Beebe, Rick George, and Michael Chebro, for many hours of help with the most random of projects. I would also like to thank Mark Dudley, Gary Lavigne, Dr. Lichun Zhang, and Dr. Roger Ristau for all of their help with the instrumental and technical aspects of my research.

My fellow research group members have also been a large part of my life here, and all of this would not have been possible without them. Firstly, I would like to thank Dr. AJ Oyer, who was my first mentor. He truly helped lay down my foundation in graphene research. Second, I would like to thank Dr. Chetan Hire, who was another mentor who first helped me develop my scientific thinking. He also helped me with any number of odd projects that had nothing to do with his own research. Next, I would like to thank Jen Bento, Garrett Kraft, and Reihaneh Mohammadi who were both great assets in research and in making lab work enjoyable. Deepthi Varghese is also deserving of my thanks, as she was extremely patient as I taught her the deeper aspects of graphene composite research. I am certain she will carry the torch of graphene research well. Finally, I would like to thank the rest of my group members: Dr. Zhenhua Cui, Dr. Andre Martinez, Dr. Kevin Huang, Taoran Hui, Harish Kumar, Elizabeth Brown, Shawn Ward, Chau Vy, and Drona Madugula, as well as my undergraduates Adam, Tom, Mike, Chris, Dan, and Sam. I have been extremely fortunate in that all of my lab mates have not only been great people to work in lab with, but also great friends.

Next, I would like to thank my family and friends. They have supported my education from the very beginning. More importantly, they have supported me in whatever I have done. I cannot even begin to express how grateful I am for everything they have done for me. I would personally like to thank my parents, Greg and Maria, for all the sacrifices they made for me. My mother from a young age taught me the joys of cooking, which led to my pursuing chemistry. My father also taught me to always be curious, and always encouraged me to take things apart. I carry that curiosity on to this

day. I am also lucky to have amazing in-laws, Ed and Suzanne, that have been there to support me my entire time at UConn. I would also like to thank my siblings, Alexei, Kate, Gregory, Becky, Chris, and Mary for being my closest friends and best companions in life. Anthony has also been like an adopted brother to me. My new sisters, Lizzy and Caroline, have also been some of my biggest supporters, and for that I am thankful. I also thank my grandparents, Witold, Svetlana, Eugene and Rosalie for all of their support in life. I have also had extremely supportive aunts, uncles, and cousins. I am extremely thankful for everything they have done for me. I would be remiss if I did not mention in a special way my uncle and aunt, Eric and Mare, who have been to every event I have had since childhood. Bub also taught me to truly use my brain by bestowing the gift of Bridge upon me.

Finally, I would like to thank my wife. She was actually the one who first recommended that I attend the University of Connecticut. She has also been the one who has supported me the most as I have pursued this goal. I would not have been able to do this without her.

Table of Contents

List of Figures

List of Tables

Chapter 1: Introduction to Graphene

1.1 Introduction

First isolated in 2004,[1] graphene is a two-dimensional allotrope of carbon that has gained much attention in the scientific community in recent years because of its outstanding properties. Graphene is made up of sp^2 hybridized carbon atoms arranged in a hexagonal, honeycomb shaped lattice. It is sometimes called the mother of carbon allotropes, as it can be thought of as the building block for all other forms of carbon: it can be folded to make fullerenes, rolled to make carbon nanotubes (CNTs), and stacked to make graphite, which can then be converted to diamond through heat and pressure (Figure 1-1).[2]

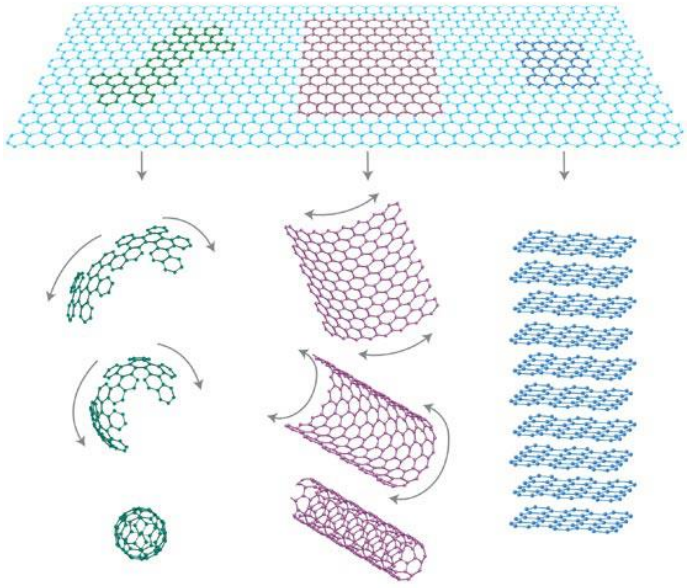

Figure 1-1: A diagram showing graphene as the basis for other carbon allotropes.[2]

Graphene has been the focus of a large amount of research because of its outstanding physical properties. It has excellent thermal conductivity of around 5000 W/mK,[3] which is an order of magnitude higher than copper. Graphene also has a very high theoretical surface area of ~2600 m^2/g,[4] and a relatively low density, 2.2 g/cm^3, as compared to conducting metals such as copper (density = 8.96 g/cm^3). Graphene's tensile modulus of ~1 TPa[5] is significantly higher than steel's value of ~200 GPa. Finally, graphene has an electron mobility of $2.5*10^5$ cm^2/Vs,[6] compared to silicon's value of 1400 cm^2/Vs and carbon nanotubes' value of $1*10^5$ cm^2/Vs.[7]

In 1947, P. R. Wallace theorized the existence of graphene to explain 3-dimensional graphite. However, at that time graphene was considered thermodynamically unstable as a free standing two-dimensional material.[2] It is now thought to have been observed for the first time in the 1970s, grown using epitaxial growth,[8] but they did not fully understand what they had made, and there were many problems with the system such as the overlapping of orbitals between the graphene and the substrate.

Novoselov and Geim first demonstrated and proved the production of pristine graphene in 2004 using a technique called micromechanical exfoliation.[1,9] Pristine graphene is graphene that has minimal oxygen functionalities or other structural problems that degrade its properties. The procedure they performed to acquire pristine graphene was actually quite simple, and will be discussed in a later section. Due to scaling difficulties, however, discovering new procedures for the production of graphene has been a very active field in materials chemistry. Beyond mere exfoliation, the utilization of graphene in various functional materials has been highly sought after. To

give a few examples: graphene based materials can be used in filtration,[10,11] energy storage,[12–15] sensing,[16–18] and as transparent electrodes.[19–22]

1.2 Outline

This dissertation focuses both on the exfoliation and utilization of pristine graphene as it acts as a two-dimensional surfactant. First, in order to better understand the foundation from which our work stems, the various methods of graphene production will be discussed, as well as the pros and cons for each. There will then be a brief overview of the types of graphite used in this research. Next, as this dissertation focuses on pristine graphene acting as a surfactant, there will be a brief introduction into traditional surfactants. From there, the dissertation will delve into the investigations carried out as part of my PhD studies.

Part I investigates the utilization of the interface trapping method to produce macroscopic conductive thin films of pristine graphene sheets. Using the same general theory, Part II covers the infusion of fabrics with a mixture of pristine graphene and graphite to impart electrical conductivity. Part III then delves into utilizing pristine graphene to form stable oil/water emulsions to template the creation of porous composite materials. Part IV explores the formation of flexible variants of these composites.

Chapter 2: Traditional Methods of Graphene Production

2.1 Micro-Mechanical Exfoliation

Andre Geim and Konstantin Novoselov are credited with the first isolation and characterization of pristine graphene in 2004. Their method, micro-mechanical exfoliation, is surprisingly simple and elegant. Starting with a piece of highly ordered pyrolytic graphite (HOPG), they placed scotch tape against the surface. By pulling the scotch tape up from the surface of the graphite, several layers of graphene were exfoliated (pulled apart from the bulk piece). By repeating this method, more and more layers were peeled off from each other until a single layer was left on the tape.[9] The tape was then dissolved, and the graphene transferred to different substrates for analysis.[1] Although elegant, the obvious difficulties in scaling this procedure have led to a variety of alternative methods, which shall be discussed below.

Figure 2-1: A lump of graphite (top left), a graphene transistor (bottom left), and a tape dispenser (right) donated by Andre Geim and Konstantin Novoselov to the Nobel Museum.[23]

2.2 Chemical Vapor Deposition and Epitaxial Growth

Chemical vapor deposition (CVD) is a process that starts with a metal substrate heated in a low-pressure environment. A carbon-based gas, such as methane, is then blown over the substrate. The heated system then absorbs carbon into the metal. Once the temperature is lowered, the carbon atoms can no longer stay in the metal substrate, so they are expelled and a thin layer of the most thermodynamically stable form of carbon, graphene, on the surface (Figure 2-2). [24–26]

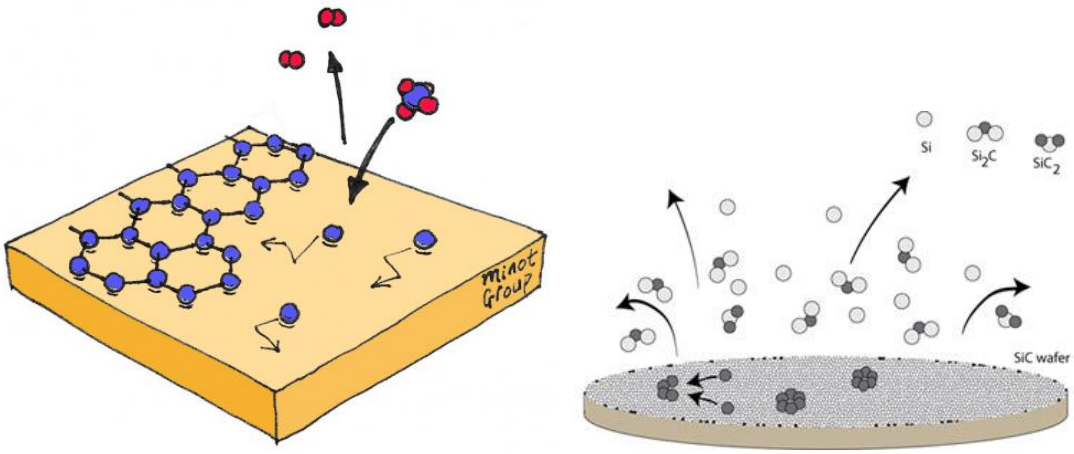

Figure 2-2: Simple illustrations of chemical vapor deposition[27] (left) and epitaxial growth (right) of graphene.[28]

Similar to CVD, epitaxial growth uses a substrate. In this case, however, it is silicon carbide, SiC. The system is heated to high temperatures either under an inert atmosphere or high vacuum. The silicon atoms then sublime out of the substrate, leaving behind a layer of graphene (Figure 2-2).[29–31] Both of these methods produce large sheet sizes and high quality graphene, although they are also expensive and difficult to optimize. CVD and epitaxial growth are extremely sensitive to the conditions used and always require extensive experimentation to determine a good procedure.

2.3 Oxidation and Reduction of Graphite

The process of producing graphene through oxidation and reduction is currently widely used. The first appearance of graphite oxide in the literature dates back to the 1800s, by Brodie.[32] Although it was not known then, this was a potential route to the production of graphene through the exfoliation of graphite oxide into graphene oxide (GO). Since then, Brodie's method, as well as two others – Staudenmaier's[33] and Hummer's[34] – have been the standards used to produce graphite oxide as a step in the production of graphene, with a modified Hummer's method being the most popular

today. During the oxidation process, oxygen functionalities are introduced to the structure. These groups are more bulky, thus leading to increased spacing between the layers that make up the stacked structure. The increased spacing results in a lowering of the van der Waals forces holding the sheets together, thus making it much easier to exfoliate into separate sheets.

Graphene oxide is an interesting material in its own right. It has many of the properties of graphene, although most are inferior to the pristine material. For example, the tensile modulus of GO is about one fifth of that of pristine graphene.[35] It is also an insulator, due to the oxygen functionalities severely disrupting the delocalized electron network throughout pristine graphene. One beneficial property that GO has is that it may be dispersed in a wide variety of polar solvents because of the oxygen functionalities present on the sheets.

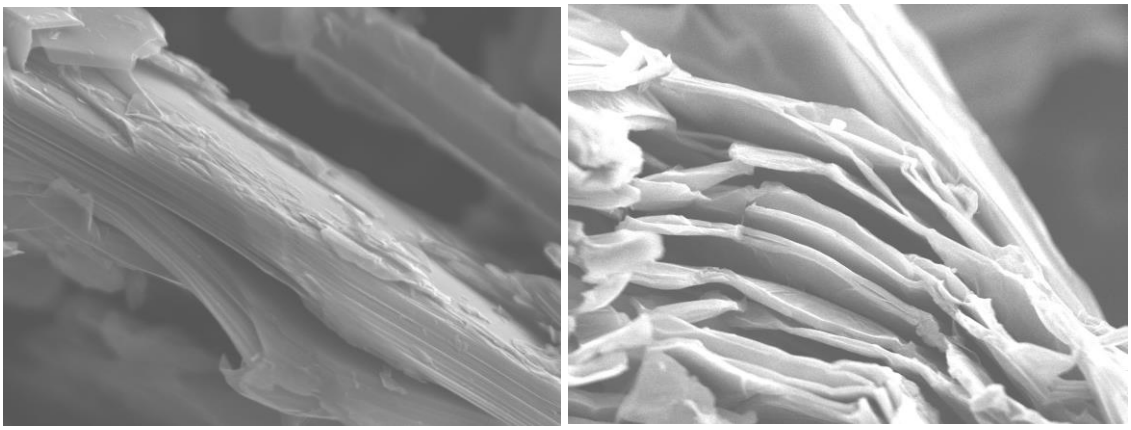

Figure 2-3: Graphite before (left) and after (right) oxidation.

The inferior properties just discussed often necessitate the reduction of GO to graphene, although it is more specifically called reduced graphene oxide (RGO). RGO differs from pristine graphene in that during the reduction process, the removal of oxygen leaves behind defects in the honeycomb lattice, such as dislocations and

residual oxygen groups. Although its conductivity and strength are better than GO, they are still considerably less than pristine graphene made from other methods, with the highest conductivity value at around 1000 S/m.[36] Again, this is due to the functional groups and defects disrupting the network of delocalized electrons.

There are many possible ways to reduce graphene oxide to RGO, although the two most prominent are chemical and thermal. Ruoff, et al. proposed the reduction of GO to RGO using hydrazine hydrate.[37] Schniepp, et al. proposed an alternate synthesis, where the RGO was made through thermal reduction at 1050 °C.[38] In this method, the sheets were reduced and exfoliated simultaneously. There are various other methods,[39–41] but the thermal method is by far the most convenient, since there are no chemicals that have to added or be removed after the reduction.

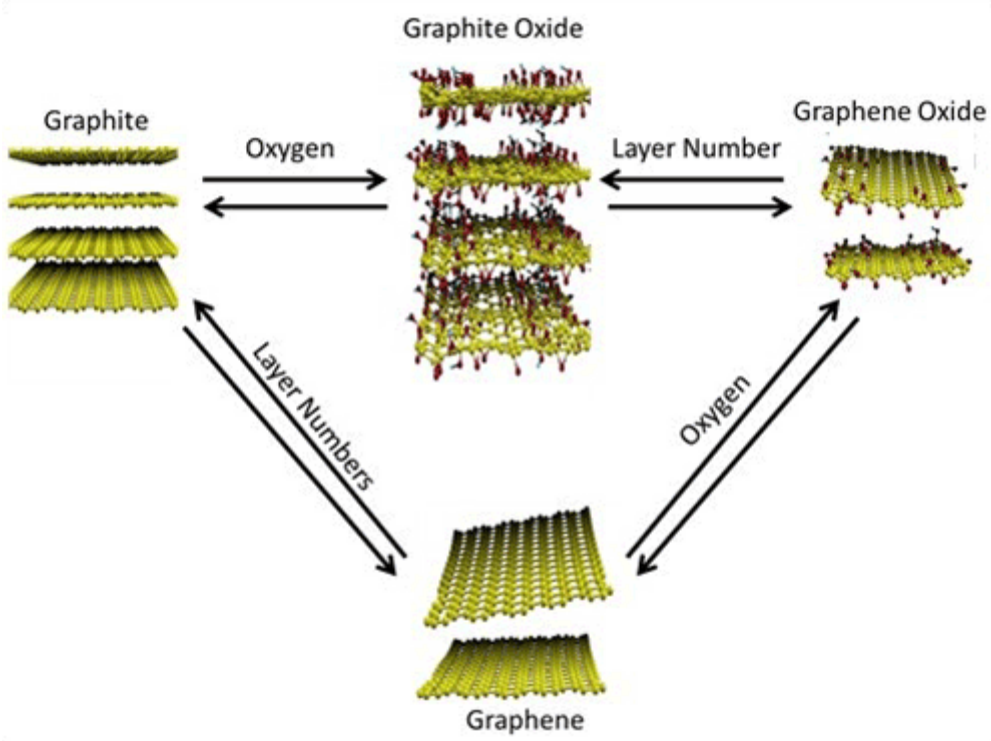

Figure 2-4: Process of producing graphene from graphite using the oxidation and reduction method.[42] Graphite is first oxidized to graphite oxide, where the interlayer spacing is increased. Due to a decrease in van der Waals interactions between the

sheets, they may be exfoliated into graphene oxide. From there, reduction yields graphene. It must be noted, however, that graphene derived from this method has many defects left from the harsh oxidation and reduction processes.

2.4 Solvent Exfoliation and Surfactant Aided Exfoliation

In both the solvent exfoliation method and the surfactant aided exfoliation method, graphene sheets are exfoliated from bulk graphite in a solvent. Energy is required for this process, and it often comes from sonication (bath or tip). Normally, the sheets quickly re-stack due to lack of stability. In the solvent exfoliation method, a solvent is chosen that hinders the restacking with some kind of interaction stronger than van der Waals forces.[43] The downside to this method is that the concentration of graphene in the solution is very low, typically around 0.01 mg/mL. In surfactant aided exfoliation, a surfactant is added that adsorbs to the graphene sheets and prevents restacking.[44] Again, there is a downside, as the surfactant must be removed using harsh chemicals or heat.

Chapter 3: Common Graphites Used

Throughout this dissertation, the work utilizes various types of graphite. The morphologies of these different graphites have a significant effect on the final materials. This chapter will focus on electron microscopy studies of the graphites used. They have all been generously provided by Asbury Carbons.

3.1 Asbury Grade 3243

Asbury grade 3243 is a natural flake graphite that is milled to around 55 um. Figure 3-1A shows the distribution of the lateral size of the graphite stacks. In Figure 3-1B, the stacks of graphite that make up the larger aggregates are seen. Figure 3-1C shows the thickness of a sample stack, as well as some of the layering.

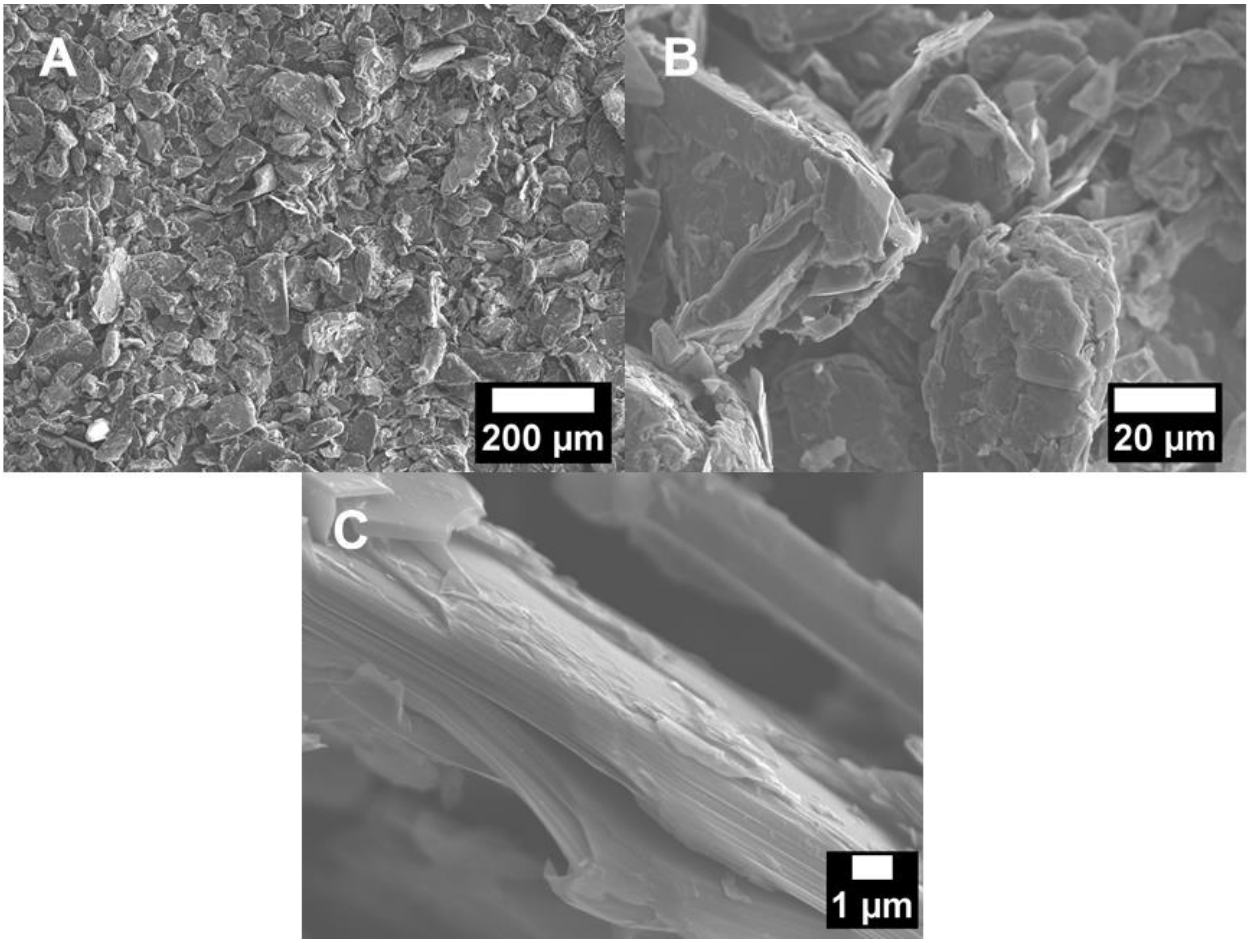

Figure 3-1: Scanning electron microscopy images of Asbury Carbons graphite grade 3243.

3.2 Asbury Grade 2299

Asbury grade 2299 is derived from a natural graphite parent. Its average lateral size is on the order of a few microns. In Figure 3-2A, B, and C, the average sheet size is seen, as well as the low amount of aggregation.

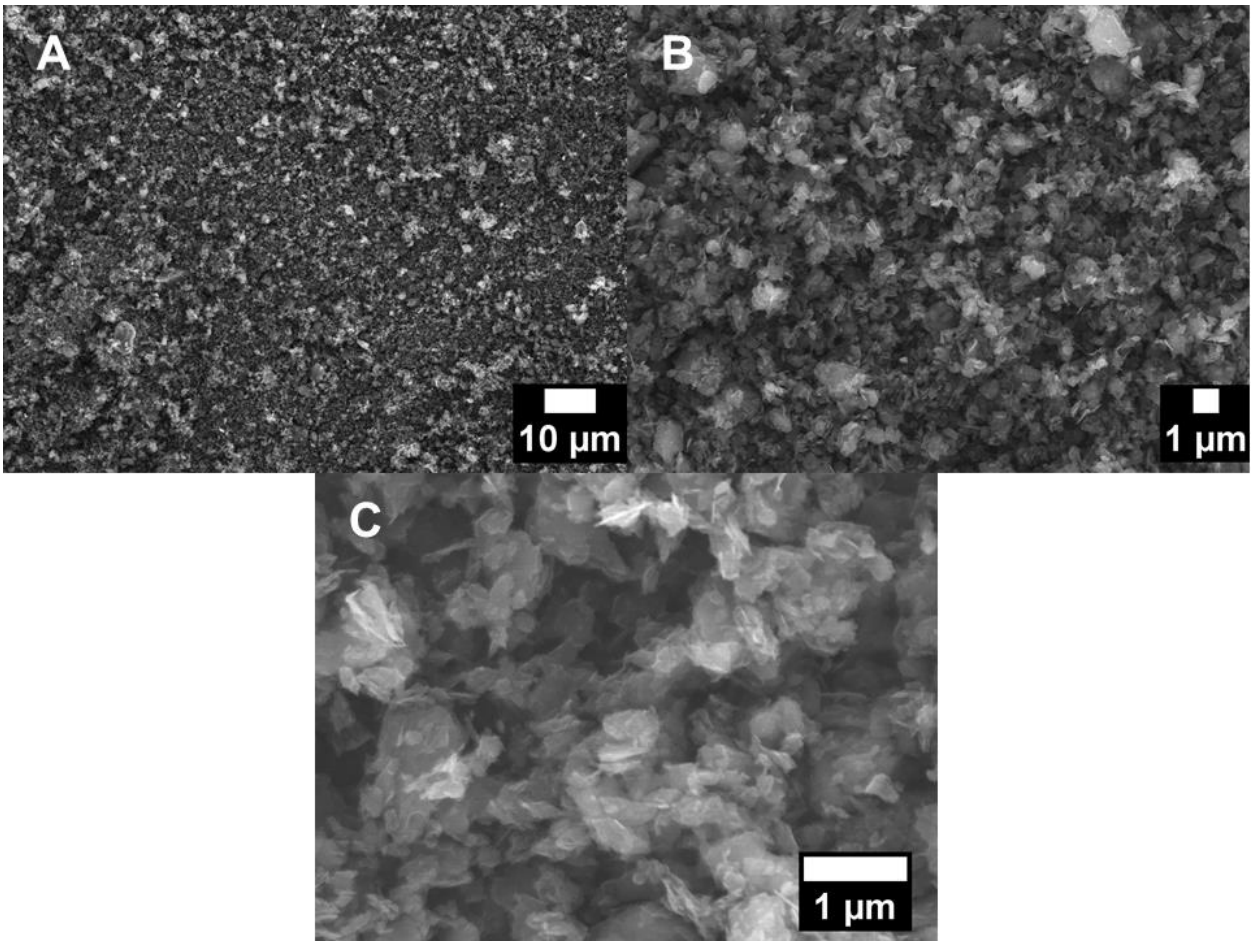

Figure 3-2: Scanning electron microscopy images of Asbury Carbons graphite grade 2299.

3.3 Asbury Grade Nano 24

Asbury grade Nano 24 is derived from a synthetic graphite parent. It is very similar to Asbury grade 2299 in shape and size. This may be seen in Figure 3-3A, B, and C.

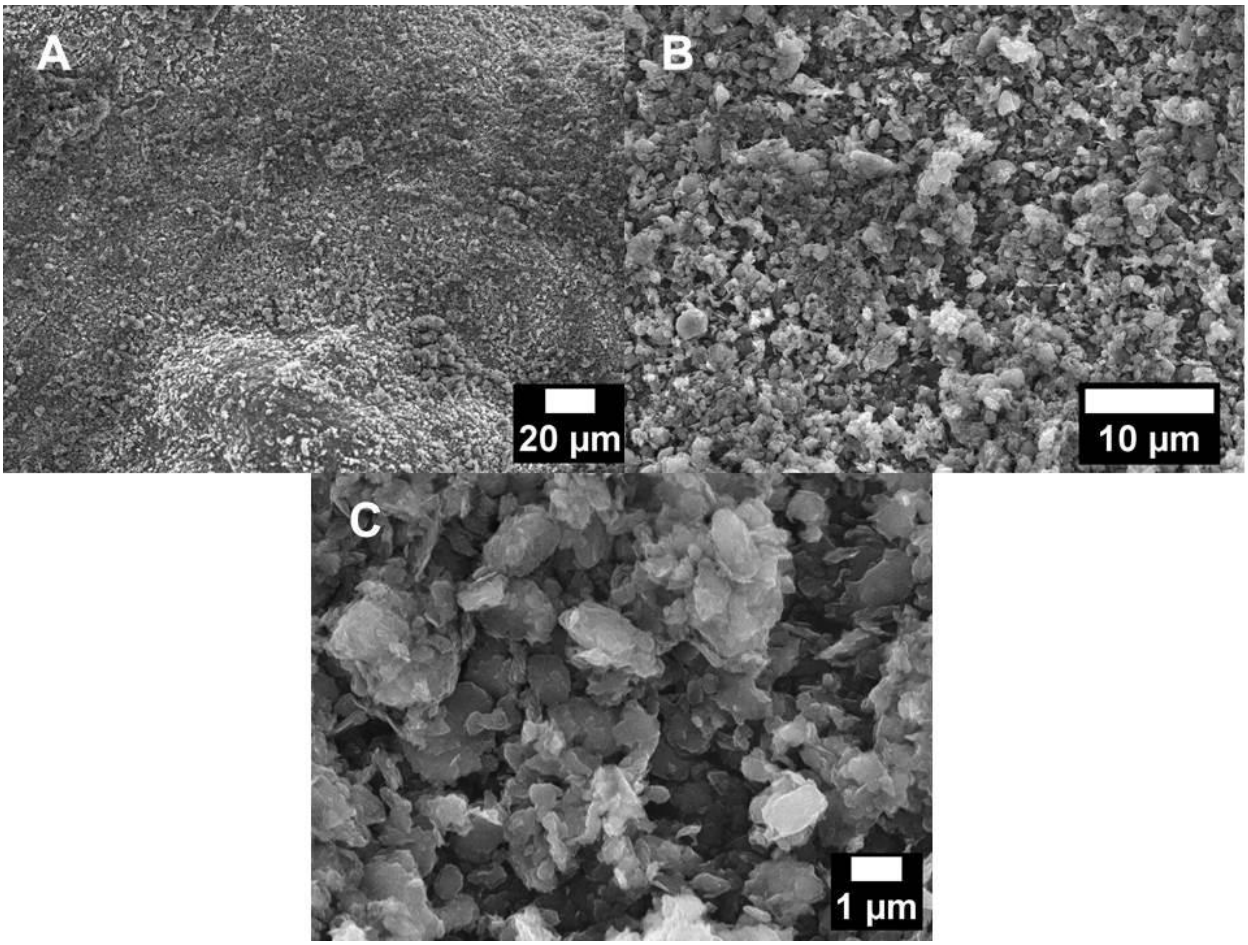

Figure 3-3: Scanning electron microscopy images of Asbury Carbons graphite grade Nano 24.

3.4 Asbury Grade Micro 890

Asbury grade Micro 890 is a natural flake graphite with an average lateral size of around 10 um. It may be seen below in Figure 3-4: A, B, and C.

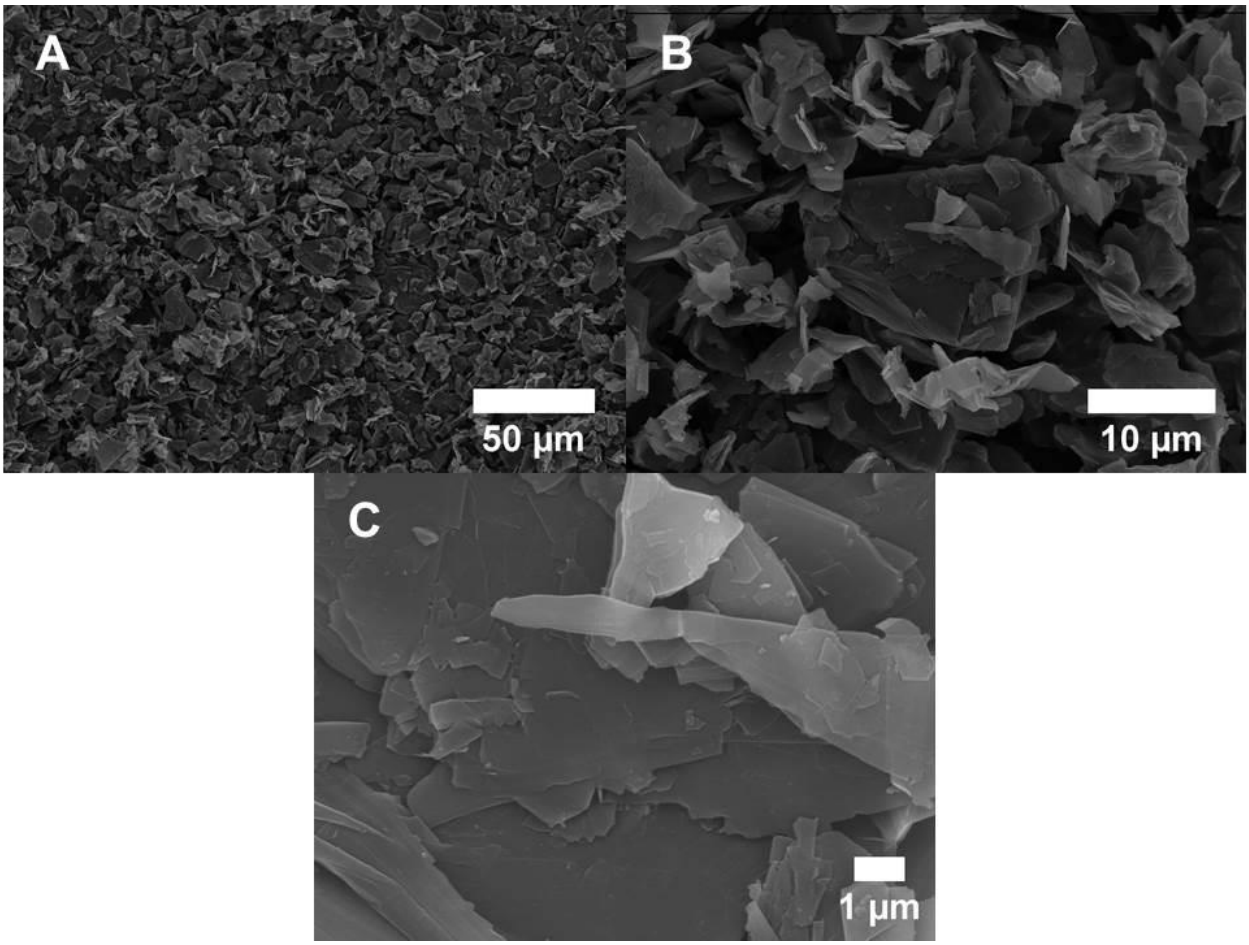

Figure 3-4: Scanning electron microscopy images of Asbury Carbons graphite grade Micro 890.

Chapter 4: Introduction to Traditional Surfactants

Traditional surfactants are amphiphilic, meaning one part of the molecule being hydrophilic, while the other part is oleophilic. There are three types of classical surfactants: nonionic, ionic, and zwitterionic. In general, the hydrophobic (oleophilic) part of the molecule is made of an alkyl chain. In a nonionic surfactant, the hydrophilic head has no charge (Figure 4-1A). Ionic surfactants may have either a negatively or positively charged head (Figure 4-1B, C). Zwitterionic surfactants have both a negative charge and a positive charge in the hydrophilic part of the molecule (Figure 4-1D).

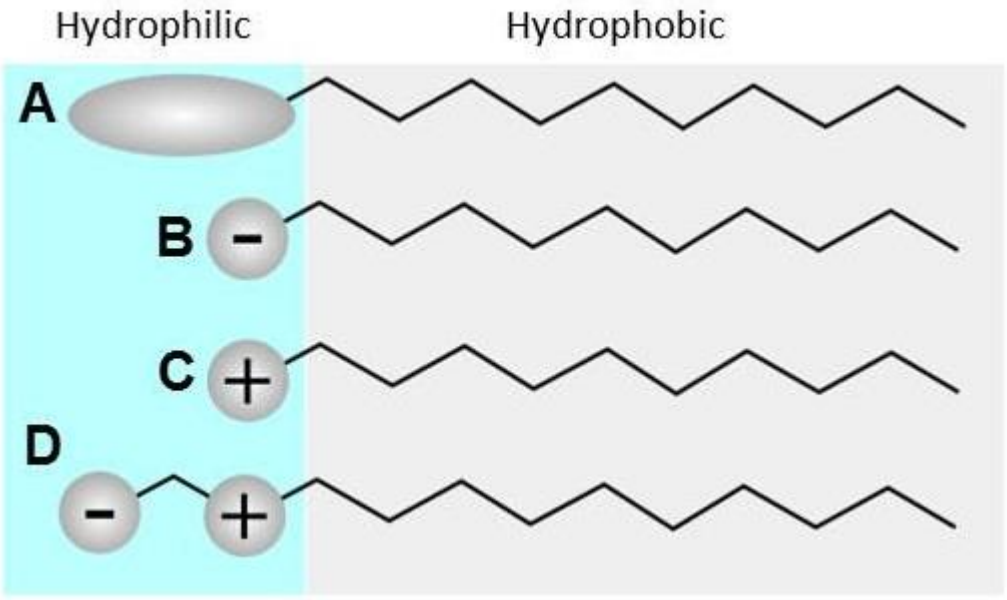

Figure 4-1: Types of traditional surfactants. (A) Nonionic, (B) and (C) Ionic, and (D) Zwitterionic. Adapted from[45]

When placed in a mixture of oil and water, the molecule sits at the interface in order to be at its lowest energy state. At the interface, the hydrophilic end of the molecule lies in the water phase, while the hydrophobic end lies in the oil phase. It must be noted that traditional surfactants can be thought of as one-dimensional. In this dissertation, we shall discuss the use of pristine graphene as a two-dimensional surfactant.

Part I: Conductive Thin Films of Pristine Graphene by Solvent Interface Trapping

Chapter 5: Introduction

The availability of inexpensive,[46] transparent and conductive pristine graphene films has the potential to revolutionize solar power harvesting, photonics, and flexible electronics technology.[22,47,48] Graphene's insolubility and its intrinsic tendency to aggregate, however, have necessitated the use of either reduced graphite oxide[49–52] or chemical vapor deposition (CVD)[19,26,53,54] sources of graphene. Chemical modification of graphene significantly reduces film conductivity,[55] while vapor deposition requires high production costs. It would be tremendously advantageous to use pristine graphene to lower the cost and boost film conductivity.

In this chapter, we describe a one-step technique to produce laterally macroscopic, transparent and conductive films from pristine (untreated and unmodified) natural flake graphite with well-controlled thickness. The films are one to four graphene layers thick and inexpensive to produce. Furthermore, there are no theoretical limitations to film lateral dimensions, and such films can be easily transferred to various substrates. This technique may be the first step in the wide spread utilization of natural graphene as a substitute for materials such as indium tin oxide (ITO) in applications such as solar panels, organic electronics, and batteries. The conductivity of graphene films formed by our interface trapping method shows values on the order of 400 S/cm.

Chapter 6: Experimental Methods

6.1 Preparation of Graphene Film

The typical sample preparation method we used was as follows: 2 mg of bulk pristine graphite was first put into a 20 mL glass scintillation vial. 5.0 mL of n-heptane (Fisher Scientific, HPLC grade) was then added and the system was briefly bath sonicated (Branson 80W B2510DTH) to break up any large particles. It was then tip sonicated (Cole-Parmer 750 Watt Ultrasonic Processor) for 15 minutes at 40% power to disperse it into the heptane. After the sonication, 5 mL of water was added and the system was bath sonicated again briefly to help move the graphene sheets to the interface. The mixture was then tip sonicated with the tip right above the main liquid-liquid interface a second time for 15 minutes at 40% power. After the second tip sonication, the system was shaken to create emulsion spheres, which upon coalescence generate a film that climbs the walls of the vial, or a glass slide inserted into the system.

6.2 Transferring of Graphene Film

To transfer the film to various other substrates, using the method above, but before the water dries under the graphene layer, the slide was dipped into a beaker of water. The film detached from the slide and floated on top of the water. Depending on the substrate, the film was transferred by either putting it under the water and lifting the film onto it, or pushing the substrate through the interface while near the film. After the transfer, the film was either dried in open air, or in an oven to speed the process.

6.3 Characterization

6.3.1 Raman Spectroscopy

Using a Renishaw 2000 Raman Spectrometer, we analyzed the 2D peak of the graphene in a film prepared on a glass slide as in the method described in section 6.1 This peak is indicative of the number of layers of graphene making up the film (Figure 6-1). The spectrum from our film may be seen in section 7.3.

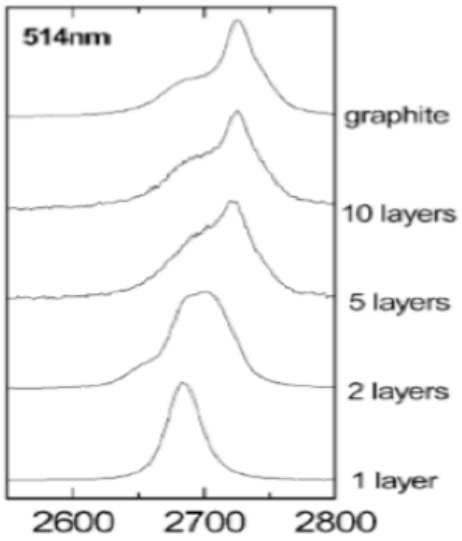

Figure 6-1: Evolution of Raman spectra at 514 nm with the number of layers.[56]

6.3.2 Ultraviolet – Visible Spectroscopy

Transparency was determined using a Cary 5000 UV-VIS-NIR Spectrophotometer. The film was created using the method described in section 6.1 with graphite (Asbury Carbons grade 2299), although we used as little graphite as possible that still resulted in a continuous film. The slide with the film on it was then taken out of the vial to dry, with some aggregation of the film occurring as the heptane evaporated.

The instrument was first zeroed using a clean glass slide as a control. This spectrum may be seen in Figure 6-2. After that process was completed, a slide with a graphene film on it was tested. The spectrum may be seen in section 7.3.

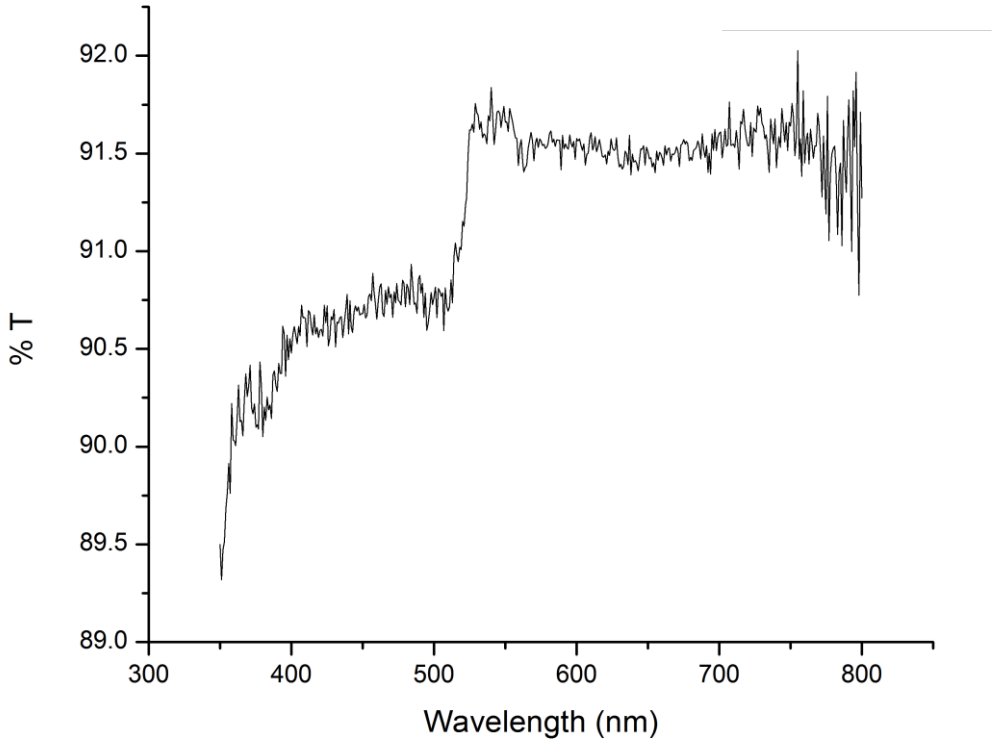

Figure 6-2: UV-VIS spectrum of the control glass slide used as a substrate for our films.

6.3.3 Transmission Electron Microscopy

Transmission Electron Microscopy (TEM) images were obtained using a FEI Tecnai T12 TEM, where we were able to confirm the average size of the sheets, as well as determine the percent coverage of the film through image analysis to be 82%. An example of a TEM image used to determine surface coverage is shown in Figure 6-3.

Samples were first prepared using the method described in section 6.1 and transferred to a TEM grid using the method described in 6.2.

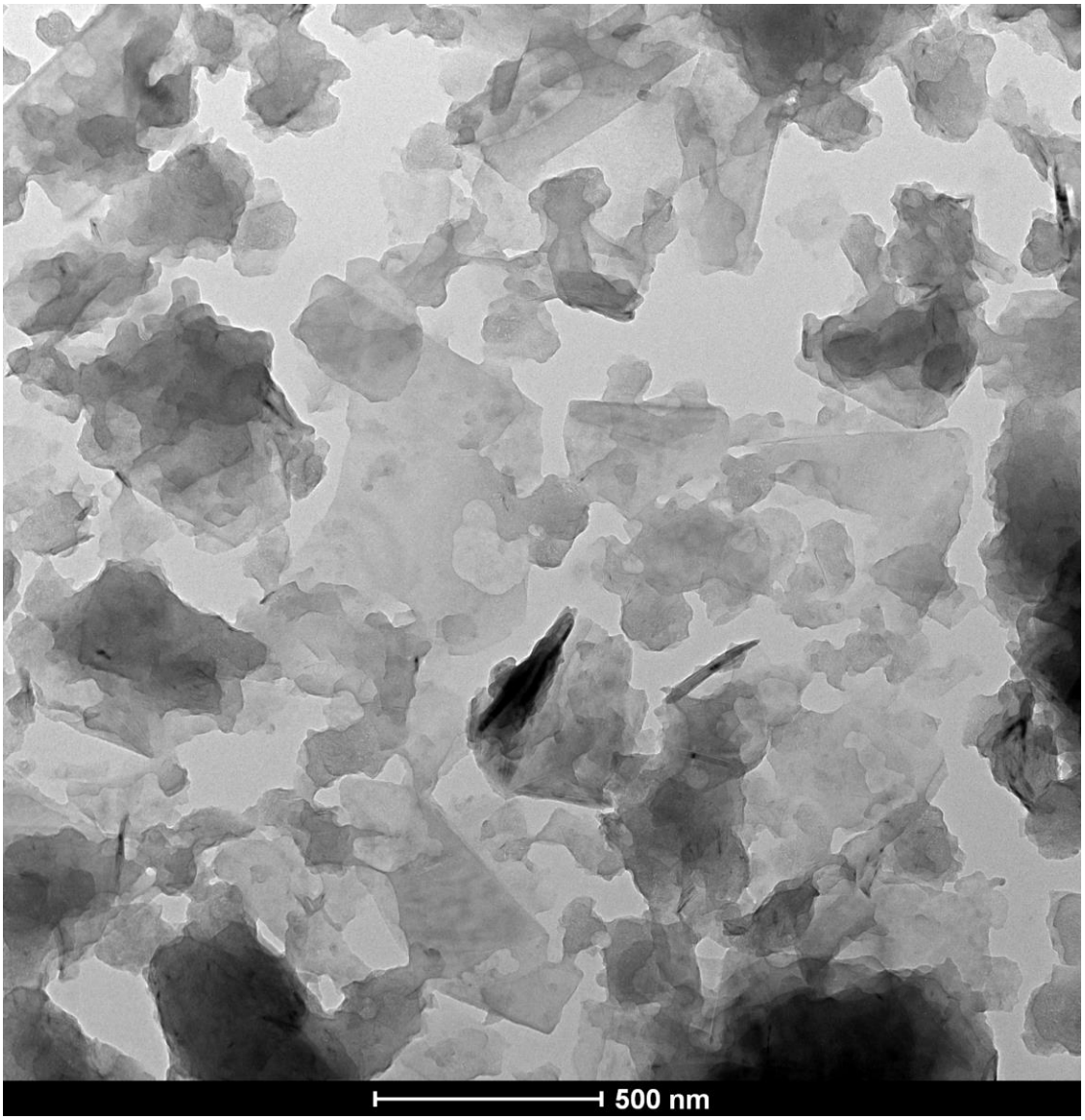

Figure 6-3: TEM image of typical graphene film.

6.3.4 Field Emission Scanning Electron Microscopy

Field Emission Scanning Electron Microscopy (FESEM) images were obtained using a JEOL JSM 6335F FESEM. The graphene film samples were prepared on a

glass slide as in section 6.1. They were then transferred to an aluminum SEM stub using the method described in section 6.2.

6.3.5 Conductivity Measurements

A typical conductivity measurement was made as follows: a graphene film was formed on a glass slide with graphite (Asbury Carbons grade 3243) using the method described in section 6.1. Four strips of copper tape were placed on the film with 1 cm spaces in between to form a 4-line probe. The conductivity was then measured using a Keithly Model 2420 SourceMeter.

Chapter 7: Results and Discussion

7.1 Film Formation

The film formation occurs at the interface of a phase-separated mixture of water and heptane. While graphene does not form a stable suspension in either water or heptane, when placed in a mixture of the two, with mild sonication, the graphene sheets assemble at the water/heptane interface to form a uniform macroscopic film that remains stable for an indefinite period of time. Figure 7-1 shows graphene film formation at the water/heptane interface, with graphene shells stabilizing a water/heptane emulsion. The size of the drops is a function of the volume fraction of water and heptane, as well as the amount of graphite added.

Figure 7-1: Emulsion of water in heptane stabilized by pristine, natural flake graphene. The ratio of heptane to water is 19:1.

When placed in a water/heptane solvent mixture of approximately 1:1, the graphite, after mild sonication, exfoliates at the solvent interface. In addition, the graphene sheets climb the sides of the hydrophilic glass vial. As the glass of the vial is hydrophilic, a thin layer of water is present on the surface and is in contact with the heptane vapor, leading to a high-energy interface. Graphene sheets “climb” this surface to minimize the interfacial energy, leading to thin graphene films. This phenomena is shown in Figure 7-2A. The graphene film, even after centrifugation at forces greater than 300,000 g, remains stable at the interface below the heptane and above the water. If, however, the heptane is allowed to evaporate, the heavier graphite will fall through the water and precipitate at the bottom of the vial, showing that the graphene is not simply suspended on the water by surface tension.

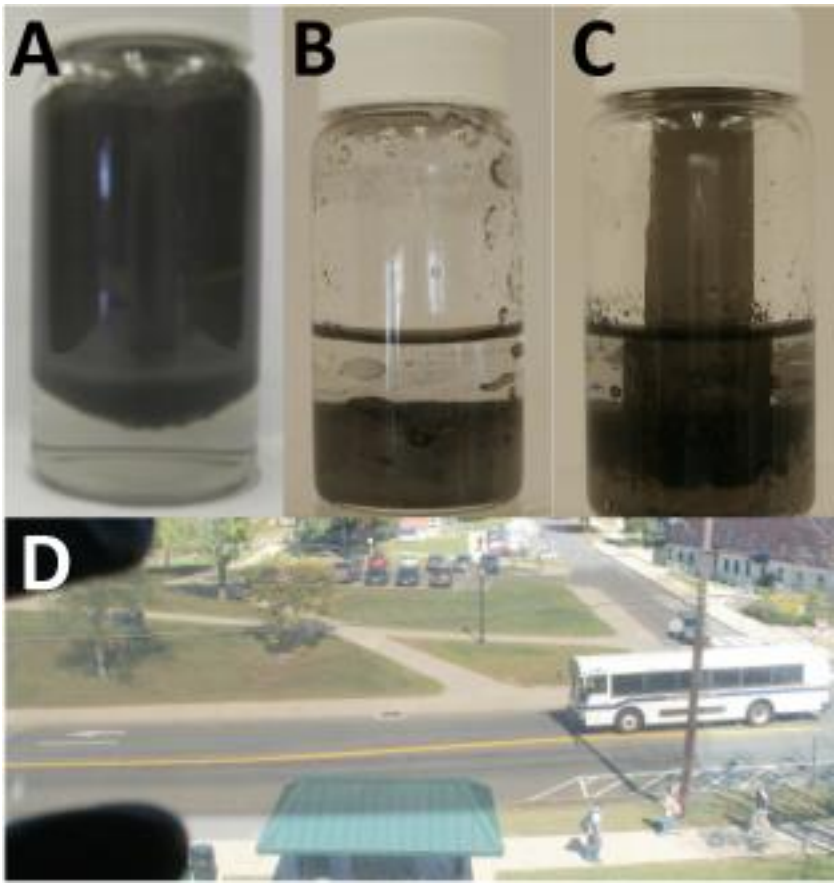

Figure 7-2: Images of graphene film. (A) Glass sample vial containing water, heptane, and graphene showing graphene film climbing the glass from the water/heptane interface to the top of the vial. (B) Glass vial whose interior surface has been made hydrophobic by treatment with a chlorosilane. Graphene is observed at the water/heptane and water/hydrophobic glass interface of the lower phase, but no climbing is observed above the water layer. (C) Vial as in B, but with an untreated glass slide inserted. The graphene climbs the slide even as it does not climb the hydrophobic glass vial. (D) Macroscopic transparent film of graphene on a glass slide formed by interface trapping.

When a glass slide is introduced to the system, the film also climbs both sides of the slide. As the glass provides a hydrophilic surface necessary to form the water/heptane interface, a hydrophobic surface will not lead to climbing. Polyethylene vials show graphene at the liquid interface, but no climbing. The same effect is seen by treating the inside of a glass vial with trimethylsilyl chloride to make the walls of the vials hydrophobic. As seen in Figure 7-2B, the graphene no longer climbs the vial walls,

instead partially coats the now hydrophobic walls in contact with the water phase. Placing an untreated glass slide in the treated vial, as shown in Figure 7-2C, results in graphene climbing the slide. Figure 7-2D illustrates such a film on a glass slide, with a graphene layer on both the back and front of the slide.

The formation of the graphene films is explained by reassembly of graphene sheets at the oil/water interface driven by minimization of interfacial free energy of the system. Indeed, the surface energy of graphene γ_g=54.8 mN/m[57,58] lies nearly in the middle between the surface tension of water, γ_w=72.9 mN/m, and the surface tension of heptane, γ_h=20.1 mN/m, at 20 °C.[59] This results in a positive spreading parameter value of $S \cong 6.6$ mN/m.[60] The climbing of the graphene indicates that the corresponding Hamaker constant of the glass/water/graphene/heptane vapor system is negative.[60] The capillary forces holding the graphene at the interface of the two liquids is substantially stronger than the gravitational force as long as the graphene film is thinner than the corresponding capillary length of ~0.7mm.[61]

7.2 Computational Simulations

The strong affinity between graphene and the water/heptane interface is also seen in detailed molecular dynamics simulations preformed with several graphene sheets dispersed at a water/heptane interface (see Section 23.1 for simulation details). During simulations, graphene sheets move along the interface forming stacks two and three sheets thick. Figure 7-3A shows the number fraction distribution normal to the interface (z-axis) in simulations with nine graphene sheets. Graphene stacks are located at the water/heptane interface with a slight preference towards the heptane phase. We never observe the formation of stacks with more than three sheets. The

further restacking of graphene flakes is suppressed by an increase in aggregate bending energy.

The strength of attraction between graphene stacks and heptane/water interfaces is evaluated by calculating the potential of the mean force between a three-sheet stack and interface in a system with a total of nine graphene sheets (see Figure 7-3B). The minimum of the potential is located at the water/heptane interface. The potential is steeper towards the water phase, confirming that the water is a poorer solvent for graphene than is heptane. In the heptane phase the potential saturates at distance z larger than 4 Å. The magnitude of the potential in the plateau regime is on the order of 4.5 *R*T (where *R* is the gas constant and T=300 K). This confirms a strong affinity of graphene stacks for the water/heptane interface. Note that in a real system, consisting of larger graphene sheets, this energy difference should be even greater, pinning graphene to the interface even more strongly. Also, for larger sheets, the formation of thick aggregates is suppressed due to both the necessity of diffusing large distances along the interface and the aggregate bending energy penalty to add a new sheet to a stack. This lack of restacking traps graphene at the liquid-liquid interface.

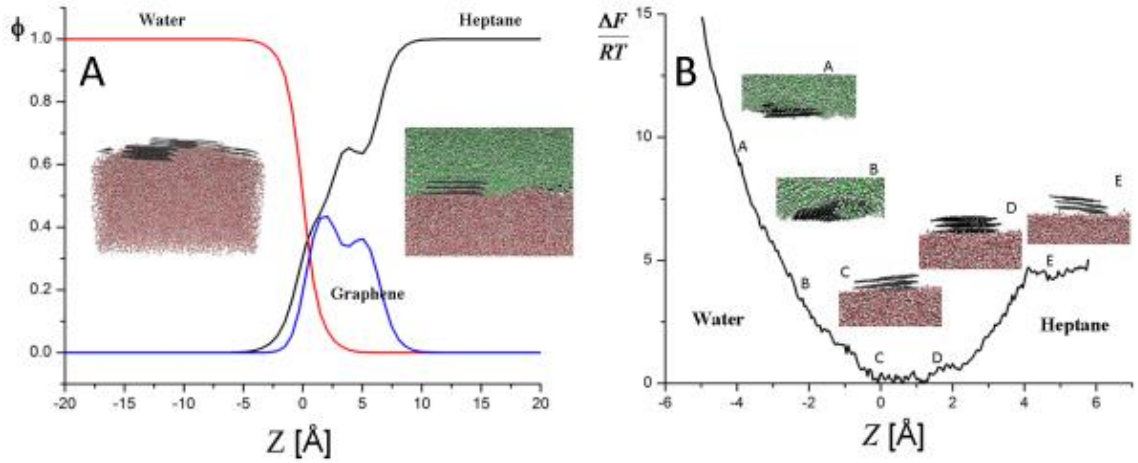

Figure 7-3: Computational study of graphene films. (A) Number fraction distribution of water, heptane and graphene along the z-axis, normal to the water/heptane interface. Insets show snapshots of the simulation box. In left inset heptane is transparent. In insets, hydrogen atoms are shown in light gray, oxygen atoms are colored in red, carbon atoms belonging to graphene are black and carbon in heptane is green. (B) Potential of the mean force for three-layer graphene flake assembly. Insets show typical configuration of the graphene flakes. The solvent into which the graphene assembly is pulled is transparent.

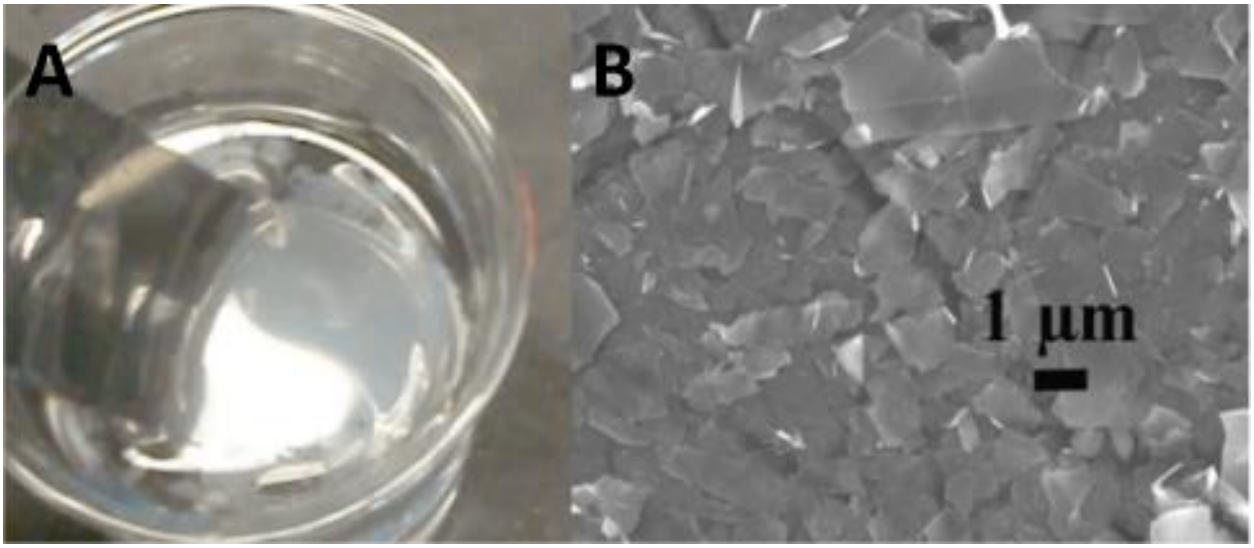

Figure 7-4: Images of pristine graphene films. (A) Graphene film formed on a glass slide by climbing being floated onto a water surface. (B) FESEM image of pristine graphene film. The sheets have lateral dimensions on the µm size scale and form an overlapping arrangement consistent with TEM images. The valleys seen are from the sample holder.

The use of an interface to produce non-transparent oxidized and reduced graphite films has been demonstrated elsewhere.[62–65] The formation of transparent conductive graphene films from modified graphitic precursors was reported recently, however in all previous investigations, dispersing the graphitic materials in one of the solvent phases was the initial step.[43,66–68] The requirement of first forming a dispersion is the major reason for the wide spread use of the water dispersible graphene oxide despite the damage caused to the graphene by oxidation.[69] Unlike the previous studies, we have used the lack of graphite solubility to our advantage. Placing graphene at the

interface of two immiscible liquids results in a condition where the graphene stabilizes the liquid/liquid interface and lowers the total energy of the system. We have found that using systems in which the graphitic material can be dispersed in one of the solvents does not lead to the climbing phenomenon that forms our transparent films. The use of functionalized graphene sheets produced by the thermal exfoliation and reduction of graphene oxide, does not result in climbing graphene, nor does the use of solvents such as NMP or DMF.

7.3 Characterization of the Graphene Film

The graphene film is formed on a glass slide simply by placing the slide in the vial where it intersects the water/heptane interface. After film climbing, the slide is removed and the heptane allowed to dry. The film can also be floated off of the glass slide onto the surface of water as illustrated in Figure 7-4A. This allows for the transfer of the film to other surfaces, an important aspect of the system for both applications and characterization. This lift off technique can be repeated several times to produce thicker films. By lifting the film onto an SEM stub, images such as that shown in Figure 7-4B are obtained. The film is shown to be composed of overlapping graphene sheets with roughly micron lateral dimensions. These large sheets are possible due to only brief, mild sonication used to speed the graphene exfoliation. The trenches in Figure 7-4B are characteristic of the aluminum stub used to mount the sample.

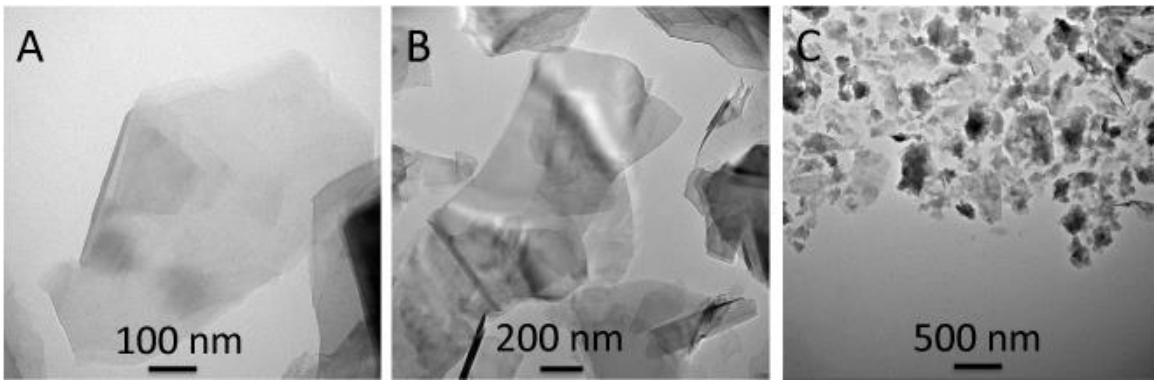

Figure 7-5: TEM images of graphene film. (A-C) illustrate the one to four layer, overlapping network morphology of the graphene films. The films contain open regions, single sheets, and stacked sheets.

The float off technique is also employed to obtain TEM images such as those shown in Figure 7-5A, B, and C. The film is observed to be composed of a network of overlapping graphene sheets. Spaces containing no graphene are also observed, and analysis of the TEM images indicates that nearly 20% of the film surface contains no graphene. The overlapping graphene sheets serve to hold the film together. The thickness of the film is also analyzed by Raman spectroscopy, comparing the spectra of our films, as shown in Figure 7-6A, with literature examples indicates a stacking of approximately two sheets.[56] The transparency of the graphene films is as high as 95% (Figure 7-6B). A single graphene sheet has been shown to absorb 2.3% of incident white light, with hydrocarbon contamination causing slightly lower transmission below 500 nm.[70] Four graphene sheets would be expected to lead to ~91% transmittance. With 20% of the surface free of graphene, the transmittance is expected to be ~93%. As shown in the TEM images and indicated by Raman spectroscopy, the film averages less than 4 sheets, thus the observed value of ~95% transmittance is consistent with these observations.

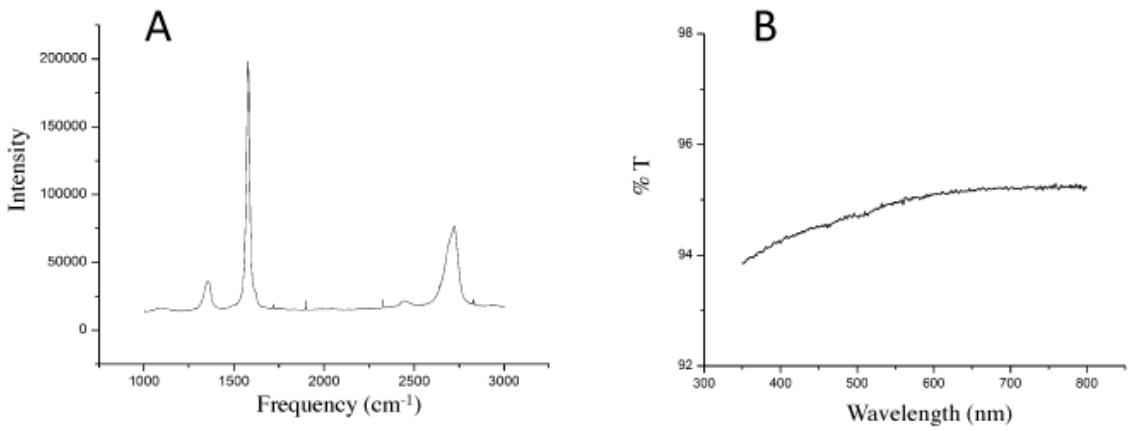

Figure 7-6: Spectroscopy of pristine graphene films. (A) Raman spectrum of graphene film. The shape of the 2D peak is consistent with two layers of graphene. (B) UV-Vis spectrum of the graphene film on a glass slide. Lower transparency at shorter wavelengths is thought to arise from the adsorption of hydrocarbons on the surface.

We find experimentally that the films formed by graphene climbing are consistently 4 or fewer sheets. The films formed at the bulk solvent interface, however, can be much thicker depending on the concentration of graphite. This discrepancy is due to the climbing phenomena being driven by lowering the interfacial energy between the water absorbed on the hydrophilic glass walls and the heptane vapor in the headspace of the vial. Once graphene occupies the interface, the driving force for climbing is diminished and no additional sheets are drawn up.

7.4 Conclusions

We have demonstrated the formation of a transparent and conductive graphene film by trapping exfoliated graphene sheets at a liquid interface. Computational studies have shown that this interface trapping process is the result of the strong affinity of the graphene sheets to the interface. The film deposition technique is simple, inexpensive,

applicable to a wide range of surfaces, scalable, utilizes pristine, natural flake graphite with no prior treatment, and requires no post-treatments such as chemical reduction or heating. It has the potential to revolutionize application of graphene films in transparent electrodes in solar panels and organic electronic devices.

Part II: Infusion of Fabrics with Pristine Graphene / Graphite

Chapter 8: Introduction

Smart textiles, also known as E-textiles or electronic textiles, are gaining attention due to potential applications in biosensors, heat generation, and wearable electronics.[71–75] However, current methods of imparting conductivity, such as the incorporation of metals[76–78] or conductive polymers,[79,80] often give less than optimal conductivity and can result in the loss of fabric flexibility, significant weight increases, undesirable changes in fabric texture, or skin irritation. In an effort to meet these challenges, a new approach, based on kinetically trapping pristine few layer graphene (FLG) from natural flake graphite, is presented. This approach enables electrically conductive fabrics incorporating FLG sheets on the surface of fibers. The fabrics show no degradation of properties, yet demonstrate remarkable electrical conductivity.

A popular approach to impart conductivity to fabrics is the incorporation of metal fibers and coatings, but their high density and undesirable interactions with the skin has led to the exploration of other materials, especially carbon-based materials. Carbon nanotubes[74] (CNT) and carbon black[81] have both been used to impart conductivity, yet low conductivity and concerns of possible CNT toxicity have limited their use. Graphene, with its outstanding mechanical and electrical properties,[2] is an attractive candidate for producing conductive textiles. It is non-toxic, inexpensive, and has even shown signs of being a viable antibiotic.[82]

Previous approaches to creating conductive fabrics based on graphene and graphite have included making graphene fibers from graphene oxide, (GO)[83–85] infusing fabric with GO followed by its reduction to graphene, transferring a patterned film made through chemical vapor deposition (CVD),[75] and dispersing graphene with a surfactant,

followed by the removal of the surfactant with nitric acid.[86] Although an improvement compared to metals, these methods all have their limitations: graphene produced through the reduction of GO has significantly reduced electrical and mechanical properties,[55] CVD grown graphene is not cost effective for bulk material production, and harsh chemical treatments for the removal of surfactants adversely affects the mechanical and tactile properties of the fabrics.

Chapter 9: Experimental Methods

9.1 Preparation of Graphene Infused Fabric

A typical laboratory procedure started with 100 mg natural flake graphite (Asbury Carbons Grade 3243) placed in a 20 mL glass scintillation vial. The vial was charged with 5 mL *n*-heptane (Fisher Scientific, 99% Optima), followed by 10 seconds of bath sonication (Branson Model 2510). This was then followed by tip sonication using a Cole-Parmer 750 Watt Ultrasonic Processor (20 kHz operating at 40% power) for 15 minutes. The initial bath and tip sonication broke up large aggregates that are common in the graphite used. De-ionized water (5 mL) was then added and the mixture was once again bath sonicated and then tip sonicated at 40% power for 15 minutes. The second bath sonication facilitated the exfoliation and migration of FLG to the liquid-liquid interface. A 2.5 cm x 2.5 cm piece of fabric (for example, poly(ethyleneterephthalate) simulated leather, non-woven) was then placed into the scintillation vial. The vial was topped off with heptane, and placed into the bath sonicator for 1 hour. After removal,

the sample is placed in the oven for drying at 80 °C The solvents and FLG/graphite left in the vial could be reused for future samples.

Control samples were also prepared. The sample preparation is the same as above, but the solvents used were different. One control used only water as a solvent, and the other control used only heptane.

9.2 Characterization

9.2.1 Determination of Percolation Threshold

The percolation threshold was determined using a four-line probe method with a Keithley 224 Programmable power supply (I_{max} = 101.1 x 10^{-3} A), while a 196 system DMA was used to measure the voltage. Samples were first prepared as described in section 9.1, although at varying concentrations. Resistance was first measured by creating an I-V plot with at least 10 data points. The sheet resistance was then determined using the relation $R_S = R(w/l,)$ where w is the width of the sample and l is the distance between the leads.

9.2.2 Field Emission Scanning Electron Microscopy

Field Emission Scanning Electron Microscopy images were obtained using a JEOL JSM 6335F FESEM. The graphene infused fabric samples were prepared as in section 9.1. They were then cut and attached to an aluminum SEM stub using carbon tape.

9.2.3 Tensile Testing

Samples were first prepared as described in section 9.1. Mechanical testing was carried out using a 2.5 cm x 1.25 cm sample at a strain rate of 10 mm/min. Control samples were also tested.

9.2.4 X Ray Diffraction

A sample was first prepared as in section 9.1. It was then tested in a Bruker D2 Phaser. The angle was varied from a 2θ value of 40 to 5.

9.2.5 Temperature Dependence of Resistance

A sample was first prepared as in section 9.1. The resistance of an infused fabric containing 14.7 wt % FLG was measured over the temperature range of 10 - 400 K using a standard four-line probe technique with a Physical Property Measurement System (Quantum Design).

Chapter 10: Results and Discussion

10.1 Exfoliation of FLG

The major difficulty encountered in the use of natural flake graphite is suspending it in solution for infusion into a fabric. The past use of GO and surfactants were efforts to solve this difficulty. Here, using a recently developed interfacial trapping method,[87] the challenge of suspending FLG in a solvent for fabric infusion is overcome without the need for surfactants or chemical modification of the graphite. Figure 10-1 illustrates a demonstration of the kinetic trapping method and shows images of fabric before and after infusion with FLG. The method produces a fabric infused with a combination of

graphite and pristine FLG, resulting in an electrically conductive fabric produced in a scalable and cost effective manner, while retaining the fabric's mechanical strength and feel.

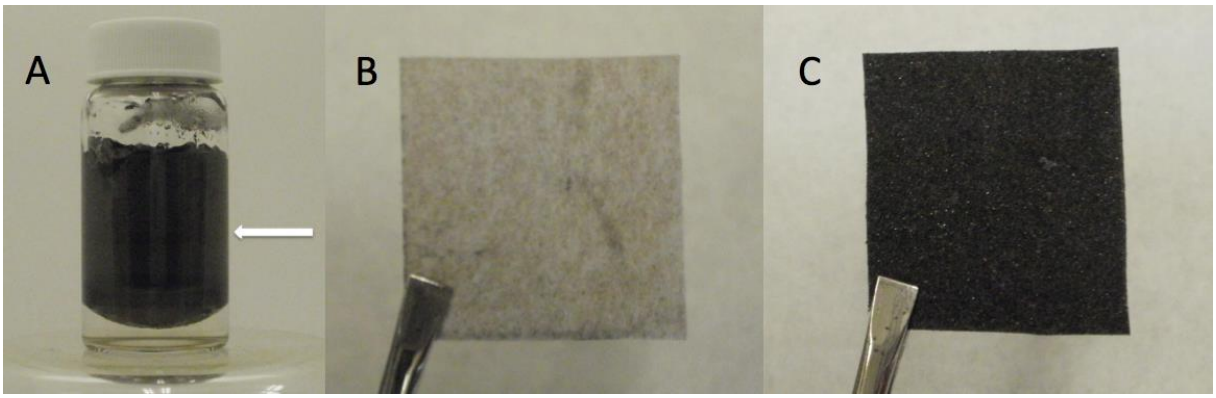

Figure 10-1: (A) Climbing of FLG/graphite up the walls of a scintillation vial. The vial contains heptane, water, and FLG/graphite. The arrow indicates the heptane-air interface, with the FLG film climbing from the heptane/water interface up the walls of the vial. (B) Fabric before treatment and (C) after the infusion of FLG/graphite.

The kinetic trapping approach utilizes a mixed solvent system of water and heptane. As both water and heptane are poor solvents for graphene,[88] neither one by itself will form stable FLG suspensions. The lack of good solvents for graphene has posed problems in the past, but the interfacial trapping relies on this insolubility. When the graphite is added to a water/heptane mixture it is initially found at the solvent interface where it serves to minimize the high interfacial energy of the two solvent phases. Once there, mild sonication speeds the exfoliation of the graphite into FLG sheets and these sheets spread to cover the interfaces, including climbing hydrophilic surfaces in contact with heptane vapor, as illustrated in fig. 1a where FLG climbs the hydrophilic glass walls of the sample vial.

Rather than approach the challenge of graphite exfoliation and suspension by chemically modifying the graphite through defect forming oxidations, or by adding

difficult to remove surfactants, we create a system in which the bulk stacked graphene sheet morphology of graphite is not the most thermodynamically stable arrangement. We start by creating a high-energy system composed of oil and water interfaces. Placing graphene sheets at these interfaces lowers the energy of the system and thus drives exfoliation and coating of hydrophilic surfaces possessing thin water layers, such as the glass vial walls shown in Figure 10-1A or individual fibers of a fabric. The force holding the pristine FLG sheets at the liquid-liquid interface is substantial, as the sheets remain at the interface even under centrifugation forces exceeding 300,000 *g*. As graphene is not soluble in either the oil or the water phase, the kinetic barrier to forming graphene stacks more than 3 to 4 layers thick is very large, effectively trapping the sheets at the interface in their exfoliated state. The uptake of FLG and graphite by the fabric as described in this report is driven by this mechanism.

10.2 Infusion of Fabric

The infusion of FLG into the fabric involves sonication of the fabric in a heptane/water mixture containing graphite, where a heptane/water interface is created at the surface of the slightly hydrophilic fibers of the fabric. Graphite is drawn into the fabric, and FLG is deposited on the fibers. As can be seen in the scanning electron microscopy images in Figure 10-2, graphite particles are trapped between the strands of the fabric (Figure 10-2**A**), while FLG flakes attach themselves to the fibers (Figure 10-2**B**). Using this approach, the fabric can be loaded with as much as 15 wt% graphitic material.

Control experiments using only water or only heptane show very different results. If only water is used as the solvent, almost no graphite is infused into the fabric and no

conductivity is observed. With only heptane, it is only possible to load the fabric with approximately 10 wt% graphite. As the fabric always contains some moisture, this is not unexpected; the real difference lies with the conductivity. Comparing fabrics infused with nearly identical loadings of graphite but with one infused in both solvents and one infused with only heptane, a forty-fold difference in conductivity is observed. Although containing roughly equal amounts of graphite, the lack of an extensive water/heptane interface in the latter sample results in far less exfoliated FLG, and thus much less efficient overlap of the FLG material. FESEM micrographs of both samples are shown in Figure 10-3.

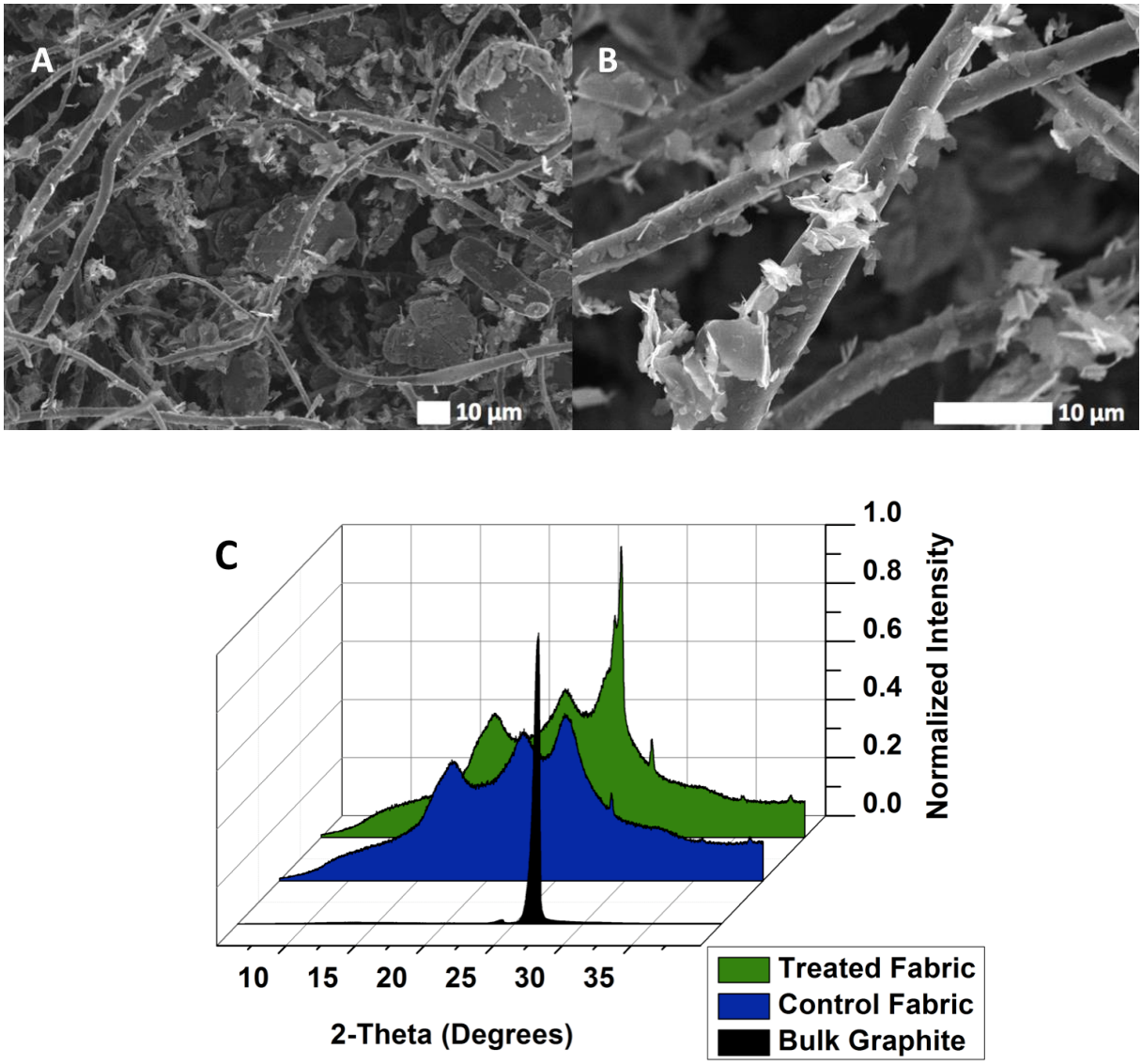

Figure 10-2: (A,B) Scanning Electron Microscopy Images of the treated fabric. The bulk pristine graphite can be seen caught between the fibers of the fabric, and FLG flakes can be seen attached to the fibers themselves. (C) X-Ray Diffraction Pattern of bulk pristine graphite, the control fabric, and treated fabric indicate no degradation of the graphitic species.

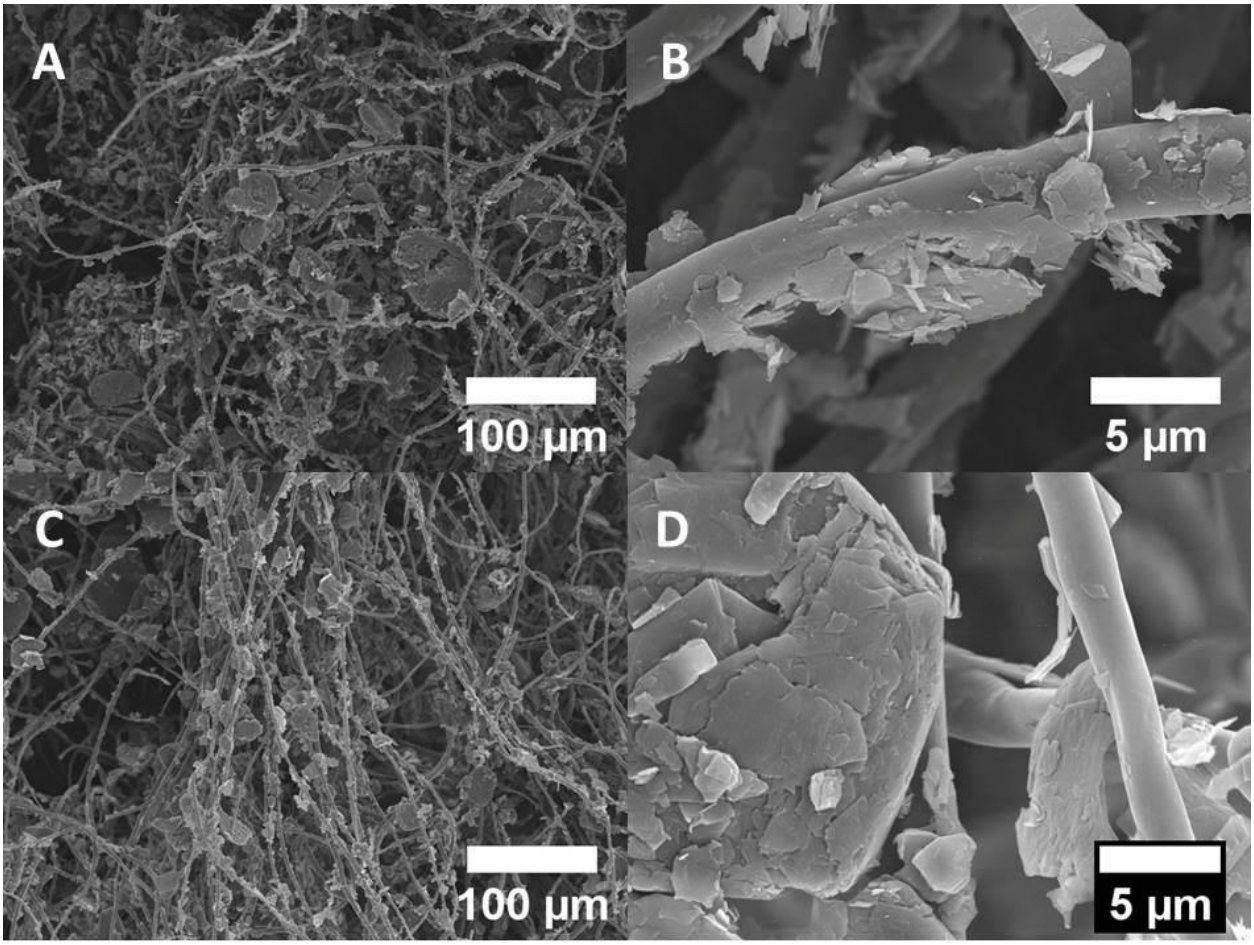

Figure 10-3: Scanning electron micrographs of samples prepared using only heptane (A,B) and only water (C,D).

As can be seen in Figure 10-3, using only one of the two solvents leads to less exfoliation of the graphite into pristine FLG sheets. In the images of the heptane only system, flakes can be seen attached to the fibers as with the two-solvent system; however, they are clearly many sheets thick as opposed to the FLG we see in the two-solvent system. In the water only system, even fewer flakes are seen attached to the fibers, and they show an even larger apparent number of sheets. This lack of connecting graphene decreases the conductivity in the one-solvent system to 40 times less than that of the two-solvent system.

To further demonstrate the applicability of the kinetic trapping mechanism to the graphite infusion of fabric, the fabric is melt-pressed to form a flat surface without the porosity of the original fabric. This is followed by placing the flattened fabric in a water bath to fully hydrate the surface, then placing it into a vial containing heptane, water, and natural flake graphite - a typical setup for producing climbing films in the original kinetic trapping investigation. Upon shaking, the film climbs the melt-pressed fabric just as it does a glass slide, indicating the same kinetic trapping and climbing phenomenon that occurs on glass occurs with the fabric as well.

10.3 Mechanical and X-ray

After infusion of the FLG/graphite mixture, the fabric has the same feel and flexibility as the initial sample, which is desirable for any practical commercial applications. The mechanical properties of the infused fabric are tested against a control using an Instron Model 1011 in tension mode and the results are shown in Figure 10-4. There is no significant change in strength between the control and the treated fabric. The treated fabric is also analyzed using X-Ray Diffraction (Bruker D2 Phaser) to see if there is any change in the FLG/graphite during the process. A fabric control, bulk pristine graphite, and a treated sample are all analyzed, and as can be seen in Figure 10-2C, no significant alteration of either the graphite or fabric is observed by XRD.

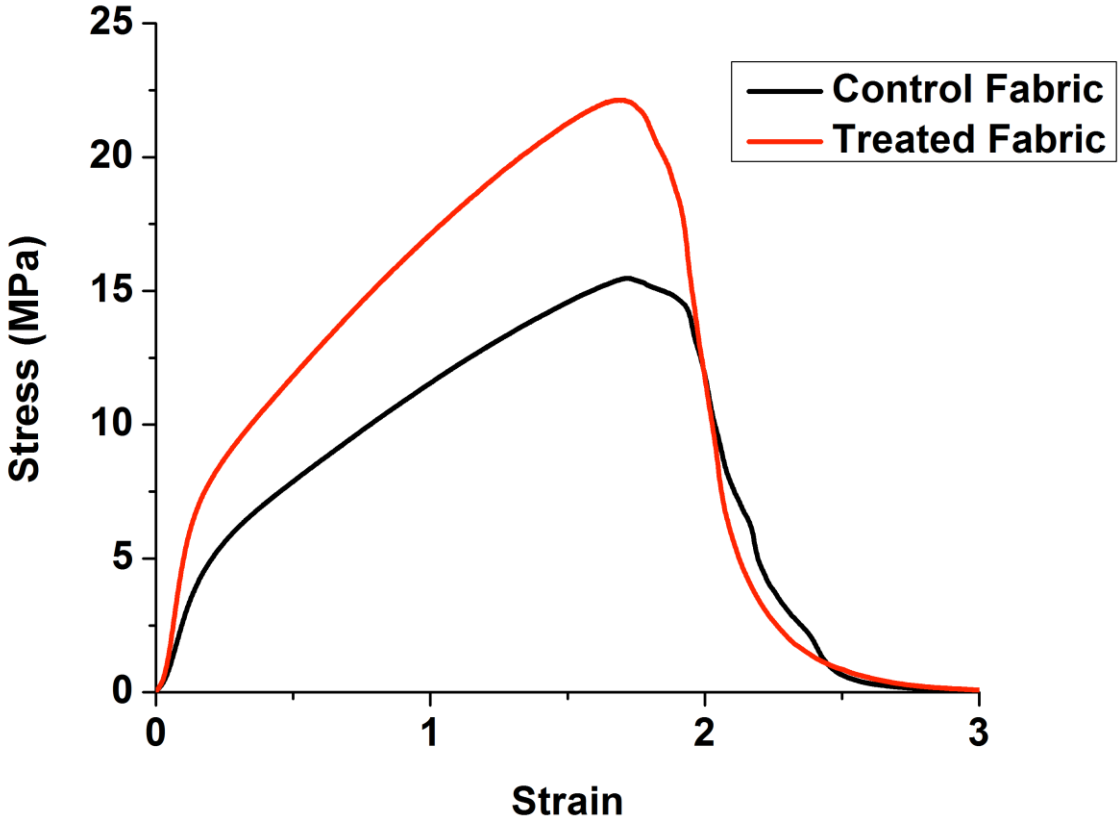

Figure 10-4: Stress-Strain curves for both the control fabric and the treated fabric.

10.4 Electrical Conductivity

Although nearly 15 wt% of graphite can be loaded into the fabric, electrical percolation occurs at a much lower level. Figure 10-5A shows the sheet resistance as a function of concentration of FLG in the fabric. The measurements are carried out using a four-line probe technique at room temperature and all samples are 2.5 cm x 2.5 cm. As expected, the sheet resistance decreases with increasing FLG concentration in the fabric. At loadings of 2.5 wt% FLG, the sheet resistance is 77.9 MΩ/sq; while at 10.7 wt% the sheet resistance is 2.5 KΩ/sq, a four orders of magnitude decrease in

resistance. Percolation is observed at 7.4 wt% loading, where the sheet resistance is 3.6 KΩ/sq. This value is roughly an order of magnitude lower than the best value reported for graphene-related materials in fabric to date.[89]

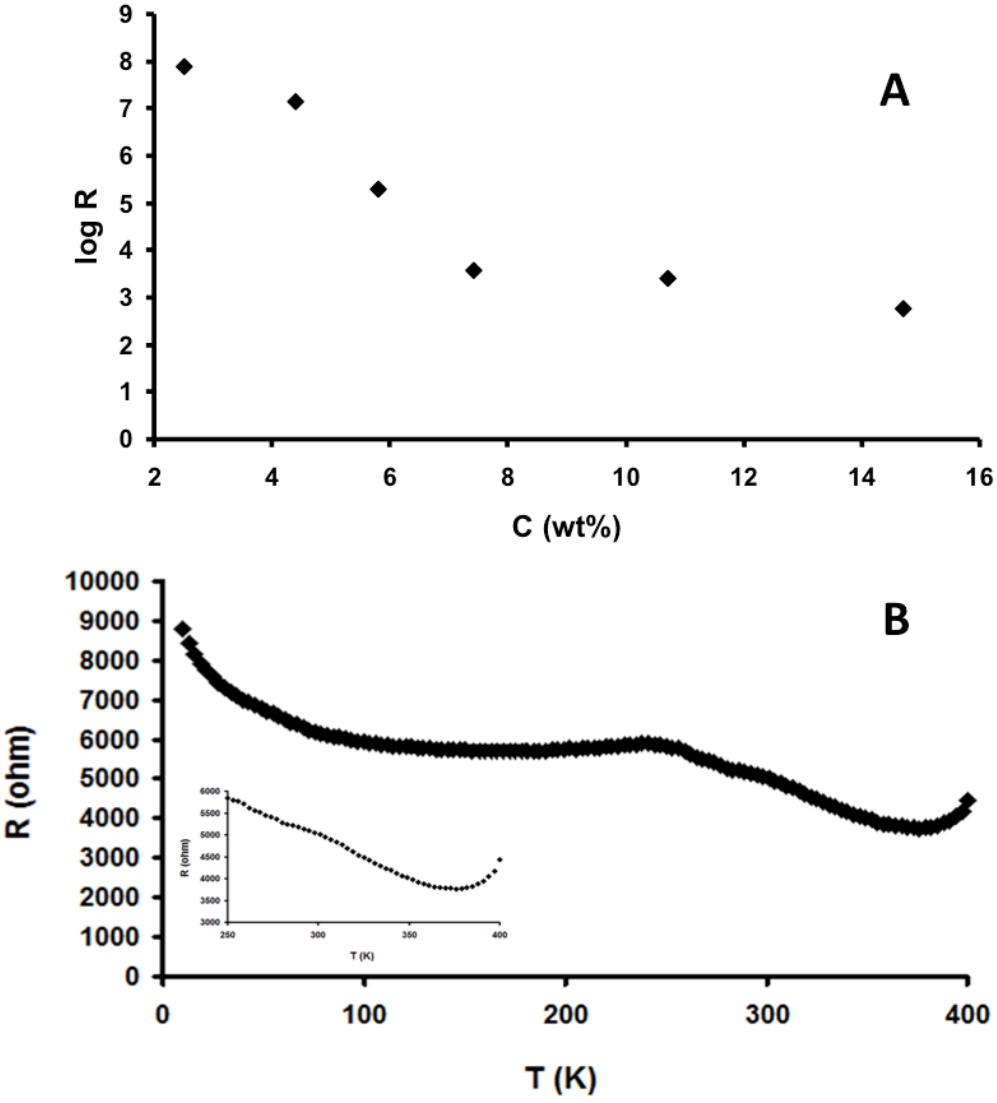

Figure 10-5: (A) Sheet resistance as a function of concentration of FLG/graphite infused into the fabric. The percolation threshold can be observed to be around 7 wt%. (B) Resistance vs. temperature plot of the infused fabric. A clear semiconductor-metal transition may be observed near 350 K (inset).

10.5 Temperature Dependence

To investigate the nature of the conductivity imparted by the FLG, the resistance of an infused fabric containing 14.7 wt % FLG is measured over the temperature range of 10 - 400 K using a standard four-line probe technique with a Physical Property Measurement System (Quantum Design). As shown in Figure 10-5B, the resistance decreases with increasing temperature from 10 to 100 K and from 250 to 350 K, consistent with semiconducting behavior. In the range of 100-250 K, the resistance is relatively constant. The change in the resistance over the entire region is about 5 KΩ. At 350 K the conductive fabric has a clear insulator-metal transition (inset of Fig. 3b**),** indicating a modulation in the band gap from gap to no gap. In addition, it is observed that the material has its lowest resistance near room temperature, where most smart textile applications will be used.

10.6 Conclusion

In summary, using an interfacial trapping technique with natural flake graphite, we are able to produce conductive fabric in a safe, facile, and cost-effective manner. The conductive fabrics thus produced suggest the possibility of bringing smart textile technology into everyday use. The use of smart textiles in communication, medicine, and energy applications has great potential, but without a feasible approach to produce these conductive fabrics, the potential will not be met. This work provides a significant step forward to realizing this potential.

Part III: Pristine Graphene / Polystyrene Foams Templated by Graphene Sheet Stabilized Emulsions

Chapter 11: Introduction

The excitement surrounding the potential of graphene as a nano-filler in composite materials is driven by its unique set of electrical and mechanical properties.[1–3,5,15,90–93] A common theme in previous studies of graphite and graphene based composites has been that the lack of graphene solubility is viewed as a challenge to be overcome. Solutions to graphene's insolubility include: employing graphene oxide (GO) or reduced graphene oxide (rGO),[35,94–99] harsh *in-situ* chemical reduction steps,[100,101] the use of high boiling and difficult to remove solvents,[102] and extended sonication treatments that result in the breaking of sheets due to shear stress.[103] All of these approaches pay a price in terms of degraded graphene properties. An approach that does not view graphene's insolubility as a limitation and thus utilizes pristine, unaltered graphite would have major advantages in terms of properties, cost, and environmental impact.

In this part of the dissertation, we report the results of a combination of experimental, theoretical and computational techniques to demonstrate the affinity of pristine graphene sheets to a water-oil interface and describe the use of this surface activity to stabilize water-in-oil emulsions. In particular, we take advantage of graphene/graphite's inherent insolubility and the large interfacial energies between aqueous and organic solvents by adding graphite to a mixture of two immiscible solvents and observing the spreading of graphene sheets at the high-energy liquid-liquid interface. There, the spreading is driven by a lowering of the total free energy of the system. The sheets then become trapped at the interface of the two solvents, playing the role of a stabilizing agent for emulsions of water droplets dispersed in a

continuous oil phase. In this context graphene sheets can be viewed as two-dimensional surfactants with internal bending rigidity.

While to the best of our knowledge the stabilization of emulsions by pristine graphene sheets has not been demonstrated previously, there are recent reports of GO being used as an emulsion stabilizer. The emulsions created with GO or GO derivatives are oil-in-water emulsions, as opposed to the water-in-oil emulsions we find with pristine graphene. This results in the formation of spherical polymer beads coated with GO, rather than a continuous composite material. For instance, Gudarzi *et al.* produced a "nanocomposite powder" with GO and PMMA,[104] Dao *et al.* synthesized surface functionalized rGO to make "microspheres,"[105] Zhang *et al.* used functionalized rGO to make a PS-based "solid powder,"[106] and Yin *et al.* reported GO coated PS microspheres.[107] A recent extensive study of GO-stabilized emulsions concluded that GO emulsions were best described as Pickering emulsions and that only oil-in-water emulsions were formed.[108]

Using a monomer as the oil phase, we demonstrate how pristine graphene-stabilized water-in-oil emulsions template solid graphite composite foams. After polymerization of the continuous phase, the water filled spherical cavities are lined with a graphitic skin consisting of overlapping pristine graphene sheets. A gentle evaporation process removes the water, leaving an open cell foam composite with exceptional mechanical strength, electrical conductivity, and low density, with cells sizes easily controllable by varying the mixture composition. This environmentally friendly approach to graphite utilization in polymer composites avoids the use of chemical treatments, the input of large amounts of mechanical or thermal energy, or the addition of stabilizers

such as surfactants or high boiling solvents that can be difficult to remove. Potential applications of these low cost materials include strong and lightweight building materials, filters, ultra capacitor electrodes, and conductive catalyst supports.

Chapter 12: Traditional Methods of Graphene Nanocomposite Production

12.1 Introduction

Polymer nanocomposites have been investigated thoroughly in the past few decades. The smaller sized filler particles (with at least one dimension less than 100 nm), are able to provide benefits like conductivity without creating problems in mechanical strength, processing, and weight.[99,109] In the recent past, carbon nanotubes have been the focus of research in the polymer nanocomposites field. There are, however, several problems that have prevented their wide scale use: limited availability, high cost, and issues arising from bundling.[99,110] Graphene, on the other hand, has attracted a lot of attention because of its low cost, high availability, and easy processing. There are three general methods that have been used to produce polymer/graphene nanocomposites, which shall be outlined in the following sections.

12.2 Solvent Processing

There are three main steps to producing polymer/graphene nanocomposites using the solvent processing method. In the first step, graphene is dispersed in a solvent; this is normally achieved through sonication. The next step is the incorporation of the polymer. The final step is the removal of the solvent, which is normally the most difficult. The compatibility of the solvent and the polymer must also be considered.

In general, there are two problems associated with this procedure. The first is that graphene is not easily dispersed. One route that has been taken to circumvent this problem is using GO, which will readily disperse in hydrophilic solvents. However, the incorporation of GO necessitates a reduction step, which is normally done in situ and requires harsh reduction agents.[111] The other problem is the removal of solvents once the polymerization is complete. As more solvent evaporates, the viscosity of the mixture increases, and it becomes harder for the solvent to further evaporate.

12.3 Melt Blending

The second method used to produce polymer/graphene nanocomposites is by melt blending. It is as simple as it sounds: melting a polymer and incorporating the graphene filler through mixing. This is somewhat easier than the previous method, and RGO can be used instead of GO, so there is no in situ reduction needed.

There are, however, several problems associated with this method as well. The first is that issues arise in dispersion of the graphene because of viscosity, especially at higher loads.[112] The second problem is that there is often breaking and crumpling of the graphene sheets due to the high shear stress from the mixing process. The wrinkling and breaking decrease the aspect ratio, which are both bad for conductivity and for dispersion.[103]

12.4 In Situ Polymerization

In this method, the nanofiller is dispersed in the monomer, which is then polymerized. Again, one of the problems associated with this method is that graphene does not disperse well in most monomers/solvents, so GO or some other type of

functionalized graphene is used.[92] Another problem is that increases in viscosity during the polymerization limit the loading.[103] Finally, phase separation often occurs, as the graphene that was suspendable in the monomer is not suspendable in the formed polymer.

Chapter 13: Experimental Methods

13.1 Preparation of a Graphene / Polystyrene Composite Foam

For a typical graphene composite foam, an Erlenmeyer flask was charged with 880 mg of graphite (Asbury Carbons Grade 2299, although others such as Asbury Carbons Micro 890 and 3243 have been used successfully as well), along with 150 mL water (Deionized), 50 mL styrene (Acros Organics, 99.5%), 12 mL divinylbenzene (Aldrich, 80%), and a stir bar. The contents were then mixed on a stir plate for 30 seconds, followed by 30 seconds of bath sonication (Branson 80W B2510DTH). This procedure results in a graphene concentration of 4.4 mg/mL and a 3/1 water/styrene ratio. Composites with other ratios and concentrations are simply adjusted accordingly, keeping the initial graphite to total water and styrene ratio constant. The sonication was not necessary to obtain emulsions, but utilized simply to break up large clumps of graphite. 150 mg of azobisisobutyronitrile (AIBN) (Aldrich, 98%) was then added to the same flask. The system was then mixed on a stir plate for a minimum of 15 minutes while being purged with Ar gas (Fisher). After the purging process, the contents of the flask were poured into a Waring Commercial Blender (Model 33BL79) under an Ar

atmosphere. The blender was then turned on for 1 minute. The newly formed emulsion was placed into a 250 mL jar and sealed under Ar gas. The jar was then placed in an oven (Thermo Electron Corporation, Model 6500) at ~70 °C for 24 hours. After the reaction was complete, the composite samples were removed from the jars and heated at ~80 °C for ~2 days to remove all water. Excess bulk polystyrene was cut off of the top if necessary.

13.2 Characterization

13.2.1 Emulsion Droplet Size Analysis

The size of the dispersed aqueous phase droplets was determined with a DT-100 Acoustic Spectrometer from Dispersion Technology Inc. The attenuation spectra were analyzed using Dispersion Technology software for polydisperse emulsions.[113] The distribution was obtained from ultrasound attenuation spectra in the frequency range between 1 and 100 MHz.

The emulsion sample used in the measurement utilized heptane rather than styrene as the continuous phase. A flask was charged with 880 mg of graphite (Asbury Carbons Grade 2299), along with 150 mL water (deionized), 62 mL heptane (Fisher Optima), and a stir bar. The contents were then mixed on a stir plate for 30 seconds, followed by 30 seconds of bath sonication (Branson 80W B2510DTH). The sonication was not necessary to obtain emulsions, but utilized simply to break up large clumps of graphite. The system was then mixed on a stir plate for about 30 seconds. After the mixing, the contents of the flask were poured into a Waring Commercial Blender (Model

33BL79). The blender was then turned on for 1 minute. The contents were then poured into a jar for transportation, and then directly into the instrument.

13.2.2 Electron Microscopy

Samples were first prepared as in section 13.1. To prepare composite samples for the electron microscope, they were first cut with a razor blade. The slices were then mounted on aluminum stubs and coated with Au/Pd in a sputter coater (Polaron Unit E5100). The samples were characterized with a JEOL 6330 field emission scanning electron microscope with a 10 kV accelerating voltage.

13.2.3 Optical Microscopy

The emulsion samples in Figure 14-1A,C, and D utilized heptane rather than styrene as the continuous phase as described above. A flask was charged with 880 mg of graphite (Asbury Carbons Grade 2299), along with 150 mL water (Deionized), 50 mL n-heptane (Fisher Scientific, HPLC grade), and a stir bar. The contents were then mixed on a stir plate for 30 seconds, followed by 30 seconds of bath sonication (Branson 80W B2510DTH). The sonication was not necessary to obtain emulsions, but utilized simply to break up large clumps of graphite. The system was then mixed on a stir plate for a minimum of 15 minutes. The contents of the flask were then poured into a Waring Commercial Blender (Model 33BL79). The blender was then turned on for 1 minute. The newly formed emulsion was placed into a 250 mL jar. A wide-mouth pipet was used to transfer some of the emulsion to a glass slide. These slides were then analyzed using a Nikon Labophot with an IDS UI-3370CP Color camera in full color (C,D) or monochrome (A) mode.

13.2.4 Electrical Measurements

Samples were first prepared as described in section 13.1. To prepare the samples for electrical conductivity testing, they were first cut into rectangular prisms on the scale of a few centimeters in length. The ends were then covered with silver paint (Ted Pella) and allowed to dry. Copper tape (Ted Pella) was then attached to the silver contacts and the resistance was measured using a Keithly Model 2420 SourceMeter.

13.2.5 Thermal Analysis

Samples were first prepared as described in section 13.1. 20 mg of each of the composites was crushed to a fine powder and analyzed in a TA Instruments TGA Q-500 to determine the graphene loading. The samples were heated in a platinum pan in a nitrogen filled chamber from 20 °C to 800 °C at 10 °C per minute. The mass of the sample left at 700 °C was taken to be purely graphene, since all of the polymer burned off by this point.

13.2.6 Mechanical Measurements

Samples were first prepared as described in section 13.1. To prepare the samples for testing, they were first cut into cylinders around 5 centimeters in diameter (the diameter of the glass jars they are prepared in) and a few centimeters in height. They were then tested using an Instron Model 5869 in compression mode.

Chapter 14: Results and Discussion

14.1 Graphene Stabilized Emulsions

The affinity of graphene sheets to a water/oil interface and their emulsion stabilization is studied with emulsions formed by water/heptane/graphite mixtures. Emulsions are produced as described in the Methods section. Figure 14-1A shows the structure of a graphene stabilized water-in-heptane emulsion under optical microscopy. Heptane is the continuous phase surrounding graphitic skin-stabilized spherical water droplets with diameters varying between 20 and 200 μm. Note that there is some coalescence during the transfer process to the glass slide used for imaging. The droplet size distribution in a water-in-heptane emulsion can be seen in Figure 14-1B.[113] The average size of the droplets is 55 μm, consistent with optical image analysis of the resultant emulsion shown in Figure 14-1A. That the water droplets are stabilized with a graphitic skin and not by chunks of graphite is shown in Figure 14-1C and D. These images of droplets before and bursting upon evaporation of the heptane continuous phase clearly show the skin surrounding the droplets is made of sheets, not graphite particles. Further, the skin displays different degrees of transparency, indicating differences in the number of sheets forming the skin and providing strong evidence for skin thicknesses of a few graphene layers.

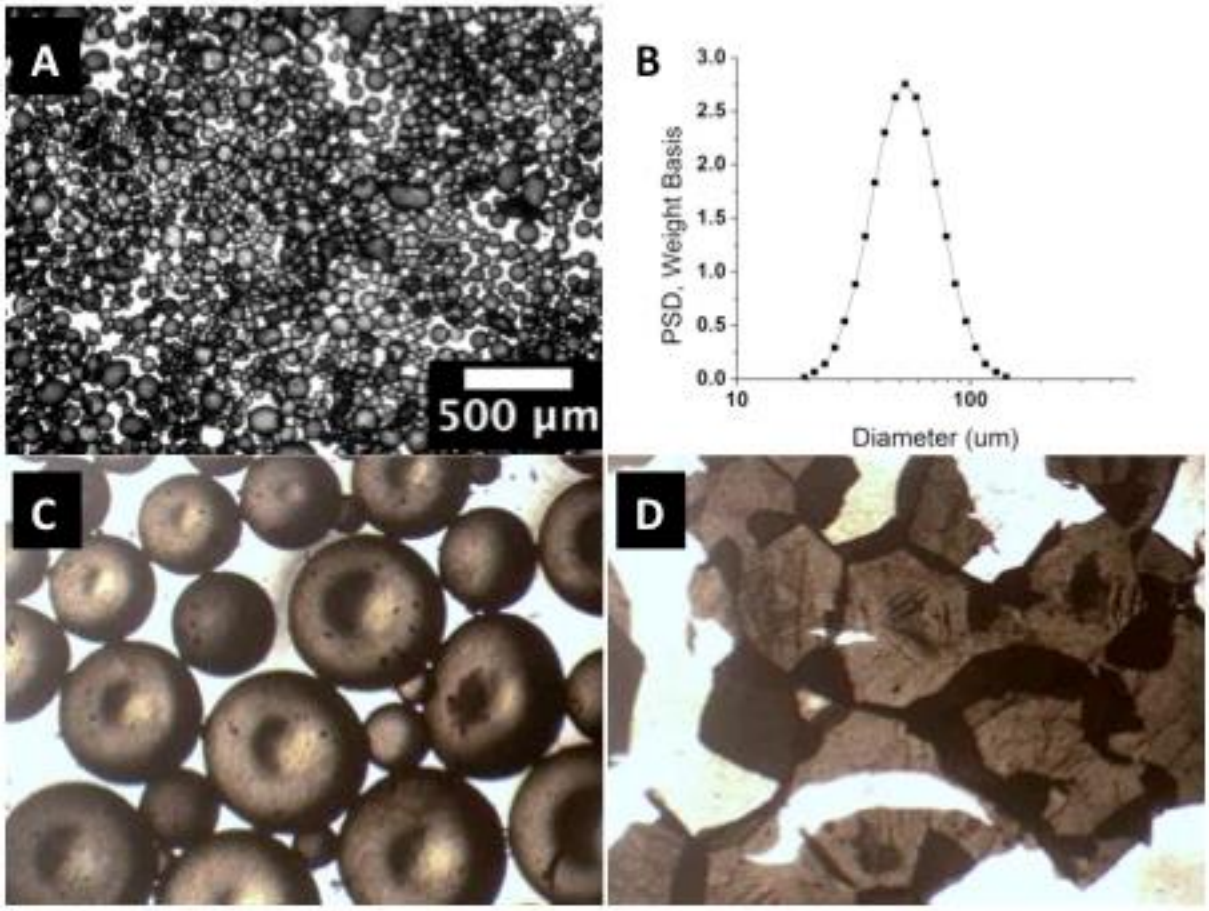

Figure 14-1: Graphitic Skin Stabilized Emulsions. (A) Optical microscopy image of graphitic skin stabilized emulsion in 50:34:0.44 mass ratio water/heptane/graphene mixture, (B) Droplet size distribution of graphite skin covered water droplets with average diameter 55 µm in 50:34:0.44 mass ratio water/heptane/graphene mixture as determined by acoustic measurements. (C) Magnified optical microscopy image of the initial structure of the water droplets covered with graphene skin before heptane evaporation. (D) Optical image of the graphitic skin left behind after heptane evaporation and droplet burst.

14.2 Computational Simulations

Corroborating the observation of few layer thick skin are results of our recent all atom molecular dynamics simulations of graphene flakes in a water/heptane mixture.[87] These simulations show that graphene flakes associate at the water/heptane interface forming stacks consisting of two to three graphene flakes. These graphene stacks are

localized at the water/heptane interface with slight preference toward the heptane phase. The system free energy change required to move a graphene flake into the heptane phase is $|\Delta g| \approx 2.2 mN/m$. Thus for a 100 X 100 nm graphene sheet, the work required to move it from the water/heptane interface into the heptane phase is on the order of 5300 $k_B T$ (where k_B is the Boltzmann constant and T = 300 K). Note that the penalty to move a graphene sheet into a water phase would be even higher. This energy cost effectively traps the graphene sheets at the water/heptane interface, a phenomenon similar in some ways to the trapping of nano- and micro-particles at a water/oil interface in Pickering emulsions.[114]

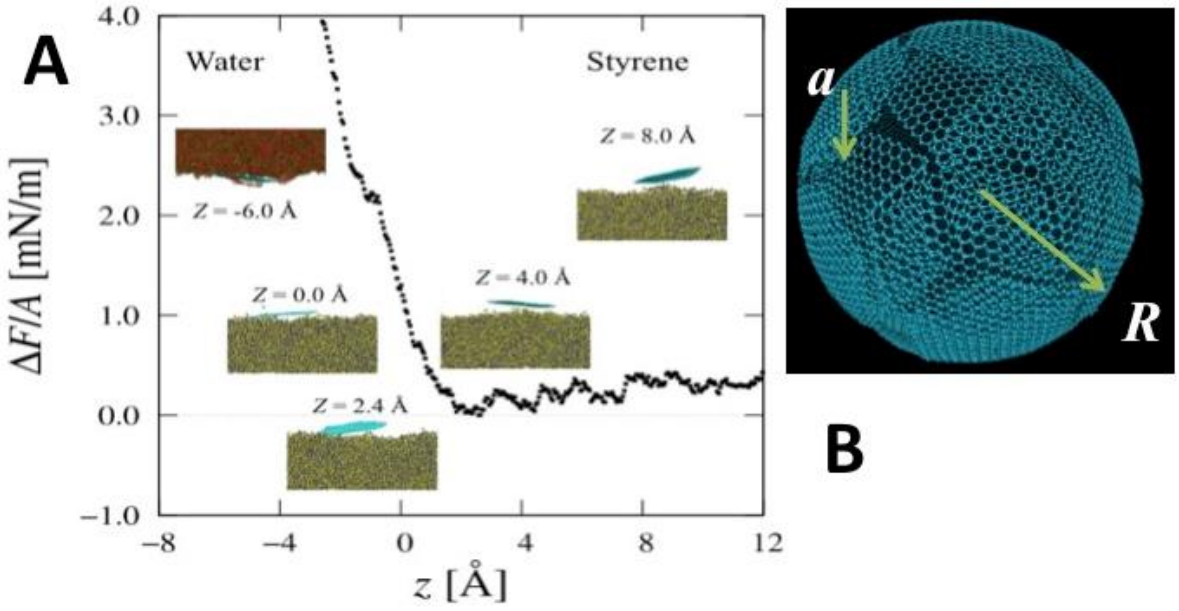

Figure 14-2: **(A)** Potential of the mean force for a graphene flake calculated along z-axis normal to water/styrene interface. Insets show typical graphene flake configurations. The solvent into which the graphene flake is pulled is transparent. In the insets, the hydrogen atoms of water molecules are yellow, oxygen atoms of water are blue, the carbon atoms belonging to styrene are red, and the hydrogen atoms of styrene are green. Graphene flakes are shown in cyan. **(B)** Schematic representation of a water droplet with size *R* covered with a graphene skin formed by flakes of size *a*.

In order to compare graphene affinity in heptane/water emulsions with that in the styrene/water emulsions used to make the reported composites, we have performed all atom molecular dynamics simulations to calculate the potential of the Mean Force between a graphene flake and water/styrene interface. In these simulations we use the Generalized Amber Force Field[115] for the atomistic model of styrene and graphene. The graphene flake is modeled as a polycyclic aromatic hydrocarbon consisting of eight generations of carbon rings terminated by hydrogen, $C_{384}H_{48}$.[87,88] The partial charges on the styrene and the graphene flakes are obtained from the Mulliken population analysis from *ab initio* calculations using the Gaussian09 simulation package with the 6-31G(d) basis set and B3LYP DFT method[116] as described in the work of Woltornist,[87] Oyer,[88] and section 23.2. For water we use the TIP3P force field potential.[117] The system consists of 9,360 water molecules, 1,360 styrene molecules and one graphene sheet. The simulations are performed following methodology developed for modeling of the graphene flakes in heptane/water mixture,[87] with details of the simulation procedure describe in SI1. In order to determine the surface activity of a graphene sheet in a water/styrene system, the Weighted Histogram Analysis Method[118] is used to calculate the potential between the graphene sheet and the water/styrene interface.

All simulations are performed at constant temperature *T* equal to 300 K. The variation of the potential of the mean force along the z-axis normal to the interface is shown in Figure 14-2A. The minimum of the potential is located in the styrene phase, indicating that although insoluble in both phases, the preference of graphene is for styrene rather than water. The increase of the potential in the styrene phase is not as steep as that observed in the water phase, another indication that styrene is a better

solvent for graphene than water. Oscillations seen in the potential of mean force indicate displacement of the aligned styrene molecules as the graphene flake is moved further away from the interface. The magnitude of the potential in the plateau regime is on the order of $|\Delta g| \approx 0.4 mN/m$. It is important to point out that similar calculations done for the heptane/water mixtures show that this free energy change is even higher $|\Delta g| \approx 2.2 mN/m$ for that system.[87] Using these values, we can estimate the work required to displace a 100 X 100 nm graphene sheet from the water/styrene interface into the styrene phase to be 966 $k_B T$, sufficiently strong to trap graphene sheets at the water/styrene interface. The work required to displace the graphene sheet into a heptane phase is about six times larger.

14.3 Theoretical Modeling

To model the total potential of the mean force in our system, we consider an emulsion prepared by mixing oil, water and graphite with masses m_o, m_w and m_g, respectively. The emulsion composition can be characterized by two mass ratios of graphene to water, $\phi_g = m_g/m_w$ and water to oil, $\phi_{w/o} = m_w/m_o$. The oil forms a continuous phase surrounding the water droplets with size R. *E*ach water droplet is covered by a graphitic skin of thickness h which is made of graphene sheets with average size a (see Figure 14-2B). The thickness of the graphitic skin h depends on the size R of the water droplets due to the mass conservation requirement such that $h = \beta R/3$, where we introduced parameter $\beta = \phi_g \rho_w / \rho_g$ with ρ_w = 1.0 g/cm^3 and ρ_g =2.66 g/cm^3 being the mass densities of water and graphene respectively (see SI2 for details). The volume of emulsion per water droplet V_0 can be expressed in terms of the emulsion composition

$\phi_{w/o}$ where $V_0 = 4\pi\alpha R^3/3$ with parameter $\alpha = 1 + \rho_w/\phi_{w/o}\rho_o$ and ρ_o is the oil mass density. Thus in the emulsion occupying volume V there are V/V_0 water droplets with size R. The total free energy change due to emulsion formation is the sum of contributions from individual droplets (see SI2 for derivation details). It has contributions from the graphitic skin bending energy and from the change of the oil/water interface free energy due to bringing graphene sheets to the interface. Equation (1) describes the result:

$$\frac{\Delta F_{total}}{V} \approx \frac{E}{384}\frac{\beta}{\alpha}\frac{a^4}{R^4} - \frac{3|\Delta g|}{\alpha R} \qquad (1)$$

where E is the Young's modulus of the graphene sheet (~1TPa). It follows that the affinity of the graphene towards the water/oil interface promotes the formation of smaller droplets to maximize the system free energy gains. However, graphene sheets adsorbed at the surface of smaller droplets have to bend more in order to remain at the interface, producing a bending energy penalty for each graphene sheet covering the surface of a droplet.

The size of the emulsion droplets is thus determined by a balance between the affinity of the graphene towards the solvent interface and the rigidity of the graphene sheets. The optimal size of the droplets is obtained by optimizing the system free energy ΔF_{total} with respect to droplet size R:

$$R^* \approx \left(\frac{E\beta a^4}{288|\Delta g|}\right)^{1/3} \qquad (2)$$

Equation 2 shows that we can control the size of the droplets by changing the graphene/water ratio (changing parameter β), by varying the graphene sheet size a, or by changing the identity of the oil. For example, in an emulsion with about 1% weight

fraction of graphite with respect to water, $b \approx 0.0033$, of radius a = 1.4 μm, we can estimate the diameter of the droplets in a water/heptane mixture to be on the order of 54 *μm*. This estimate is consistent with the emulsion droplet size of 55 μm observed experimentally (see Figure 14-1B). Repeating the same calculations for a water/styrene mixture, we estimate the diameter of the droplets to be 95 μm. This is consistent with the image shown in Figure 14-4B of a foam resulting from an emulsion with 80 to 90 μm diameter droplet sizes. Note that the increase in the droplet size is consistent with a decrease in the graphene flake affinity to the water/oil interface in these two systems. However, this is only an upper bound estimate for the size of the droplets covered with the graphitic skin. In reality the droplets in the emulsions are smaller due to droplets' breakup upon emulsion shearing in the homogenizer.[119] Indeed, we see a steady decrease of the average droplet size with increasing homogenization time.

14.4 Rheological Studies

The same approach is used to make emulsions with styrene as is used to make emulsions with heptane. In both cases, the graphitic skin stabilized water droplets settle to form a densely packed phase of spheres with the oil phase filling the space between them. The aggregation between graphitic skin covered droplets is due to van der Waals attraction between graphene sheets forming the skin layer. The excess of the oil phase forms a pure liquid phase above the emulsion, and the densely packed emulsion phase remains stable as confirmed by measuring G' at extended time (see Figure 14-3).

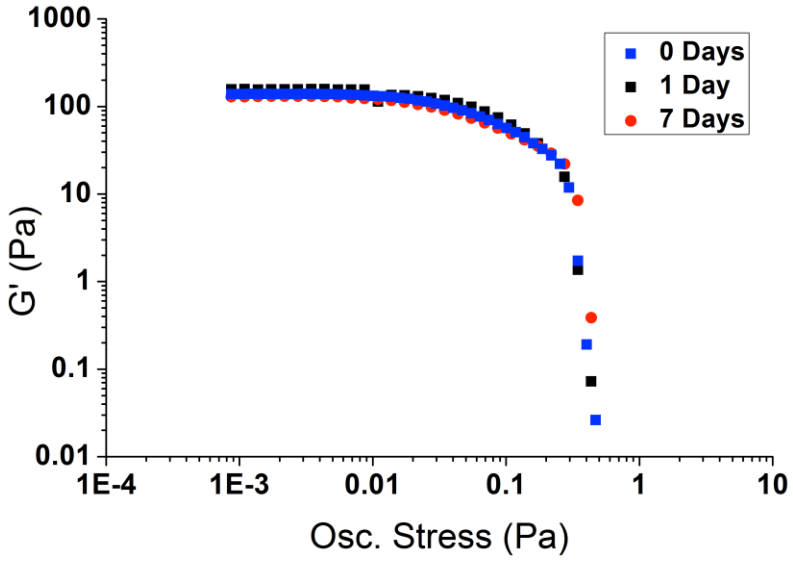

Figure 14-3**:** G’ vs Oscillatory Stress of styrene/water/graphite emulsion systems over time. Even after 7 days, the traces overlap, indicating a stable emulsion.

14.5 Styrene/Graphene Nanocomposites

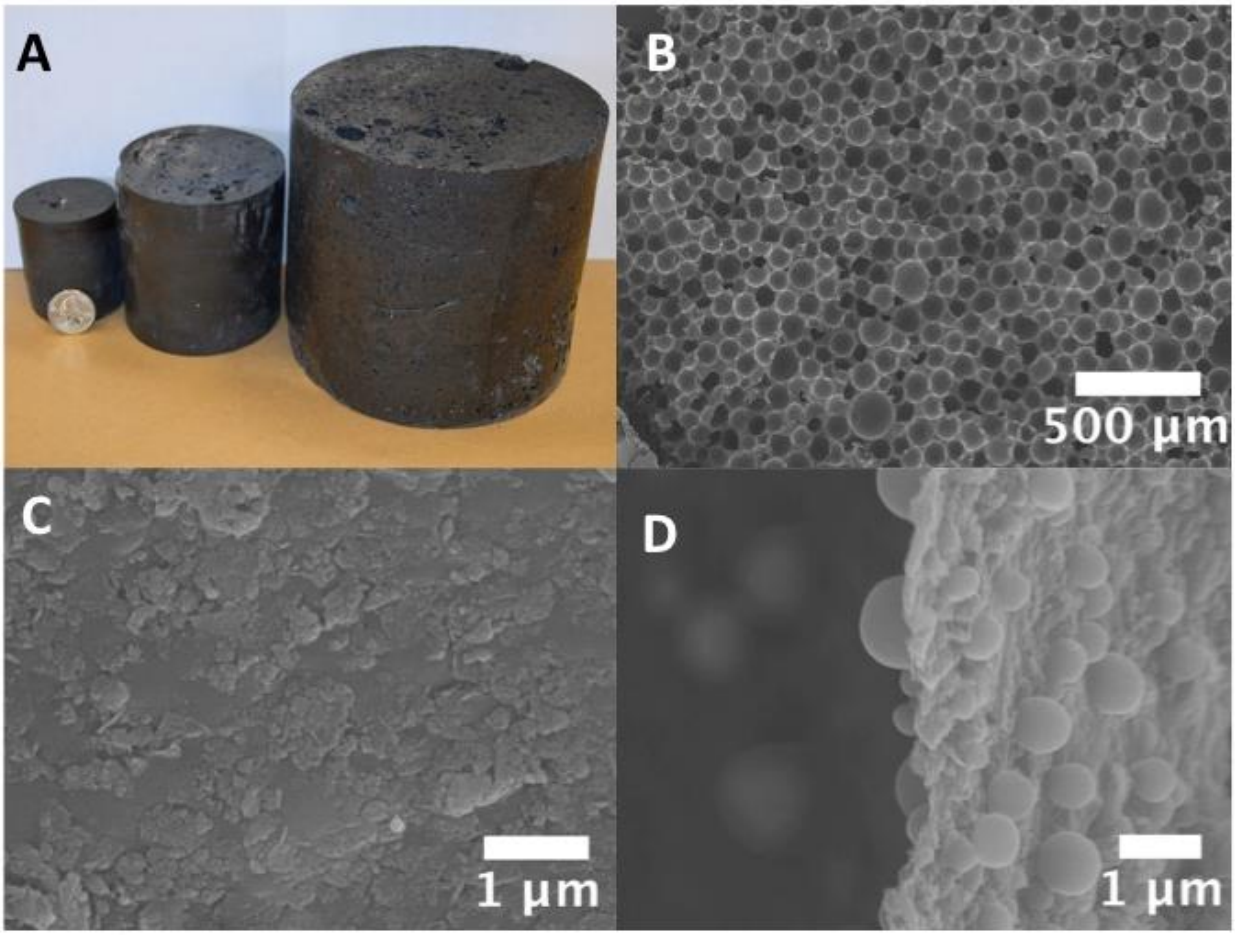

Figure 14-4: Composite Foam Morphology. (**A)** Graphene composite foams of various sizes with a US quarter for scale. (**B)** Scanning electron micrograph of a cross-section of the composite after polymerization made from an emulsion with a 50:34:0.44 mass ratio of water/styrene/graphite. **(C)** Graphene sheets seen lining the inside of the spherical cavities of the composite foams. **(D)** Micrograph of a cross section of a sphere-sphere contact point. The small spheres seen on both sides of the graphitic skin arise from the very small amount of styrene solubilized in the water phase.

In the case of styrene as the oil phase, gentle heating polymerizes the monomer. After the styrene monomers are polymerized, the graphitic skin covered water droplets are fixed in space, forming a rigid foam. This approach is highly scalable as illustrated in Figure 14-4A showing composites of increasing overall size, all with the same

underlying foam structure. A cross sectional image of a typical graphene foam using a JEOL 6330 field emission scanning electron microscope (FESEM) is shown in Figure 14-4B. The imaged surface is much like that of a golf ball, with concave dimples covering the entire surface. A higher magnification image of the interior of a dimple, shown in Figure 14-4C, clearly shows a layer of graphene sheets lining the interior of the cavities. Figure 14-4D shows where the emulsion droplets make contact, with little or no polymer observed, only a thin layer of overlapping graphene sheets. This structural feature is crucial to the electrical conductivity of the composites as it provides the contact between graphene sheets of different spheres. The spheres observed on the surface of the graphitic skin in Figure 14-4D are the result of a very small amount of dissolved styrene in the water phase that polymerizes and precipitates out. This is verified by the addition of NaCl to the water phase, reducing the solubility of styrene, and resulting in nearly no small polystyrene spheres being observed in the composite (see section 15.1).

14.6 Morphology and Mechanical Strength

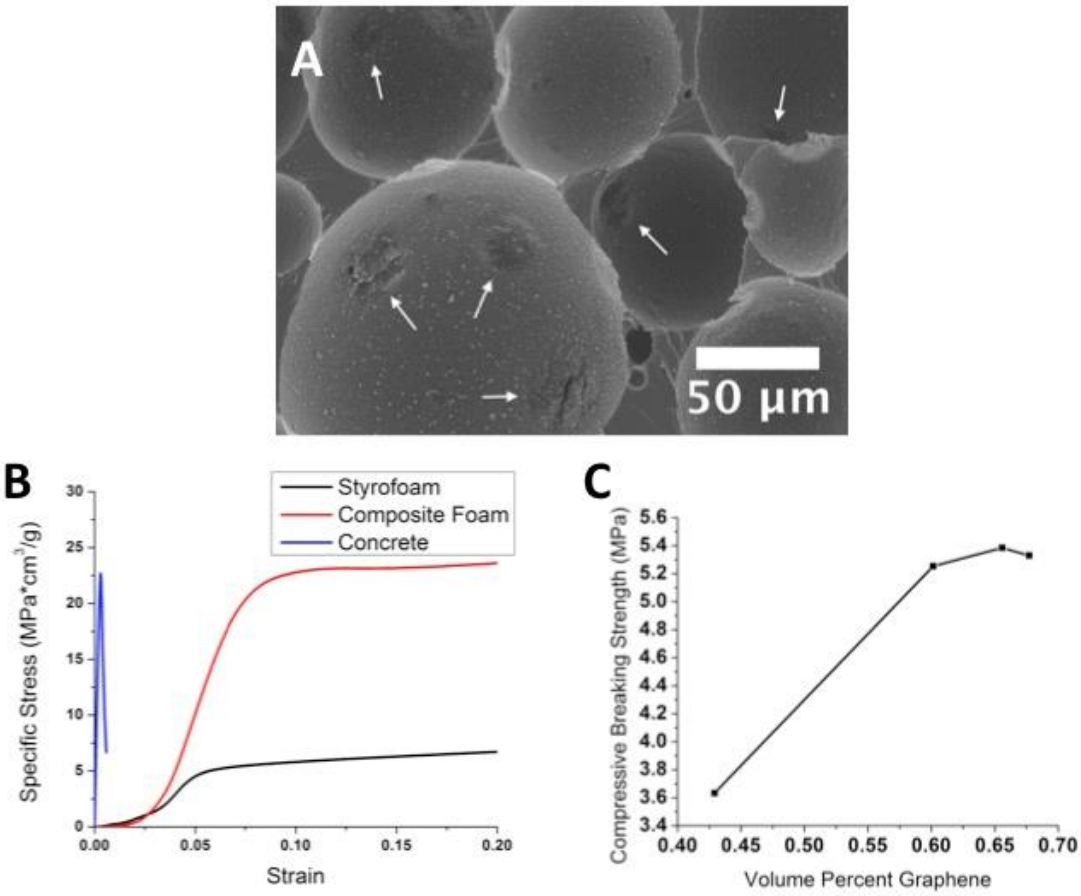

Figure 14-5: Morphology and Compressive Strength. **(A)** Scanning electron micrograph of a composite foam with visible sphere-sphere contact points indicated with arrows. These areas often sag because of the lack of supporting polymer. **(B)** Stress/Strain curves of the composite foam and other industrial materials normalized by material density.[120] **(C)** Compressive strength vs volume percent graphite of the composite samples.

The placement of these thin contact regions can be seen in Figure 14-5A. In some instances a tear can be observed in the graphitic skin, providing a pathway for water removal. If gentle heat is applied, these regions provide ample space for water to escape. Placing the water wet material in high vacuum, however, causes the water to burst out of the spheres, creating a popcorn-like effect. These openings between

spheres also allow for the infusion of various polymers into a dried foam. Adding a second polymer to the inside surface of the spheres, along with controlling the average size of the spheres, provides a powerful handle for tuning the mechanical and electrical properties of the foams. A comparison of the specific stress of the foams versus those of concrete and Styrofoam may be seen in Figure 14-5B. The foams are seen to have both the specific strength of concrete and the plateauing failure mechanism of Styrofoam. As the graphene content increases, the compressive breaking strength increases until it reaches a local maximum, as seen in Figure 14-5C.

The sphere size is controlled by altering the ratio of styrene to water in the emulsion, as well as by varying the amount of graphite. Table 14-1 shows the progression of sphere sizes from a 4/1 to a 1/1 water/styrene ratio with a constant graphene to total water/styrene ratio (and DVB to styrene ratio). The graphene concentration dependence of sphere size is shown in section 15.2. The relative amount of each solvent in the initial mixture also determines the volume fraction of the emulsion phase in the total mixture. For a 7/3 water/styrene ratio, the final volume of the sample is composed almost entirely of the emulsion. If the volume fraction of the water is less than 7/3, the system has an excess styrene phase and spheres become smaller. When the volume fraction of water is raised above 3/1, the emulsion loses its stability and the graphene spheres coalesce, leaving an excess of water and a larger average sphere size. At a 9/1 ratio and above, the emulsion structure is lost. The relationship between solvent volume ratio and emulsion volume fraction is plotted in section 15.3.

The sphere size in the foams strongly influences both compression strength and electrical conductivity, with foams composed of spheres smaller than ~160 μm diameter

having a higher compressive strength than foams with larger spheres. At diameters greater than ~190 µm, the emulsions begin to coalesce and the volume fraction of the emulsion in the mixtures becomes smaller. At a 4/1 ratio, the regular foam structure is nearly gone and an average sphere size cannot be determined. Even though the composite contains a large fraction of graphite, the collapse of the regular sphere structure results in a weak material. Our material compares favorably to commercial materials formed by dispersing graphite flakes in foamed polystyrene, and have compressive resistances on the order of 0.173 MPa at 10% yield.[121]

Table 14-1: Water/Styrene Ratio Study

Ratio Water/Styrene (volume)	Ratio Water/ Graphite (mass)	Observed Sphere Diameter (µm)	Density (g/cm^3)	Compressive Strength (MPa)	Conductivity (S/m)	Loading Percent (by TGA)
1/1	114	90	0.26	5.33	0.043	5.73
3/2	136	130	0.27	5.25	0.051	4.90
7/3	159	160	0.30	5.38	0.054	4.81
3/1	170	190	0.22	3.63	0.070	4.29
4/1	182	x	0.15	1.07	0.148	8.76

14.7 Electrical Conductivity

Unlike the mechanical strength, the electrical conductivity is observed to depend on the overall level of graphene loading rather than on the spherical structure of the foam. This results in larger sphere foams showing increased conductivity as the

emulsion phase gets smaller while the amount of graphene stays constant. The densely packed sphere structure of the graphene foam composite allows for electrical conductivity at low graphene loadings, although increased graphite loading levels in non-optimal systems can also lead to highly conductive material.

Increasing the conductivity and mechanical properties of the foams is also achieved by the addition of a second polymer to the interior of a previously dried foam. The passageways for the removal of water provide an opportunity to infuse a second polymer into the system. Submerging a composite sample in a polymer solution and placing the system under gentle vacuum, the solution replaces the air in the foam. Subsequent removal of the solvent leaves behind the dissolved polymer from the solution. Infusing the graphene composite foam with an aqueous suspension of poly(3,4-ethylenedioxythiophene):poly(styrene sulfonate) (PEDOT:PSS), followed by evaporation of the water, leaves a layer of PEDOT:PSS lining the interior surfaces of the foam. After the water evaporates, the PEDOT:PSS left behind is “draped” over the PS beads and graphene sheets as shown in Figure 14-6. A dramatic increase in conductivity and compressive strength is observed, with conductivities improved by up to two orders of magnitude, from 0.07 S/m to 7 S/m for a 3/1 initial water volume fraction sample. Compressive strengths are also improved by as much as 20%.

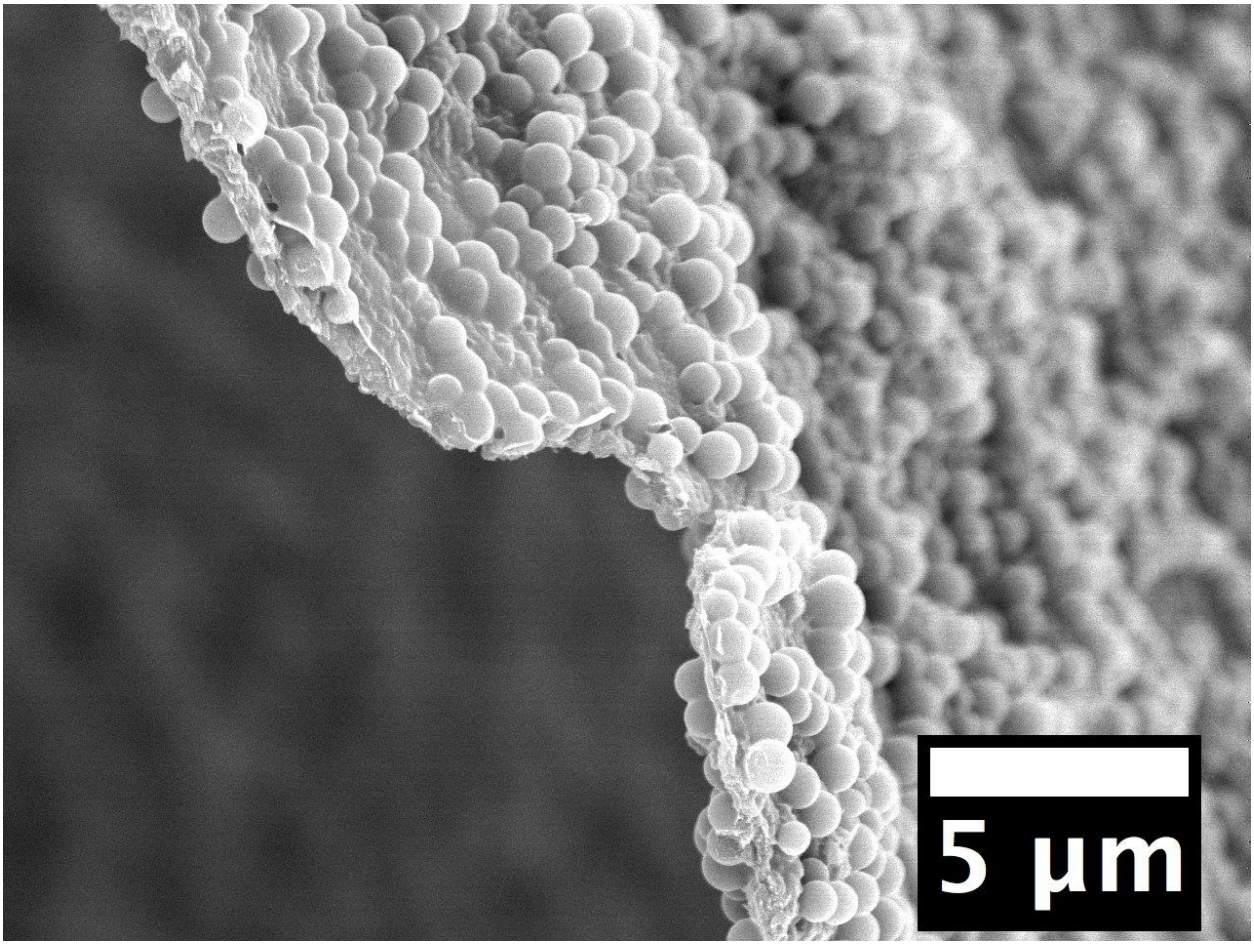

Figure 14-6**:** Film of PEDOT:PSS Draped over graphene layer.

Although the graphene foam composite described uses water with styrene as the oil phase, many other monomers have been used. These include isoprene, butyl acrylate, divinylbenzene, and butyl methacrylate. Flexible foam composites are observed with polyisoprene and ultra low densities are realized with butyl acrylate.

14.8 Conclusion

We have demonstrated the ability of graphene to serve as a two-dimensional surfactant for the stabilization of water-in-oil emulsions and have used this ability to form low density, conductive, high compressive strength graphene/graphite polymer

composites. A conductive network with low graphite loading is formed by the contact between thin graphitic skins surrounding the droplets of the closely packed dispersed phase. Computational results indicate an interface trapping mechanism operates to form the emulsions that serve as the composite template. Additionally, we demonstrated that the electrical conductivity and strength of the composite foams may be increased dramatically through control of the emulsion droplet size and the infusion of additional polymers such as PEDOT. The foams are inexpensive and their formation is environmentally friendly with no volatile organic solvents, oxidations, reductions, high temperatures, or large input of energy required.

Limitations on the choice of monomer comes from the requirement that graphene stabilize the oil/water interface.[87] The oil phase must have a surface energy less than the surface energy of graphene and be nearly insoluble in the water phase. As graphene has a surface energy of 54.8 mN/m,[57,58] and water has a surface energy of 72.9 mN/m, the surface energy of the oil phase must be below 54.8 mN/m. The low surface energy of styrene and most other monomers easily fit this criterion, making the described approach both robust and diverse. Applications such as strong and lightweight building materials, ultra capacitor electrodes, conductive catalyst supports, and filtration are expected to be enabled by these materials and are currently being investigated.

Chapter 15: Supplementary Information

15.1 Salt Studies

It was found that adding salt to the water used in composite preparation removes the small polystyrene spheres found in the hollow cavities after the reaction. This is due to the salt lowering the solubility of styrene monomer in the water prior to polymerization. The experimental procedure for sample preparation was simply modified by using 1M NaCl solution in place of the pure water. Salt crystals were left behind when the water dried, but these were removed by rinsing the sample with water prior to imaging. A FESEM micrograph of an edge of the sample without styrene spheres may be seen below in Figure 15-1:

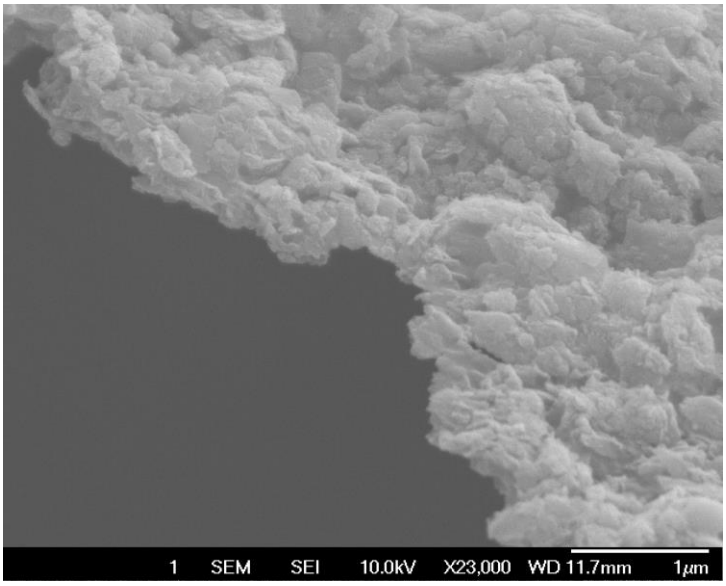

Figure 15-1**:** FESEM micrograph of salt trial**.**

15.2 Graphene Concentration Studies

Samples were prepared with various initial graphite concentrations to test the effect of graphite concentration on the system. Three concentrations were studied: the original concentration, one quarter of the original, and one eighth of the original. The FESEM micrographs of the quarter and eighth concentrations may be seen below. Note the larger sphere sizes as the concentration of graphite is decreased.

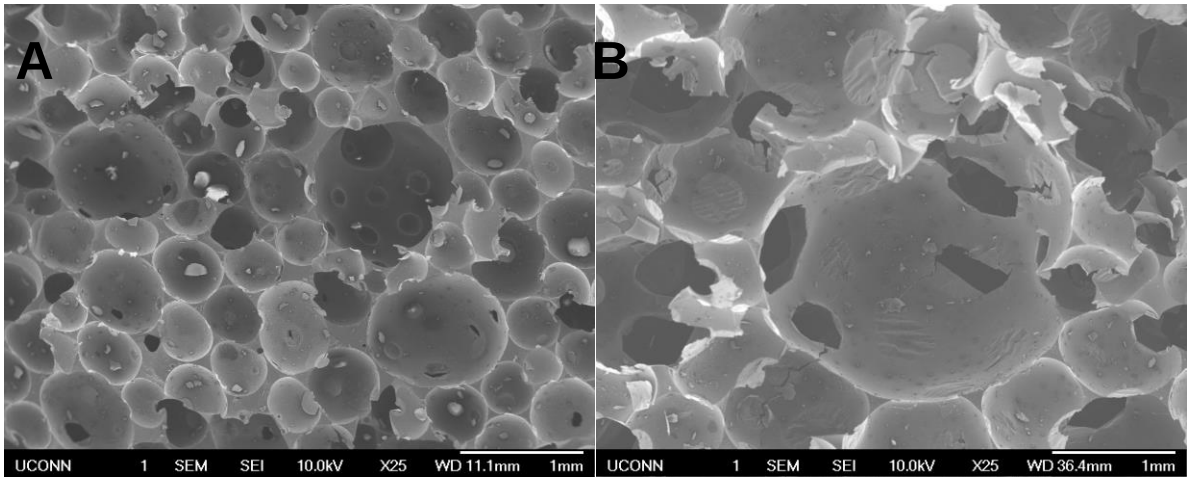

Figure 15-2: FESEM micrographs of lower concentration samples. (A) Sample with one quarter the initial amount of graphite. (B) Sample with one eighth the initial amount of graphite

15.3 Initial Solvent Volume vs Final Phase Volume

The effects of changing the initial volumes/ratios of the solvents were analyzed by making samples with initial volume ratios of 9/1 to 2/3 water/styrene. Additional styrene was added in the place of divinylbenzene. The samples were prepared exactly as described in section 13.1, except without AIBN so they would not polymerize. The samples were also allowed to sit for 1 hour to let the spheres settle. The results are plotted below:

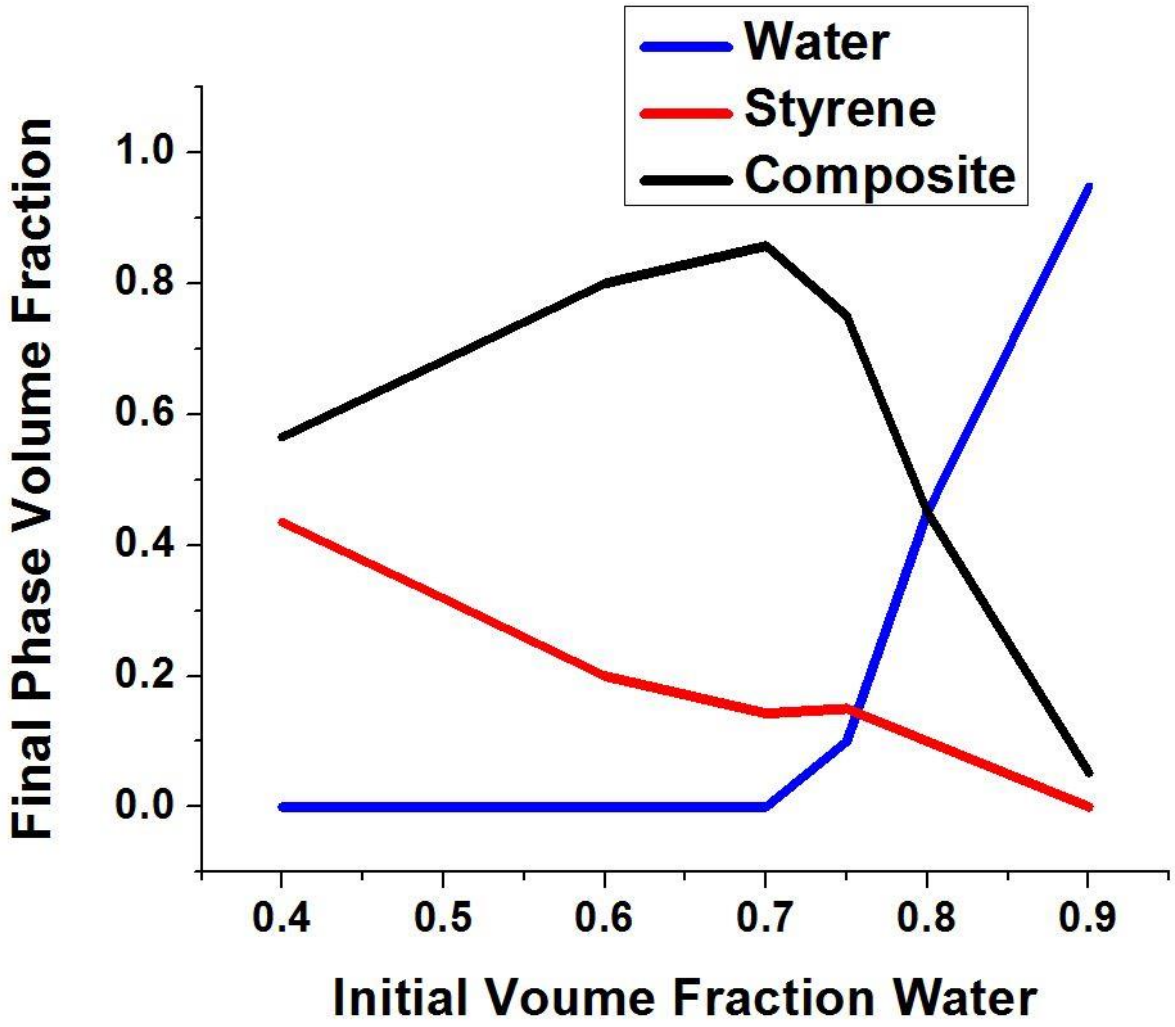

Figure 15-3: Final phase volume fraction as a function of the initial volume fraction of water in the system. The fraction of emulsion in the system goes up until it reaches the stable 7/3 ratio. After that, we start to see minor coalescence at 3/1 and major coalescence at 4/1. By 9/1, there is little, if any, emulsion.

Chapter 16: Alteration of Interstitial Polymer

16.1 Introduction

Up to this point in my dissertation, all of the composites have been templated by graphene-stabilized water and pure monomer (styrene and divinylbenzene) emulsions. This yields composites where the interstitial spaces between the graphene spheres are filled with polymer (crosslinked polystyrene). By replacing the pure monomer oil phase to one comprised of monomer and an inert oil (heptane), we theorized that the resulting foam would have voids left behind where the inert oil had been during the polymerization process. This would result in one of two different morphologies: 1) the interstitial space would be filled with a sponge-like polymer with holes where the heptane was during polymerization, or 2) the polymer would form a wall surrounding the graphene spheres with a thickness determined by the amount of heptane added to the system. The sponge-like morphology actually has been seen before, when we used what we suspect was partially polymerized butyl acrylate as the oil phase (an old bottle). This may be seen in Figure 16-1.

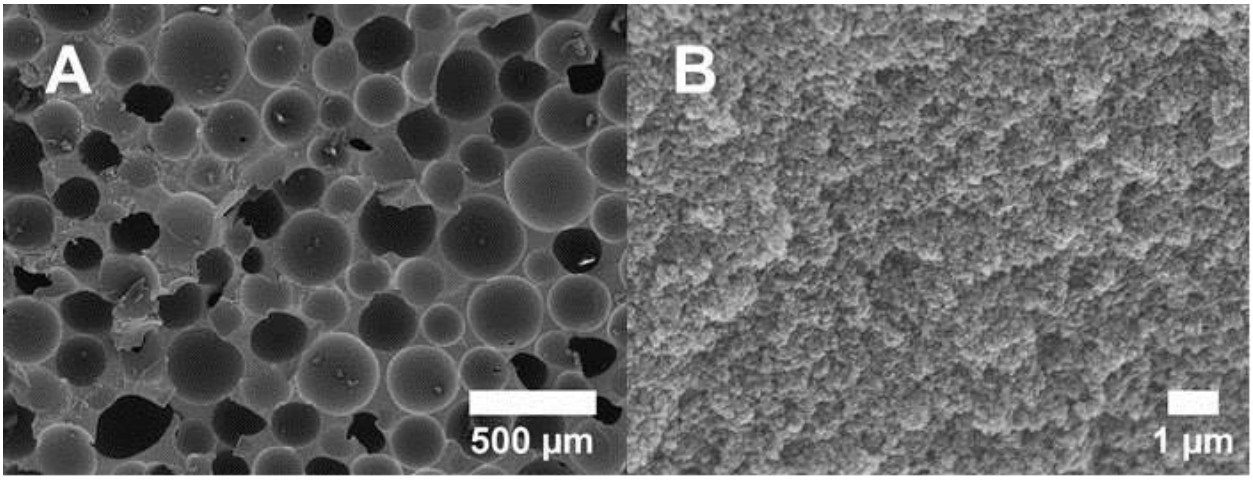

Figure 16-1: Scanning electron microscope images of composite made using partially polymerized monomer as the oil phase. (A) General structure of the foam. It is comparable to other composites made using the same technique. (B) Interstitial spacing filled with sponge-like polymer.

With either morphology, there would be a dramatic increase in surface area and void volume. This is very important for certain applications. In filtration, the increased empty space would allow higher flows. The higher surface area could also be beneficial to energy storage applications.

16.2 Experimental Methods

16.2.1 Preparation of Low Density / High Surface Area Composite Foam

A flask was charged with 629 mg of graphite (Asbury Carbons Grade Nano 24), along with 100 mL water (Deionized), 100 mL styrene (Acros Organics, 99.5%), 23 mL divinylbenzene (Aldrich, 80%), 300 mg of azobisisobutyronitrile (AIBN) (Aldrich, 98%), and a stir bar. The system was then mixed on a stir plate for 1 minute. The stir bar was removed, and the system was emulsified using a Silverson L5M-A for 1 minute. The newly formed emulsion was placed into a 250 mL jar and sealed. The jar was then placed in an oven (Thermo Electron Corporation, Model 6500) at ~70 °C for 24 hours.

After the reaction was complete, the composite samples were removed from the jars and heated at ~80 °C for ~2 days to remove all water.

The above procedure was used to make a 100/0 styrene/heptane (S/H) and 50/50 water/oil (W/O) composite. The procedure was altered to make composite materials in a matrix, where both the styrene/heptane and oil/water ratios were changed. 100/0, 90/10, 80/20, 70/30, 60/40, 50/50, 40/60, 30/70, 20/80, and 10/90 S/H sets varying the W/O ratio to 70/30, 60/40, and 50/50 were made. It must also be noted that the water to initial graphite ratio was kept constant. This was unlike in the initial study in section 13.1, where the graphite to oil + water ratio was kept constant.

16.2.2 Characterization

16.2.2.1 Electron Microscopy

Samples were first prepared as in section 16.2.1. To prepare composite samples for the electron microscope, they were first cut with a razor blade. The slices were then mounted on aluminum stubs using carbon tape and carbon glue, and coated with Au/Pd in a sputter coater (Polaron Unit E5100). The samples were characterized with a Teneo low vacuum field emission scanning electron microscope with a 10 kV accelerating voltage.

16.2.2.2 Electrical Measurements

Samples were first prepared as described in section 16.2.1. To prepare the samples for electrical conductivity testing, they were first cut into rectangular prisms on the scale of a few centimeters in length. These were cut from the bottom of the cylindrical sample, as this area was seen to have the highest conductivity. The ends

were then covered with silver paint (Ted Pella) and allowed to dry. Copper tape (Ted Pella) was then attached to the silver contacts and the resistance was measured using a Keithly Model 2420 SourceMeter.

16.2.2.3 Mechanical Measurements

Samples were first prepared as described in section 16.2.1. To prepare the samples for testing, they were first cut into cylinders around 5 centimeters in diameter (the diameter of the glass jars they are prepared in) and a few centimeters in height. These were cut from the top of the cylindrical sample, as this area was seen to have the highest compressive breaking strength. They were then tested using an Instron Model 5869 in compression mode.

16.3 Results and Discussion

In previous studies, the initial graphite to total water and oil ratio was held constant. This led to the average sphere size in the composites changing as the graphene to water ratio changed through the studies. Here, we kept the graphene to water ratio constant in order to test our previous theoretical work which states the sphere size is determined in part by that ratio. The results of our testing may be seen in Figure 16-2.

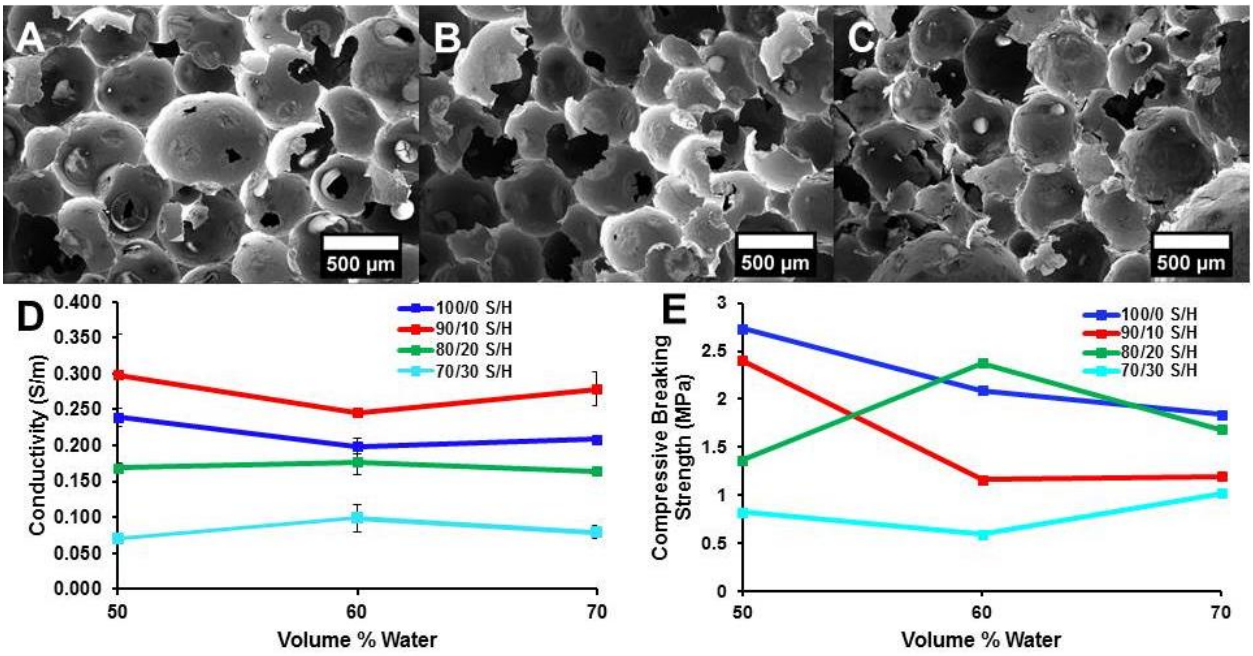

Figure 16-2: Scanning Electron Micrographs of 100/0 S/H 50/50 W/O (A), 100/0 S/H 60/40 W/O (B), and 100/0 S/H 70/30 W/O (C). Conductivity (D) and compressive breaking strength (E) of composite materials with varied S/H and W/O ratios.

The micrographs show that the average sphere size does not change as the W/O ratio is varied while the graphene to water ratio is held constant. In practice, this leads to more emulsion phase, and therefore more final composite, in the 70/30 W/O ratio samples. Furthermore, both the conductivity and compressive breaking strength data points to samples being nearly identical in the same S/H sets since the graphene to water ratio is held constant. Because of this, to simplify the data from this point forward, only samples made using the 50/50 W/O ratio will be presented.

As the amount of styrene in the oil phase is reduced and replaced with heptane, a morphology change is seen, especially in the spaces between the spheres. Scanning electron micrographs of the interstitial spacing may be seen in Figure 16-3.

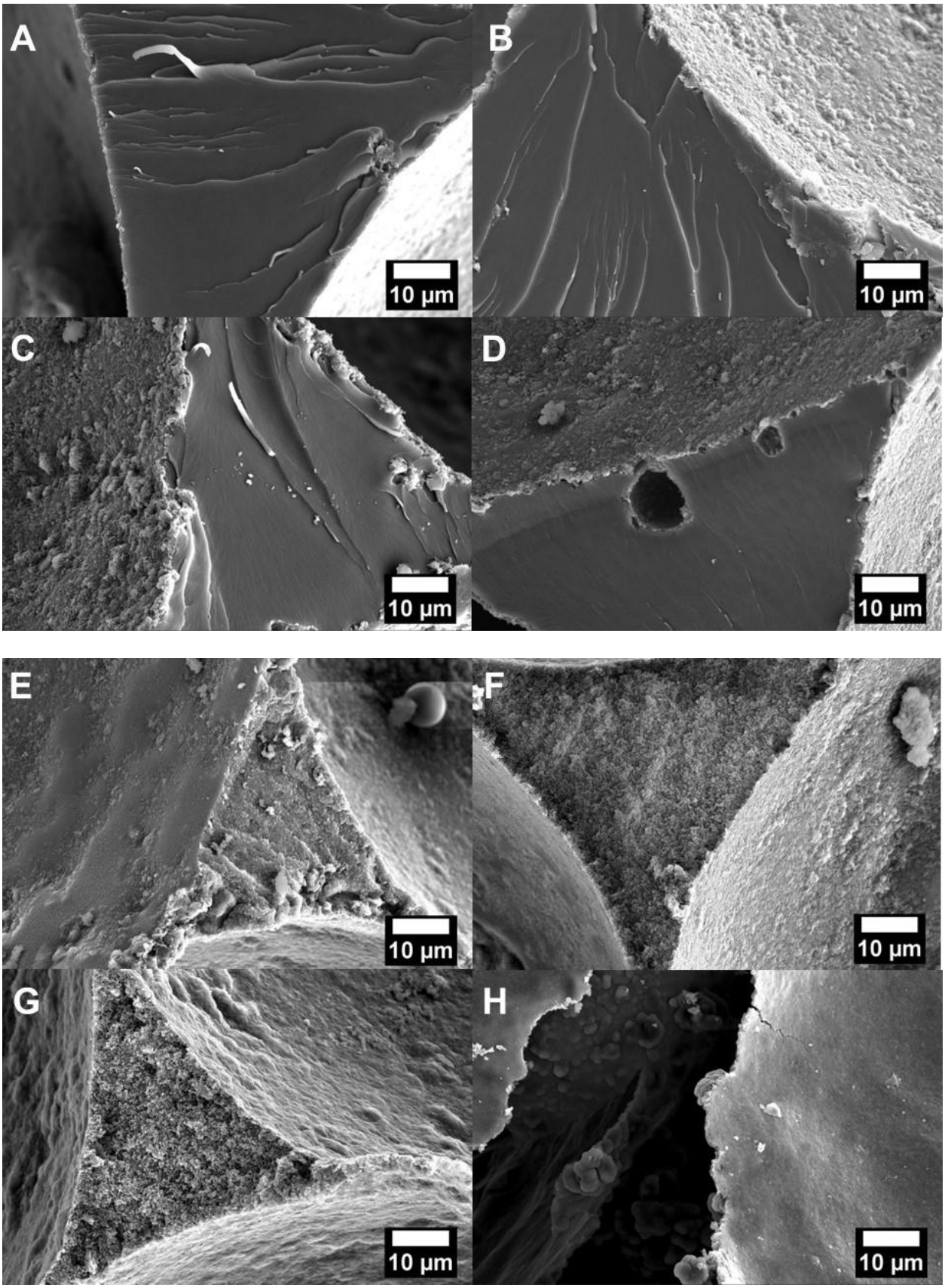
A
10 µm
B
10 µm
C
10 µm
D
10 µm
E
10 µm
F
10 µm
G
10 µm
H
10 µm

Figure 16-3: Sanning electron micrographs of the interstitial spacing of (A) 100/0, (B) 90/10, (C) 80/20, (D) 70/30, (E) 60/40, (F) 50/50, (G) 40/60,and (H) 30/70 S/H samples.

As can be seen in the figure above, as the amount of styrene is reduced, the polymer in the interstitial spacing begins to form a textured surface. Upon closer inspection, the textured surface in between the spheres is seen to actually be voids developing as the styrene amount is lowered (Figure 16-4).

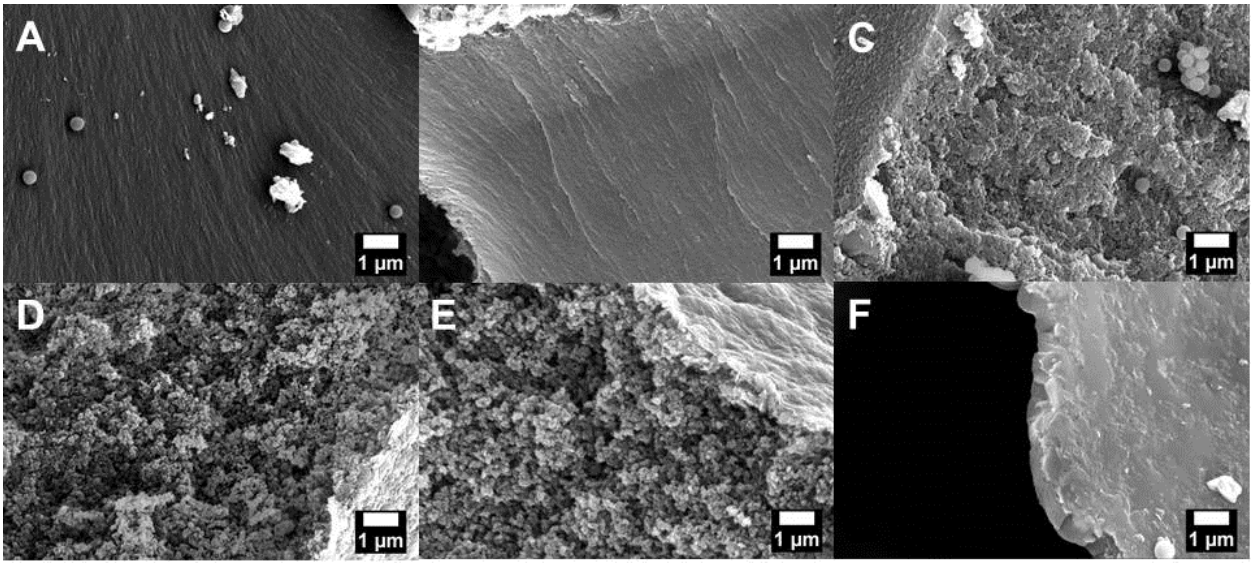

Figure 16-4: Sanning electron micrographs of the interstitial spacing of (A) 80/20, (B) 70/30, (C) 60/40, (D) 50/50, (E) 40/60,and (F) 30/70 S/H samples.

These voids are indicative of the sponge-like morphology mentioned earlier. At the 30/70 S/H ratio, however, the interstitial polymer network suddenly seems to be unstable. Note that the composite is still formed, so the emulsion network is still stable. At this point, the interstitial polymer takes on the shell morphology, where it covers the outside of the graphene sheets. Polymer “globs” are seen to cover the outer surface of the spheres in Figure 16-5.

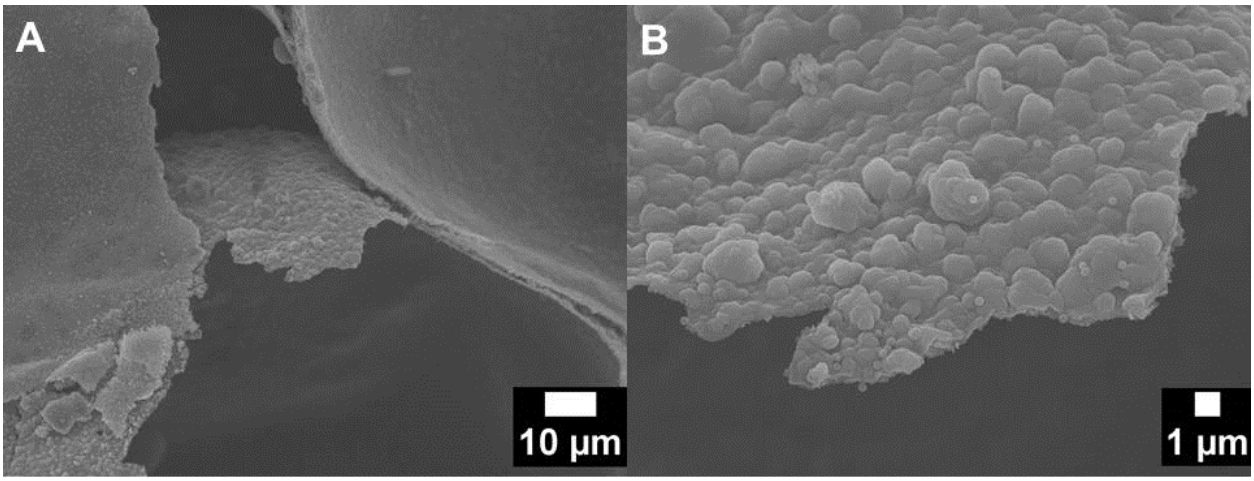

Figure 16-5: Scanning electron micrographs of a 30/70 S/H 50/50 W/O composite material. (A) The interstitial space between the spheres, with the outer shell of a sphere visible in the middle. (B) Close-up of the polymer-"glob" coated shell of a sphere.

A mechanism where the polymer coating the graphene shells comes from precipitating polymer would not seem to lead to a stable emulsion. A more likely mechanism would incorporate something seen in graphene oxide (GO) styrene/water emulsion systems:[107] styrene oligomers adsorbing to the surface of graphene due to π–π interactions. Once adsorbed, the oligomers would continue polymerization from the surface of the graphene sheets. Evidence of this has actually been seen before in our original composite samples. This may be seen in Figure 16-6.

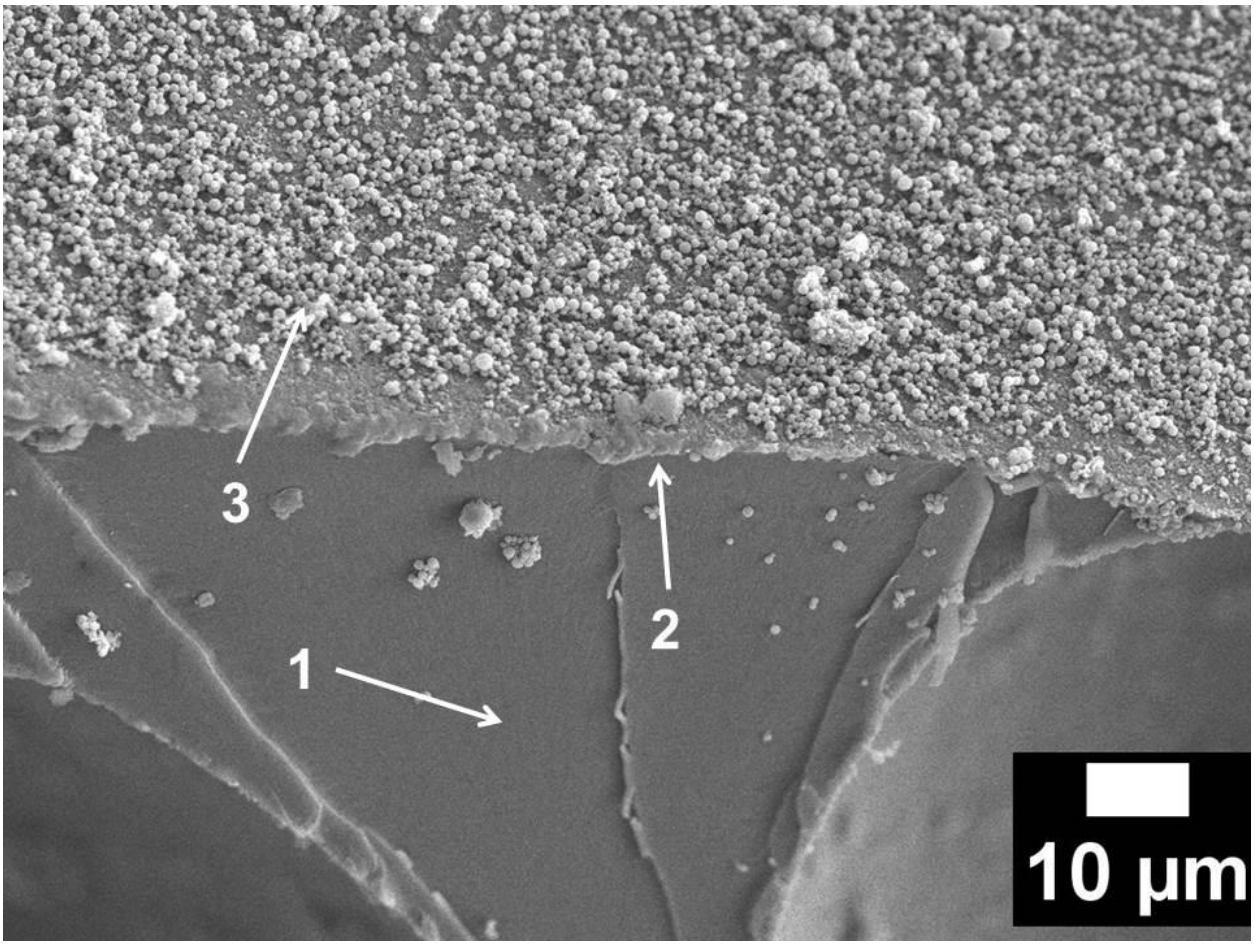

Figure 16-6: Scanning electron micrograph of interstitial polymer and inside of graphene composite sphere. (1) Bulk interstitial polymer. (2) Polymer grown from graphene sheet. (3) Precipitated polymer.

We believe that there are actually three different types of polystyrene in this image. The first is the main part of the interstitial polymer. This is the darker-colored, smooth part of the image above (Figure 16-6-1). Next, there is the polymer that appears right under the graphene sheets, and forms a lip over the bulk interstitial polymer (Figure 16-6-2). Lastly, there are the white-colored polystyrene beads that form when the styrene monomer dissolved in the water layer polymerizes and precipitates out of solution (Figure 16-6-3).

The compressive strength of several of the different S/H composites (all at 50/50 W/O) were also tested. The results may be seen in Figure 16-7.

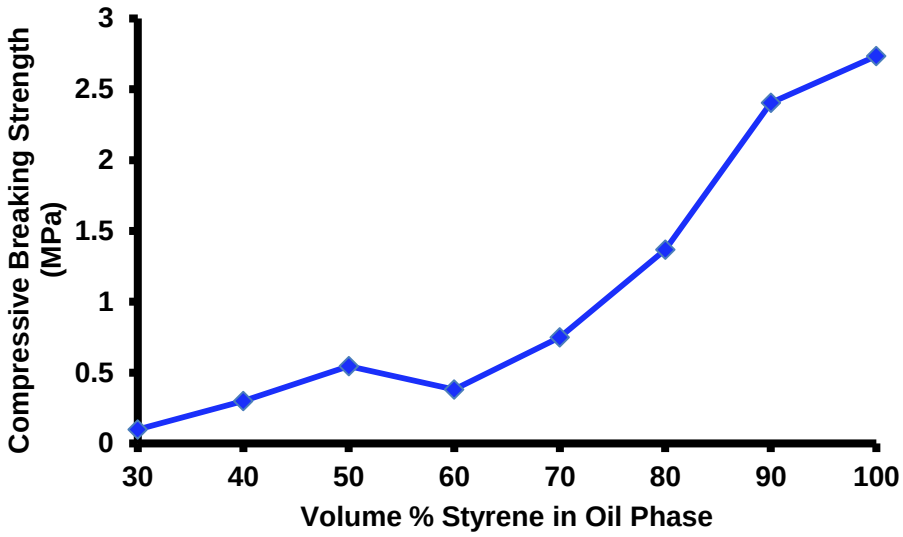

Figure 16-7: Compressive breaking strength as a function of the volume % of styrene in the oil phase.

As expected, the compressive breaking strength decreases with the decreasing amount of styrene in the oil phase.

The conductivity of the foams was also tested. In Figure 16-8, the conductivity and density of the foams is seen to decrease as the amount of styrene in the system decreases.

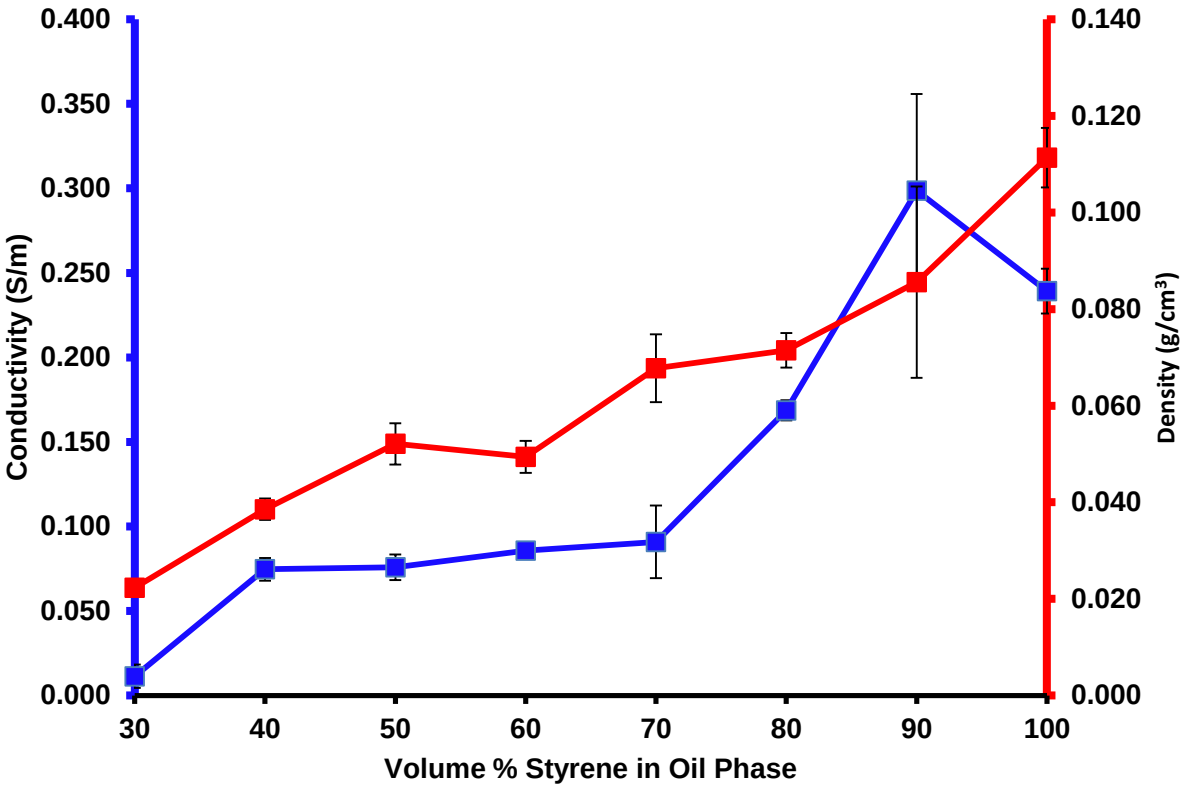

Figure 16-8: Conductivity and Density as a function of the volume % of styrene in the oil phase.

The lowering of the density of the foams with decreasing styrene in the oil phase was expected, as the space usually filled with polystyrene in the final foam was filled with voids where the heptane was. The conductivity, however, is a more curious matter. Initially, our expectation was that as the amount of styrene in the system was lowered, the conductivity would increase because there would be less polymer that could get in between the sheets. This did not prove to be the case. Somewhat subtly seen in the SEM images is that as the amount of styrene in the oil phase decreases, the amount of graphene sheets visible on the inner surface of the spheres decreases as well. Instead, a smooth polymer layer is seen to develop. We believe the answer lies in the potential of mean force diagrams of graphene in both the styrene/water and heptane/water

systems. In the styrene/water system, the graphene sheet is at the lowest energy around 2 angstroms from the interface. In the heptane/water system, the sheet is at lowest energy around 4 angstroms from the interface (Figure 16-9). This suggests that as the amount of heptane in the oil phase is increased, the sheet migrates further from the water/oil interface, and ultimately results in the sheets being encapsulated by polymer instead of exposed at the surface. This leads to more polymer between the sheets, and greater resistance.

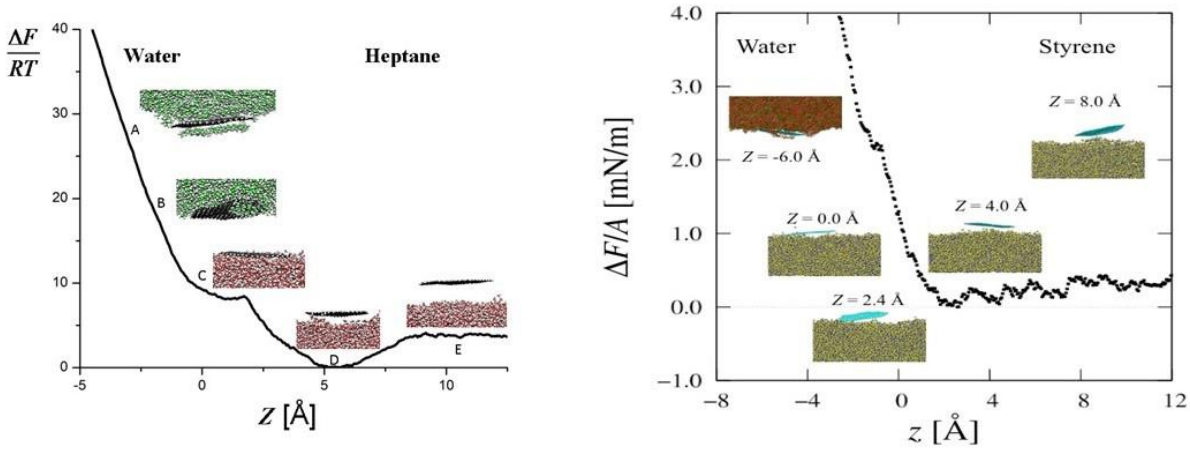

Figure 16-9: Potential of Mean Force Plots for (left) a heptane and water systems and (right) a styrene and water system.

16.4 Conclusion

Replacing the pure styrene oil phase with a mixture of styrene and heptane has resulted in low-density, high surface area composite foams. The density, strength, and conductivity are all tunable through alteration of the styrene/heptane ratios, and densities an order of magnitude lower than those previously recorded have been

achieved. Possible applications of these foams include low density sensors, as well as high-flow filters.

Part IV: Pristine Graphene / Poly(butyl acrylate) Foams Templated by Graphene Sheet Stabilized Emulsions

Chapter 17: Introduction

The creation of a bicontinuous arrangement of exfoliated few layer graphene (FLG) sheets by the thermodynamically driven self-assembly of pristine graphite provides a unique scaffold for templated polymerization. Rather than attempting to modify the hydrophobic graphite with oxidation or added surfactants, we rely on the insolubility to form an ordered scaffold that templates the polymerization of elastomeric polymer to create a bicontinuous nanocomposite with an open network of FLG lined spheres. The resulting elastomer displays electrical resistivity that is sensitive to deformation and has absorption properties that are selective for certain solvents. These properties are enabled by an interfacial trapping mechanism that utilizes pristine graphene as a surfactant and avoids the use of difficult to remove solvents,[102] extended sonication times,[103] and harsh chemical reduction treatments[100,101]

Even though the electrical and mechanical properties[1–3,15,90,91,93,122,123] of pristine graphene are superior compared to graphene oxide (GO) and reduced graphene oxide (rGO), GO and rGO are commonly used instead of graphite to impart conductivity and increase strength in polymeric composite materials.[92,104,110,124–126] Although GO and rGO have degraded properties when compared to pristine graphene, due to the disruption of the delocalized pi electron network,[35,36,94,95,97] graphene's lack of solubility in virtually all solvents hinders the application of pristine graphene in traditional nanofiller incorporation techniques. Here, we take advantage of graphene/graphite's insolubility and use it as the surfactant,[87,127,128] where it exfoliates, lowers the interfacial energy of the oil/water interface, and templates the creation of poly(butyl acrylate) graphene composite foams.

As the FLG sheets are found solely at the interface during polymerization, in the final graphene composite material they cover the surface of the empty (formerly water filled) spherical cavities. This highly ordered FLG network is conductive, and therefore could lead to potential applications in electrochemical sensing, catalyst support, and capacitive deionization. At the areas where the spheres touch, little to no polymer is found, only graphene sheets. These areas tend to be weaker than the rest of the walls, and often break to form holes that connect the spaces inside the spheres. These pathways enable oils to be absorbed readily into the system. Furthermore, the specific arrangement of the sheets, along with some kind of shape change (from swelling, physical deformation, etc.) leads to an electrical response. This opens up a wide variety of new potential applications, from chemical sensing to pressure sensing.

Chapter 18: Experimental Methods

18.1 Preparation of Typical Composite Sample

A 250 mL Erlenmeyer flask was charged with 0.88 g graphite (Asbury Carbons, grade Nano 24), 120 mL DI water, 80 mL butyl acrylate (Acros Organics, 99%), 500 uL divinylbenzene (Sigma Aldrich, 80%), 0.24 g 2,2'-azobis(2-methylpropionitrile) (Sigma Aldrich, 98%), and a stir bar. The contents were then mixed for about 1 min on a stir plate. The stir bar was then removed, and the contents were mixed at ~10,000 rpm for 1 min using a Silverson L5M-A high shear blender with a ¾" tubular blending head with the square hole, high shear screen. After mixing, the contents were poured gently into a 240 mL glass jar. The jar was then sealed and placed into a convection oven (Blue M, Stabil-Therm) at 65°C for 24 hr to react. The jar was then broken to remove the composite sample, which was then placed in the same oven for several days (~3) until dry.

18.2 Characterization

18.2.1 Electron Microscopy

Samples were first prepared as in section 18.1. To prepare composite samples for the electron microscope, they were first cut with a razor blade. The slices were then mounted on aluminum stubs and coated with Au/Pd in a sputter coater (Polaron Unit E5100). The samples were characterized with a JEOL 6330 field emission scanning electron microscope with a 10 kV accelerating voltage.

18.2.2 Swell Testing with Various Solvents

A typical composite sample was first prepared as in section 18.1, then placed in a liquid nitrogen bath for 3 s to get it to below the glass transition temperature. The sample was removed from the bath and the top and bottom (~0.5 cm each) were immediately cut off and discarded using a band saw. The sample was then submerged again in liquid nitrogen again for 3 s, and cut into 1.5 cm discs immediately after being removed from the bath. It was then submerged in liquid nitrogen for 3 s, and cut into rectangular prisms with the approximate dimensions of 1.5 cm x 1.5 cm x 3 cm immediately after removal from the bath. These samples were then used in the swell testing.

To perform the test, the cut sample was first measured and weighed. 70 mL of the chosen solvent was then poured into a 120 mL jar. The composite sample was then placed into the jar, and left to sit for 15 min. The sample was then removed and measured and weighed again. The solvents used include:

Acetone (Fisher, 99.5%)

Isopropanol (Sigma Aldrich, 99.5%)

n-Heptane (Fisher, 99%)

Dimethyl Sulfoxide (JT Baker, 99.9%)

1,4 Dioxane (Fisher 99%)

Toluene (Sigma Aldrich, 99.5%)

Ethanol (Acros Organics, 99.5%)

Diethyl Ether (Sigma Aldrich, 99%)

Methanol (Sigma Aldrich, 99.8%)

Chloroform (JT Baker, 99.8%)

Tetrahydrofuran (JT Baker, 99.8%)

Styrene (Sigma Aldrich, 99%)

Hexane (Sigma Aldrich, 98.5%)

Butyl Acrylate (Acros Organics, 99%)

Pentane (Alfa Aesar, 98%)

Acrylonitrile (Sigma Aldrich, 99%)

DI Water

18.2.3 Swell Testing with Various Crosslinking Amounts

A 250 mL Erlenmeyer flask was charged with 0.88 g graphite (Asbury Carbons, grade Nano 24), 120 mL DI water, 80 mL butyl acrylate (Acros Organics, 99%), 0.24 g 2,2'-azobis(2-methylpropionitrile) (Sigma Aldrich, 98%), a stir bar, and either 0.201, 0.403, 0.805, 1.61, or 3.22 mL divinylbenzene (Sigma Aldrich, 80%). The contents were then mixed for about 1 min on a stir plate. The stir bar was then removed, and the contents were mixed at ~10,000 rpm for 1 min using a Silverson L5M-A high shear blender with a ¾" tubular blending head with the square hole, high shear screen. After mixing, the contents were poured gently into a 240 mL glass jar. The jar was then sealed and placed into a convection oven (Blue M, Stabil-Therm) at 65 °C for 24 hr to react. The jar was then broken to remove the composite sample, which was then placed in the same oven for several days (~3) until dry.

The dried composite samples were then cut as described in section 18.2.2. Swell testing was also as in section 18.2.2, although it was performed only in acetone.

18.2.4 Swelling and Resistance / Mass Change

A typical sample was first prepared as described in section 18.1. It was then cut into a rectangular prism by first submerging it in liquid nitrogen and then cutting it with a band saw. The final dimensions were ~1.5 cm x 1.5 cm x 3 cm. Two sides of the prism were then painted with colloidal silver paste (Ted Pella, Pelco). The sample was then placed in the oven overnight to cure the paste. After removal from the oven, copper tape (3M, ¼") was placed on top of both of the ends covered with the silver coating. The tape was then painted again with silver paste to ensure it was bound to the composite. The resistance was measured using a Keithley 2420 sourcemeter. The instrument was set to start taking measurements, and then 0.5 mL of acetone (Fisher, 99.5%) was pipetted onto the top of the sample, directly in between the faces covered with silver paste. This was to ensure the sample did not swell at the location of the silver paste. 300,000 data points were taken at a sampling rate of 600 ms/pt and at 0.01 V. The experiment was repeated several times until there was no hysteresis.

After the resistance tests were completed, the sample was placed on an analytical balance (with the silver paste and copper tape). 0.5 mL of acetone was then placed on the sample in the same place as before. The mass data was taken at 5 s, 10 s, 20 s, 30 s, 1 min, 2 min, 3 min, 5 min, 10 min, 20 min, 30 min, 40 min, 50 min, and 60 min.

18.2.5 Repeated Compression Test

A typical composite sample was first prepared as described in section 18.1, submerged in liquid nitrogen for 3 s, then removed and immediately cut using a band saw to remove the top and bottom (~0.5 cm). The flat top and bottom of the sample

were then painted with colloidal silver paste (Ted Pella, Pelco). The sample was then placed in the oven overnight to cure the paste. After removal from the oven, copper tape (3M, ¼") was placed on top of both of the ends covered with the silver coating.

Before the sample was placed into the Instron 1350 for testing, the instrument was prepared by covering the compression plates with paper and tape to prevent electrical conductivity. Once the sample is placed between the plates, it was compressed 100 times to approximately 50% of its original height. The resistance was measured before, during, and after the compression cycles using a Keithley 2420 sourcemeter, taking 100,000 pts 140 ms apart with a voltage sweep from 0.001 V to 0.1 V. This measurement was repeated several times (~3) to remove any hysteresis.

Chapter 19: Results and Discussion

19.1 Foam Morphology

Polymerizing the continuous phase of the FLG stabilized emulsion holds the bicontinuous structure in place. Using a monomer that polymerizes to a flexible polymer allows us to form soft, low density, and electrically conductive materials with very low loadings of graphite. Figure 19-1A illustrates the internal structure of the material. The observed spheres range from roughly 100 to 300 μm depending on the flake size of the graphite and the processing conditions. The surface is much like a golf ball covered with dimples where the water droplets had been. As the FLG serves as a surfactant in the system, the sheets are only found at the monomer/water interface, allowing for percolation at very low loadings. After polymerization and following removal of the water by evaporation, the resulting foam is lightweight (D ~0.10 g/cm^3), flexible, and

electrically conductive. When the emulsion is formed, at the locations where the spheres touch, there is little to no polymer formed. This is also where the electrical percolation pathway continues from sphere to sphere. These areas, seen in Figure 19-1B, tend to be weak and tear, thus creating a pathway of windows for water to escape during the evaporation process.

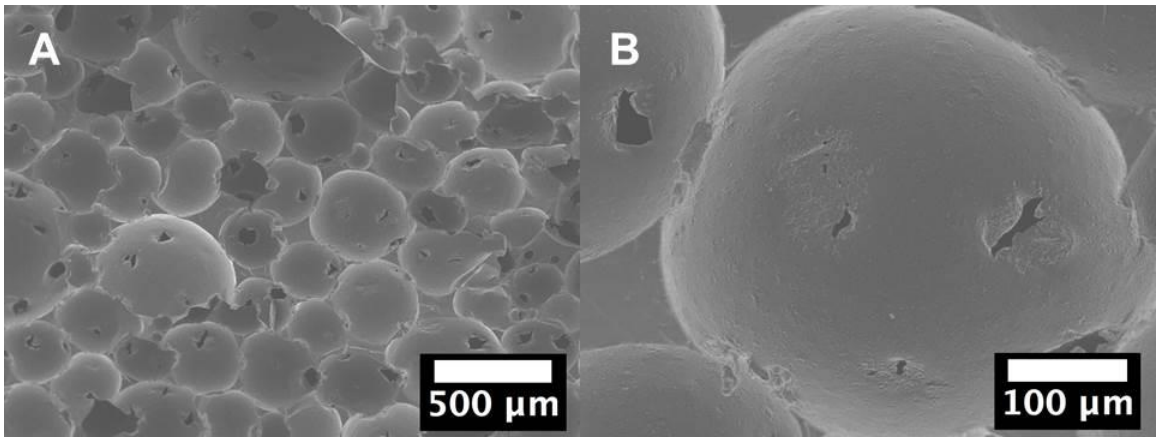

Figure 19-1: SEM image of graphene based foam showing (A) structure composed of packed spheres, (B) openings, or “windows” between spheres that allow for the passage of materials in and out of the foam.

19.2 Oil Absorption

While the openings between the spheres are important for water evaporation, they also allow other liquids to be absorbed. The high surface area, combined with significant capillary action, enables the foam to swell and absorb a wide range of organic solvents. The foam prior to swelling but after removal of the water used in its synthesis, may be seen in Figure 19-2A. Despite the role of water in the formation of the template used to produce the foam, the foam is highly hydrophobic. As seen in Figure 19-2B, pouring water on the foam results in no swelling and the foam remains the same size. The result is much different with organic solvents, however. Adding

tetrahydrofuran (THF) (Figure 19-2C) immediately swells the foam as it absorbs the liquid. Furthermore, as the solvent evaporates out of the composite material, it returns to its original shape (Figure 19-2D).

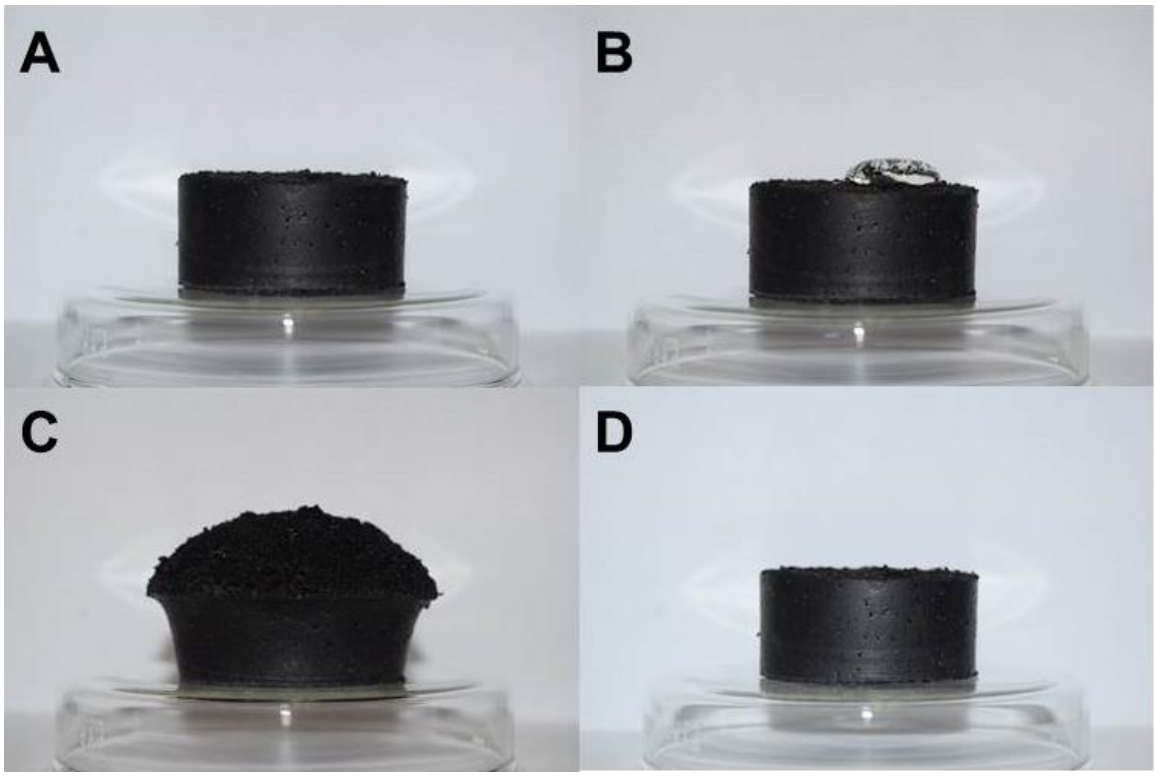

Figure 19-2: Image of graphene based polymerized high internal phase emulsion, (A) before swelling, (B) after addition of water, (C) after addition of THF, (D) after evaporation of the solvent. While water is not absorbed, THF is shown to swell the material. After the evaporation, the material is seen to return to its original size and morphology.

The volume expansion of the material with organic solvents is typically greater than the initial void volume. Due to the high surface area of the foam, the swelling and absorption take place very quickly, normally only a few seconds. All solvents do not swell the material equally, however, and to investigate the factors affecting absorption, swell tests are performed using 17 different solvents, both hydrophilic and hydrophobic. Figure 19-3A shows a histogram of the percent volume expansion for each solvent

tested. The foams clearly favor organic solvents, and solvents with solubility parameters closest to that of poly (butyl acrylate) are found to swell the material to the greatest extent (Figure 19-3B). Although the polymer does not dissolve, and solvent can be squeezed out like a sponge, the favorable interaction of solvent and polymer plays a critical role and leads to the chemically selective uptake of liquids.

This chemical selectivity can be seen when two solvents are mixed. Depending on the miscibility of the solvents, the final results can vary. When a piece of graphene composite is placed in a container that has two immiscible solvents, e.g. heptane and water, the foam absorbs the oil phase exclusively. When placed in a container with two miscible solvents, the foam swells, but to a degree between that of the two solvents if they were by themselves. This may be seen in Figure 19-3C**.** Also seen in Figure 19-3C is the fact that the swelling takes place very quickly, and then is constant over long periods of time, showing great stability.

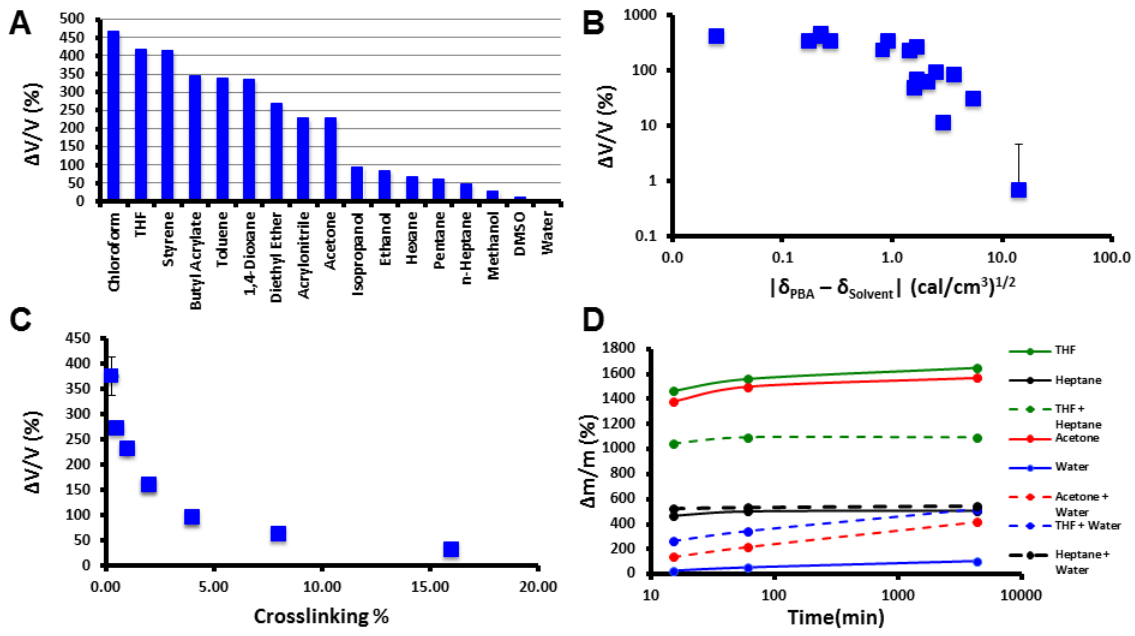

Figure 19-3: (A) Histogram of the percent volume expansion of the foam with different solvents. (B) Plot of volume expansion as a function of the solubility parameter of the

solvent. It is observed that the closer the match between solvent and polymer solubility parameter, the larger the volume expansion. (C) Expansion of the foam in acetone as a function of crosslink density. (D) Change in mass of the foam as a function of time. Also note the effect of mixed solvents.

In addition to the chemical identity of the solvent playing a role, the ability of the material to expand also contributes to the extent of swelling. Increasing the concentration of cross linker in the polymer increases its stiffness, thus hindering swelling. Figure 19-3D illustrates the effect on swelling of increased cross-link density. As would be expected, the stiffer the material, the less solvent it can absorb. The role of the graphene surface in the swelling is more difficult to elucidate. Plotting the swelling of the composite as a function of the difference in solubility parameter between graphene and solvent (see section 20.1 for details) finds no clear correlation. Although the FLG's role in swelling is not clear, it provides the necessary framework for the absorbent material.

19.3 Chemical Sensing

Beyond providing the framework, however, the FLG does play a crucial role in potential applications. As stated previously, the FLG sheets are found solely at the interface between the oil and water in the initial emulsion. After polymerization, they are found only at the surface of the spheres, between the polymer and where the evaporated water once was. Any distortion of the original arrangement of FLG sheets leads to a change in the conducting network, thus leading to a measurable change in electrical resistance. During swelling by solvent absorption, there is an increase in the internal surface area of the material that leads to an observable change in resistance. In Figure

19-4, the effect of the absorption of a small amount of acetone (0.5 mL) is shown. The stretching of the network spreads FLG sheets, increasing the distance electrons must travel and breaking contacts. The resistance thus rises with a nearly instantaneous response rate, although slightly slower than the mass. This is due to oil first going into the cavities in the foam, and then being absorbed into the polymer. As the acetone evaporates, the foam and spheres slowly return to their original shapes. As this occurs, the FLG sheets are brought back into their original alignment; there is a return to the original resistance. There is a slight difference in the speeds at which the resistance and the mass change. This is most likely due to the polymer returning to its original shape before all of the acetone has been evaporated. The complete reversibility demonstrates the robustness of the FLG network.

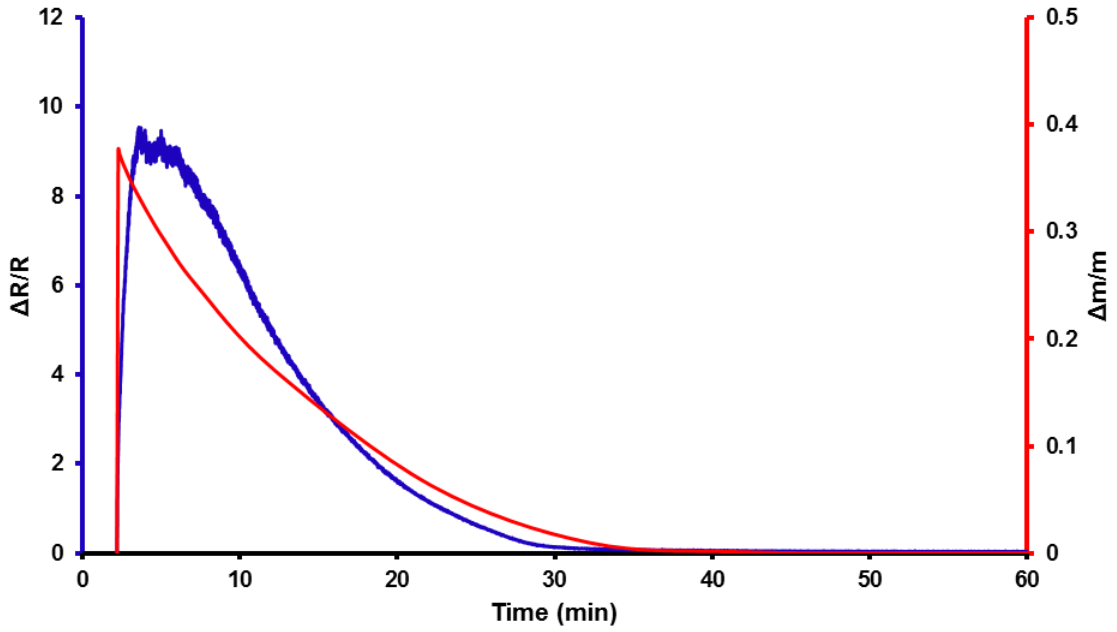

Figure 19-4: Resistance and mass change of the foam as a function of swelling.

19.4 Pressure Sensing

Alternatively, mechanical compression also distorts the spheres and causes a change in electrical resistance. In Figure 19-5A, the foam is compressed to about 50% (after about 1 hour) and held under compression. The resistance is seen to jump to over three times its original value at rest, but then slowly decreases while left under the compression. It must be noted, however, that the resistance never reaches the value of the foam at rest pre-compression. In Figure 19-5B, the foam is released from compression. Interestingly, the foam again sees a spike in resistance upon the release of the compression, and then gradually decreases until it reaches the pre-compression at rest value. As the foam is compressed, the spheres are initially distorted and yield a higher resistance value. The slow lowering of the resistance after the initial spike suggests that the spheres slowly find an equilibrated shape after a certain amount of time. Once the compressive pressure is released, the spherical shapes are again disrupted and we see an increase in resistance. From there, the spheres are able to slowly return to their usual shape, and we see the lowering of the resistance to its original value.

In Figure 19-5C, the resistance of the foam is seen over 100 compression and release cycles (50% compression). No significant degradation is observed. At the end of the cycles, there is a noticeable relaxation time while the resistance returns to its original value. As the spheres relax back to their equilibrium shape, the resistance decreases.

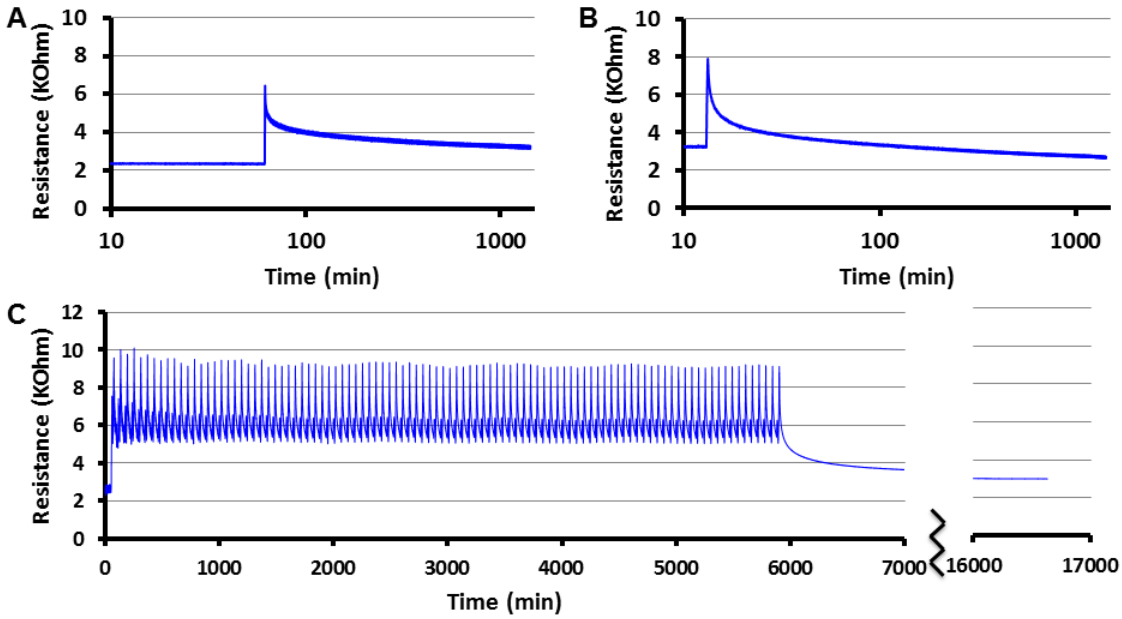

Figure 19-5: Resistance as a function of compression. (A)The foam is compressed and then left under compression. (B) The foam is released from compression. (C) The foam is compressed and allowed to recover numerous times, returning to its original resistance each time.

19.5 Conclusion

By templating poly(butyl acrylate) foams with few layer graphene sheets, we have created a material with its internal surface area covered with an ordered percolating electrical network. The foam not only has applications in oil capture because of its swelling and absorption capabilities, but also electrochemical sensing, catalyst support, pressure sensing, and oil sensing because of the FLG sheet network. Due to their ease of synthesis and use of cost effective reagents, Graphene composites have the potential to be brought to real world use quickly and efficiently.

Chapter 20: Supplementary Information

20.1 Swelling vs Graphene Solubility Parameter

Samples were prepared and tested as in the method described in section 18.2.2. When the swelling is plotted against the absolute value of the difference in solubility parameter of graphene and the solvent, no trend is observed.

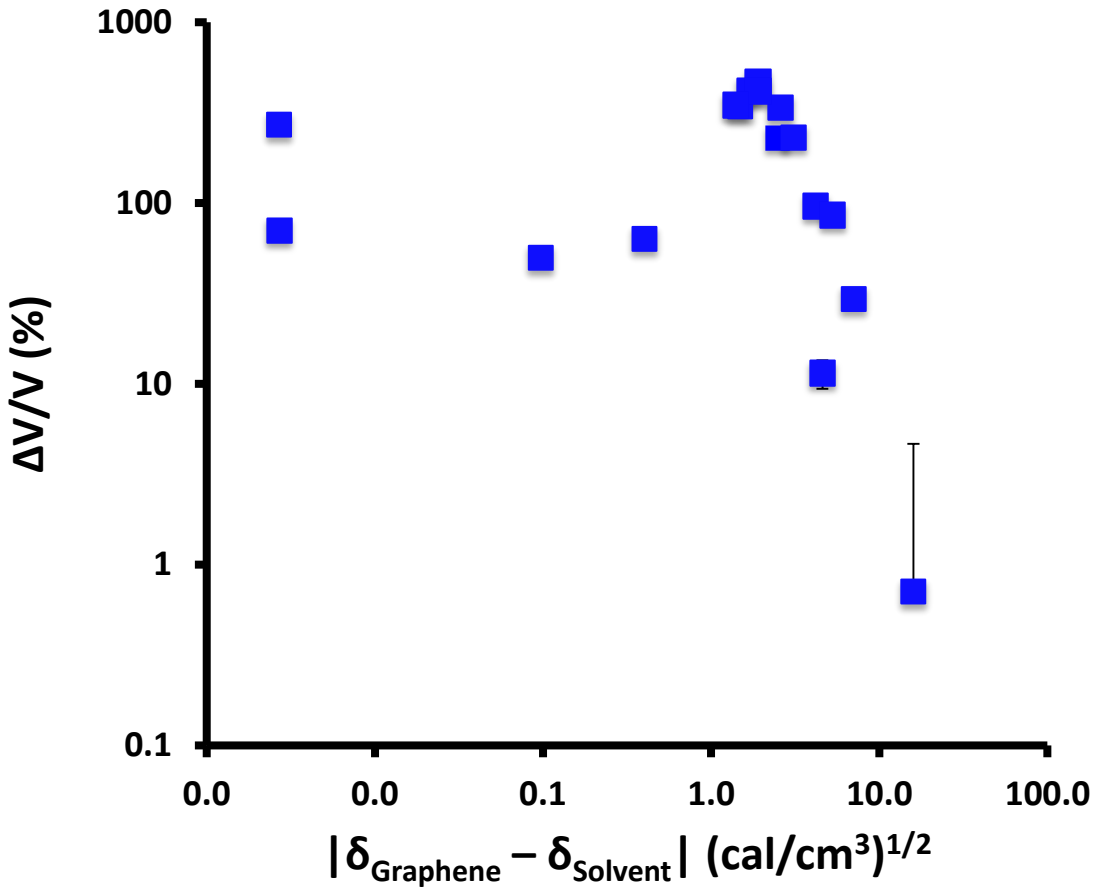

Figure 20-1: Swelling of the composite material in various solvents in relation to the difference in solubility parameter of graphene and the solvent.

20.2 Alteration of Graphite Sheet Size

In addition to the standard foams, materials were made using other starting graphites. One particular example uses Asbury Carbons Micro 890 graphite. Samples are prepared using the same method as described before, except the Asbury Carbons Nano 24 graphite is substituted for an equal mass of Micro 890 graphite (~10 um lateral sheet size).

The resulting foams are then dipped in liquid nitrogen for 3 seconds to bring them below their glass transition temperature, and then cut on a band saw to yield cylinders. A small piece is then cut off with a razor blade and attached to an aluminum SEM stub using both carbon tape and carbon glue. It is then coated with Au/Pd in a sputter coater (Polaron Unit E5100). The samples are characterized with a JEOL 6330 field emission scanning electron microscope with a 10 kV accelerating voltage and may be seen in Figure 20-2.

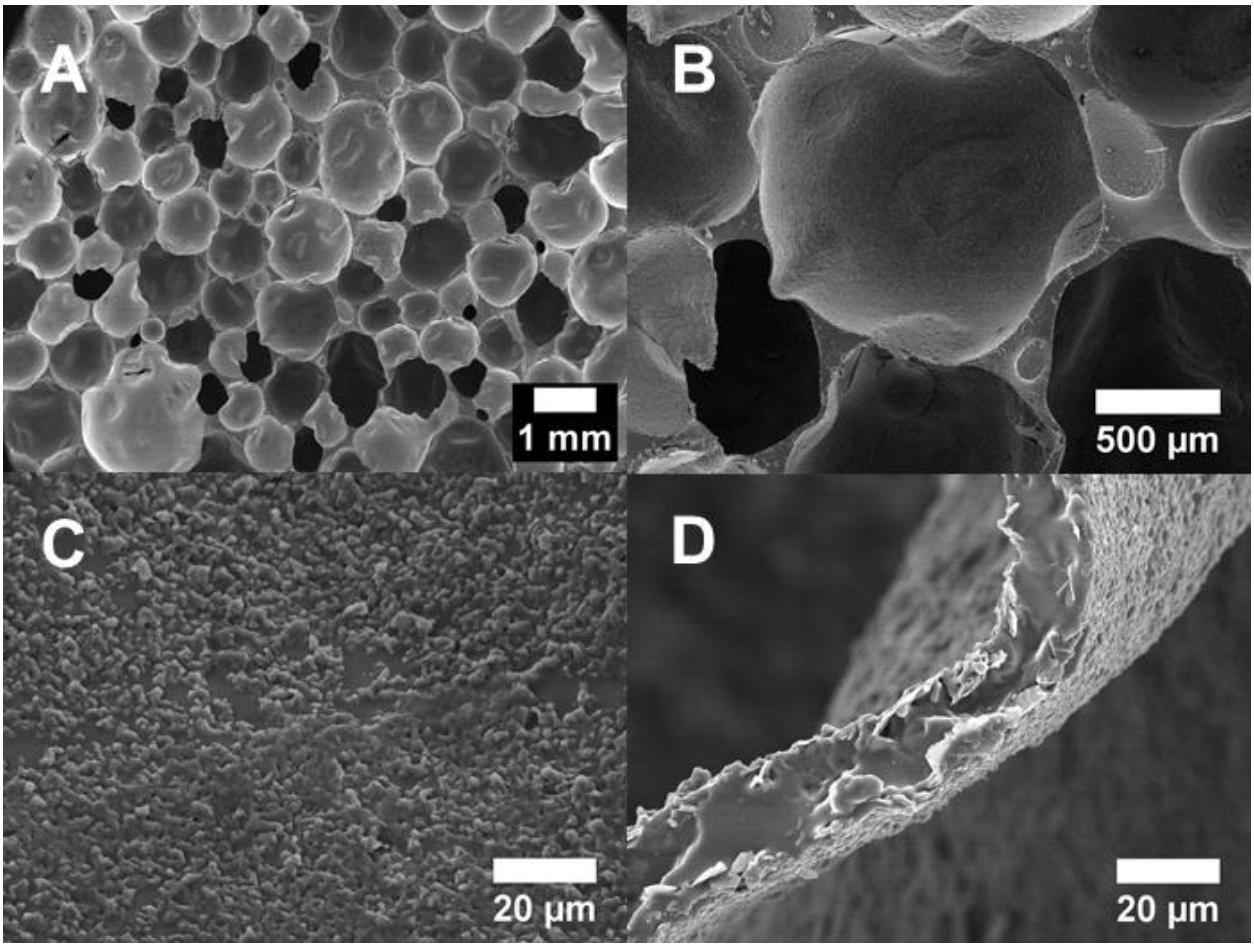

Figure 20-2: Scanning electron microscopy images of Graphene / PBA Composite made using Micro 890 graphite.

Since the Micro 890 graphite has a larger lateral sheet size than the usual Nano 24 (~10 um as opposed to ~1 um), the sphere sizes of the emulsions templated by the larger graphite are much larger than those templated by the smaller graphite. This yields the larger final composite sphere sizes we see in Figure 20-2A and B. The sheets also seem to prefer to stay a little more in the oil phase, as can be seen in Figure 20-2C, which is the surface of a sphere. In Figure 20-2D, the area where two spheres meet is seen. The graphene sheets seem to be less exfoliated, which is expected because of their larger lateral dimensions.

Perhaps most interesting about this system is that the composite is a closed cell system. We think this is due to the larger sheet size increasing the strength of the sphere-sphere contact areas. Having a closed cell system opens of many potential applications, as the aqueous phase (and anything in it) is now trapped in the spheres.

20.3 Swelling Resistance Comparison w/Polystyrene Composite

To compare the change in resistance of the poly(butyl acrylate) foam to that of a traditional polystyrene composite material, samples were first made using the following procedures. The poly(butyl acrylate) sample was made using the standard procedure outlined in the experimental section. To make the polystyrene composite sample, a 250 mL Erlenmeyer flask was charged with 0.88 g graphite (Asbury Carbons, grade Nano 24), 140 mL DI water, 60 mL butyl acrylate (Acros Organics, 99%), 14 mL divinylbenzene (Sigma Aldrich, 80%), 0.18 g 2,2'-azobis(2-methylpropionitrile) (Sigma Aldrich, 98%), and a stir bar. The contents were then mixed for about 1 min on a stir plate. The stir bar was then removed, and the contents were mixed at ~10,000 rpm for 1 min using a Silverson L5M-A high shear blender with a ¾" tubular blending head with the square hole, high shear screen. After mixing, the contents were poured gently into a 240 mL glass jar. The jar was then sealed and placed into a convection oven (Blue M, Stabil-Therm) at 65°C for 24 hr to react. The jar was then broken to remove the composite sample, which was then placed in the same oven for several days (~3) until dry.

After drying, the samples were cut using a band saw to about 1.5 cm x 1.5 cm x 3 cm. The poly(butyl acrylate) samples were frozen in liquid nitrogen for 3 seconds before being cut to ensure they were below the glass transition temperature. Two sides of the prism were then painted with colloidal silver paste (Ted Pella, Pelco). The sample was then placed in the oven overnight to cure the paste. After removal from the oven, copper tape (3M, ¼") was placed on top of both of the ends covered with the silver coating. The tape was then painted again with silver paste to ensure it was bound to the composite. The resistance was measured using a Keithley 2420 sourcemeter. The instrument was set to start taking measurements, and then 500 uL of acetone (Fisher, 99.5%) was pipetted onto the top of the sample, directly in between the faces covered with silver paste. This was to ensure the sample did not swell at the location of the silver paste. Data points were taken at a sampling rate of 600 ms/pt and at 0.01 V. The experiments were repeated several times until no hysteresis was seen. The results are seen in Figure 20-3.

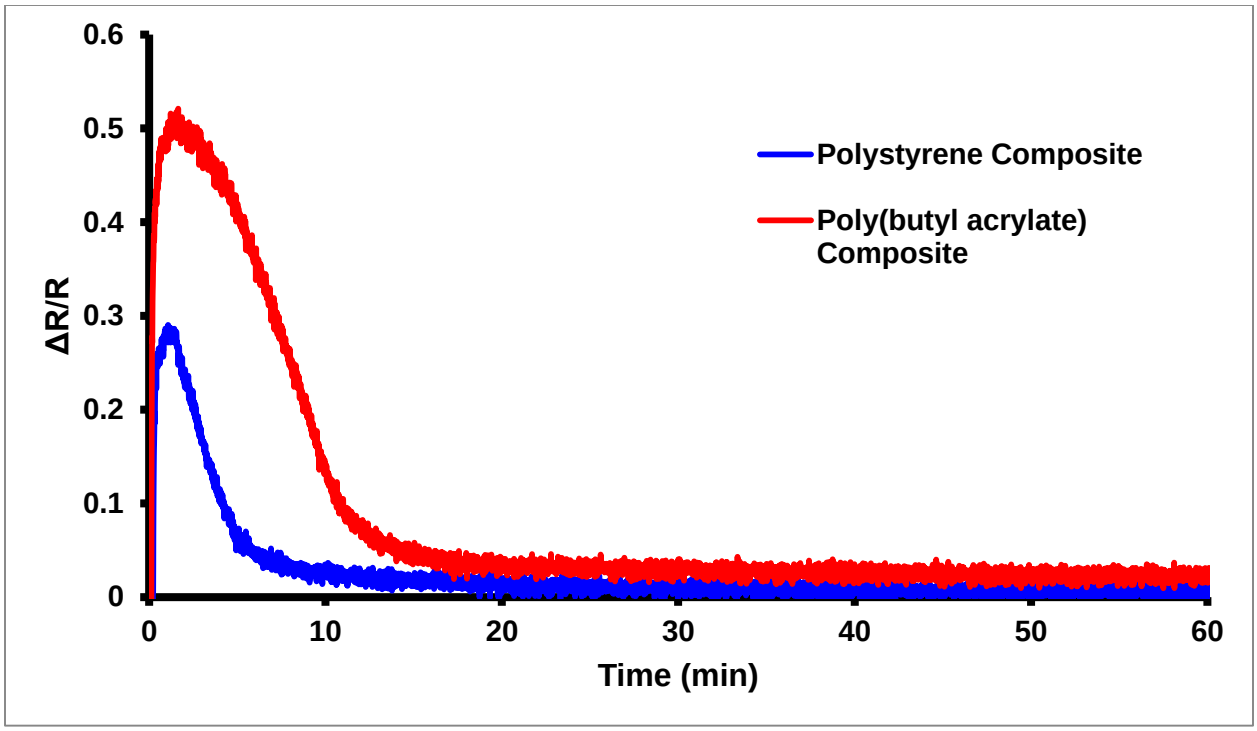

Figure 20-3: Change in resistance over time as acetone is placed on a composite sample and then evaporated.

As is clearly seen in the figure, the poly(butyl acrylate) composite showed almost twice the change in resistance compared to the polystyrene composite tested with the same amount of acetone. Furthermore, a larger amount of acetone was tested: 0.5 mL. While the poly(butyl acrylate) samples were easily able to swell to absorb the liquid (as seen in previous tests), the polystyrene samples did not swell enough to accommodate the liquid. This ultimately led to the acetone dissolving the conductive adhesive on the copper tape. In conclusion, both because of the larger change in resistance, and the ability to swell to absorb large amounts of solvent, the poly(butyl acrylate) composite material is the superior choice for chemical sensing.

Summary and Future Work

Chapter 21: Summary

A new method for the production of pristine graphene has been presented in this dissertation. The interface trapping method utilizes graphene's insolubility in virtually all solvents by trapping the sheets at the interface, where they lower the interfacial energy of the system. Once there, the sheets exfoliate and self-assemble to form a macroscopic conductive network. Part I of this dissertation saw the utilization of the interface trapping method to produce macroscopic, conductive, transparent thin films of pristine graphene. The films were first formed in scintillation vials, where they climbed up glass slides. They could then be transferred to virtually any substrate using a float-off technique. The graphene that made up the films was seen to be about 3-5 layers thick, as determined by SEM, TEM, Raman, and computational simulations. Transparencies up to 95 %T, and conductivities up to 400 S/cm were attained.

Using the same theory, a mixture of graphene and graphite was infused into fabric to impart conductivity in Part II of this dissertation. The fabrics show great promise in smart textile applications. In Part III, stable graphene emulsions were demonstrated and utilized to create graphene/polymer nanocomposite foams. This technique is extremely versatile, and can be used to create rigid and flexible foams with wide ranging applications including: chemical sensing, pressure sensing, construction reinforcement, filtration, and capacitors.

Chapter 22: Future Work

In this dissertation, I have laid out the groundwork for this novel technique. There is still much exciting work to be done.

With regard to the films: developing a continuous technique would be enormously beneficial.

Concerning the fabrics: further developing this technology with conductive polymers has shown great promise.

Finally, for practicality's sake, we only focused on a few monomers to create the foams with. In reality, almost any monomer that can undergo radical polymerization is able to be used in this process. Furthermore, it would be tremendously beneficial to develop a method to form foams using a non-radical technique. There are also a large number of application oriented projects that show great promise. These include filtration, capacitors, sensors, and construction materials to name a few.

References

(1) Novoselov, K. S.; Geim, a K.; Morozov, S. V; Jiang, D.; Zhang, Y.; Dubonos, S. V; Grigorieva, I. V; Firsov, a a. Electric Field Effect in Atomically Thin Carbon Films. *Science* **2004**, *306* (5696), 666–669.

(2) Geim, A.; Novoselov, K. The Rise of Graphene. *Nat. Mater.* **2007**, *6* (3), 183–192.

(3) Balandin, A. a; Ghosh, S.; Bao, W.; Calizo, I.; Teweldebrhan, D.; Miao, F.; Lau, C. N. Superior Thermal Conductivity of Single-Layer Graphene. *Nano Lett.* **2008**, *8* (3), 902–907.

(4) Peigney, a; Laurent, C.; Flahaut, E.; Bacsa, R. R.; Rousset, a. Specific Surface Area of Carbon Nanotubes and Bundles of Carbon Nanotubes. *Carbon N. Y.* **2001**, *39*, 507–514.

(5) Lee, C.; Wei, X.; Kysar, J. W.; Hone, J. Measurement of the Elastic Properties and Intrinsic Strength of Monolayer Graphene. *Science* **2008**, *321* (5887), 385–388.

(6) Orlita, M.; Faugeras, C.; Plochocka, P.; Neugebauer, P.; Martinez, G.; Maude, D. K.; Barra, a.-L.; Sprinkle, M.; Berger, C.; de Heer, W. a.; et al. Approaching the Dirac Point in High-Mobility Multilayer Epitaxial Graphene. *Phys. Rev. Lett.* **2008**, *101* (26), 267601.

(7) Dürkop, T.; Getty, S. A.; Cobas, E.; Fuhrer, M. S. Extraordinary Mobility in Semiconducting Carbon Nanotubes. *Nano Lett.* **2003**, *4* (1), 35–39.

(8) Oshima, C.; Nagashima, A. Ultra-Thin Epitaxial Films of Graphite and Hexagonal Boron Nitride on Solid Surfaces. *J. Phys. Condens. Matter* **1997**, *9* (1), 1–20.

(9) Novoselov, K. S.; Jiang, D.; Schedin, F.; Booth, T. J.; Khotkevich, V. V; Morozov,

S. V; Geim, a K. Two-Dimensional Atomic Crystals. *Proc. Natl. Acad. Sci. U. S. A.* **2005**, *102* (30), 10451–10453.

(10) Sint, K.; Wang, B.; Král, P. Selective Ion Passage through Functionalized Graphene Nanopores. *J. Am. Chem. Soc.* **2008**, *130* (49), 16448–16449.

(11) Cohen-Tanugi, D.; Grossman, J. C. Water Desalination across Nanoporous Graphene. *Nano Lett.* **2012**, *12* (7), 3602–3608.

(12) Wu, Z. S.; Ren, W.; Wen, L.; Gao, L.; Zhao, J.; Chen, Z.; Zhou, G.; Li, F.; Cheng, H. M. Graphene Anchored with Co3O4 Nanoparticles as Anode of Lithium Ion Batteries with Enhanced Reversible Capacity and Cyclic Performance. *ACS Nano* **2010**, *4* (6), 3187–3194.

(13) Zhu, Y.; Murali, S.; Stoller, M. D.; Ganesh, K. J.; Cai, W.; Ferreira, P. J.; Pirkle, A.; Wallace, R. M.; Cychosz, K. A.; Thommes, M.; et al. Carbon-Based Supercapacitors. **2011**, *332* (June), 1537–1542.

(14) Wang, Y.; Shi, Z.; Huang, Y.; Ma, Y.; Wang, C.; Chen, M.; Chen, Y. Supercapacitor Devices Based on Graphene Materials. *J. Phys. Chem. C* **2009**, *113* (30), 13103–13107.

(15) Stoller, M. D.; Park, S.; Zhu, Y.; An, J.; Ruoff, R. S. Graphene-Based Ultracapacitors. *Nano Lett.* **2008**, *8* (10), 3498–3502.

(16) Zhou, M.; Zhai, Y.; Dong, S. Electrochemical Sensing and Biosensing Platform Based on Chemically Reduced Graphene Oxide. *Anal. Chem.* **2009**, *81* (14), 5603–5613.

(17) He, Q.; Wu, S.; Yin, Z.; Zhang, H. Graphene-Based Electronic Sensors. *Chem. Sci.* **2012**, *3* (6), 1764.

(18) Martin, P. Electrochemistry of Gaphene: New Horizons for Sensing and Energy Storage. *Chem. Rec.* **2009**, *9* (4), 211–223.

(19) Kim, K. S.; Zhao, Y.; Jang, H.; Lee, S. Y.; Kim, J. M.; Kim, K. S.; Ahn, J.-H.; Kim, P.; Choi, J.-Y.; Hong, B. H. Large-Scale Pattern Growth of Graphene Films for Stretchable Transparent Electrodes. *Nature* **2009**, *457* (7230), 706–710.

(20) Wang, X.; Zhi, L.; Müllen, K. Transparent, Conductive Graphene Electrodes for Dye-Sensitized Solar Cells. *Nano Lett.* **2008**, *8*, 323–327.

(21) Li, X.; Zhu, Y.; Cai, W.; Borysiak, M.; Han, B.; Chen, D.; Piner, R. D.; Colomba, L.; Ruoff, R. S. Transfer of Large-Area Graphene Films for High-Performance Transparent Conductive Electrodes. *Nano Lett.* **2009**, *9* (12), 4359–4363.

(22) Bae, S.; Kim, H.; Lee, Y.; Xu, X.; Park, J.-S.; Zheng, Y.; Balakrishnan, J.; Lei, T.; Ri Kim, H.; Song, Y. Il; et al. Roll-to-Roll Production of 30-Inch Graphene Films for Transparent Electrodes. *Nat. Nanotechnol.* **2010**, *5* (8), 574–578.

(23) Graphene https://en.wikipedia.org/wiki/Graphene.

(24) Vaari, J.; Lahtinen, J. Ã.; Hautoj, P. The Adsorption and Decomposition of Acetylene on Clean and K-Covered Co (0001). *Catal. Letters* **1997**, *44*, 43–49.

(25) Starr, D. E.; Pazhetnov, E. M.; Stadnichenko, a. I.; Boronin, a. I.; Shaikhutdinov, S. K. Carbon Films Grown on Pt(111) as Supports for Model Gold Catalysts. *Surf. Sci.* **2006**, *600* (13), 2688–2695.

(26) Li, X.; Cai, W.; An, J.; Kim, S.; Nah, J.; Yang, D.; Piner, R.; Velamakanni, A.; Jung, I.; Tutuc, E.; et al. Large-Area Synthesis of High-Quality and Uniform Graphene Films on Copper Foils. *Science* **2009**, *324* (5932), 1312–1314.

(27) Minot Research Group Web Gallery

http://www.science.oregonstate.edu/~minote/wiki/doku.php.

(28) Fast sublimation growth process http://www.liu.se/senmat/fsgp.html.

(29) Forbeaux, I.; Themlin, J.; Debever, J. High-Temperature Graphitization of the 6H-SiC (0001) Face. *Surf. Sci.* **1999**, *442*, 9–18.

(30) Berger, C.; Song, Z.; Li, T.; Li, X.; Ogbazghi, A. Y.; Feng, R.; Dai, Z.; Marchenkov, A. N.; Conrad, E. H.; First, P. N.; et al. Ultrathin Epitaxial Graphite: 2D Electron Gas Properties and a Route toward Graphene-Based Nanoelectronics. *J. Phys. Chem. B* **2004**, *108* (52), 19912–19916.

(31) Berger, C.; Wu, X.; Brown, N.; Naud, C.; Li, X.; Song, Z.; Mayou, D.; Li, T.; Hass, J.; Marchenkov, a.; et al. Electronic Confinement and. *Science (80-.).* **2006**, *312* (May), 1191–1196.

(32) Brodie, B. C. On the Atomic Weight of Graphite. *Philos. Trans. R. Soc. London* **1859**, *149*, 249–259.

(33) Staudenmaier, L. Verfahren Zur Darstellung Der Graphitsäure. *Berichte der Dtsch. Chem. Gesellschaft* **1898**, *31* (2), 1481–1487.

(34) Hummers Jr., W. S.; Offeman, R. E. Preparation of Graphitic Oxide. *J. Am. Chem. …* **1958**, *208* (1937), 1937.

(35) Suk, J. W.; Piner, R. D.; An, J.; Ruoff, R. S. Mechanical Properties of Monolayer Graphene Oxide. *ACS Nano* **2010**, *4* (11), 6557–6564.

(36) Liu, H.; Zhang, L.; Guo, Y.; Cheng, C.; Yang, L.; Jiang, L.; Yu, G.; Hu, W.; Liu, Y.; Zhu, D. Reduction of Graphene Oxide to Highly Conductive Graphene by Lawesson's Reagent and Its Electrical Applications. *J. Mater. Chem. C* **2013**, *1* (18), 3104.

(37) Stankovich, S.; Dikin, D. a.; Piner, R. D.; Kohlhaas, K. a.; Kleinhammes, A.; Jia, Y.; Wu, Y.; Nguyen, S. T.; Ruoff, R. S. Synthesis of Graphene-Based Nanosheets via Chemical Reduction of Exfoliated Graphite Oxide. *Carbon N. Y.* **2007**, *45* (7), 1558–1565.

(38) Schniepp, H. C.; Li, J.-L.; Mcallister, M. J.; Sai, H.; Herrera-alonso, O. M.; Adamson, D. H.; Prud'homme, R.; Car, R.; Saville, D. A.; Aksay, I. A. Functionalized Single Graphene Sheets Derived from Splitting Graphite Oxide. *J. Phys. Chem. B* **2006**, *110* (17), 8535–8539.

(39) Wang, G.; Yang, J.; Park, J.; Gou, X.; Wang, B.; Liu, H.; Yao, J. Facile Synthesis and Characterization of Graphene Nanosheets. *J. Phys. Chem. C* **2008**, *112* (22), 8192–8195.

(40) Dua, V.; Surwade, S. P.; Ammu, S.; Agnihotra, S. R.; Jain, S.; Roberts, K. E.; Park, S.; Ruoff, R. S.; Manohar, S. K. All-Organic Vapor Sensor Using Inkjet-Printed Reduced Graphene Oxide. *Angew. Chem. Int. Ed. Engl.* **2010**, *49* (12), 2154–2157.

(41) Si, Y.; Samulski, E. T.; Hill, C.; Carolina, N. Synthesis of Water Soluble Graphene 2008. **2008**.

(42) IDTechEx Forecasts a $100 Million Graphene Market in 2018 http://www.microwavejournal.com/articles/print/18722-idtechex-forecasts-a-100-million-graphene-market-in-2018.

(43) Hernandez, Y.; Nicolosi, V.; Lotya, M.; Blighe, F. M.; Sun, Z.; De, S.; McGovern, I. T.; Holland, B.; Byrne, M.; Gun'Ko, Y. K.; et al. High-Yield Production of Graphene by Liquid-Phase Exfoliation of Graphite. *Nat. Nanotechnol.* **2008**, *3* (9), 563–568.

(44) Fang, M.; Wang, K.; Lu, H.; Yang, Y.; Nutt, S. Single-Layer Graphene Nanosheets with Controlled Grafting of Polymer Chains. *J. Mater. Chem.* **2010**, *20* (10), 1982.

(45) Roland.chem. Tenside haben hyrophile und hydrophobe Enden https://commons.wikimedia.org/wiki/File:TensideHyrophilHydrophob.png.

(46) Segal, M. Selling Graphene by the Ton. *Nat. Nanotechnol.* **2009**, *4* (10), 612–614.

(47) Bonaccorso, F.; Sun, Z.; Hasan, T.; Ferrari, A. Graphene Photonics and Optoelectronics. **2010**, *4* (August), 611–622.

(48) Geim, A. K. Graphene: Status and Prospects. *Science (80-.).* **2009**, *324* (5934), 1530–1534.

(49) Tung, V. C.; Allen, M. J.; Yang, Y.; Kaner, R. B. High-Throughput Solution Processing of Large-Scale Graphene. *Nat. Nanotechnol.* **2009**, *4* (1), 25–29.

(50) Hecht, D. S.; Hu, L.; Irvin, G. Emerging Transparent Electrodes Based on Thin Films of Carbon Nanotubes, Graphene, and Metallic Nanostructures. *Adv. Mater.* **2011**, *23* (13), 1482–1513.

(51) Stankovich, S.; Dikin, D. a.; Dommett, G. H. B.; Kohlhaas, K. M.; Zimney, E. J.; Stach, E. a.; Piner, R. D.; Nguyen, S. T.; Ruoff, R. S. Graphene-Based Composite Materials. *Nature* **2006**, *442* (7100), 282–286.

(52) Dikin, D. a.; Stankovich, S.; Zimney, E. J.; Piner, R. D.; Dommett, G. H. B.; Evmenenko, G.; Nguyen, S. T.; Ruoff, R. S. Preparation and Characterization of Graphene Oxide Paper. *Nature* **2007**, *448* (7152), 457–460.

(53) Suk, J. W.; Kitt, A.; Magnuson, C. W.; Hao, Y.; Ahmed, S.; An, J.; Swan, A. K.; Goldberg, B. B.; Ruoff, R. S. Transfer of CVD-Grown Monolayer Graphene onto

Arbitrary Substrates. *ACS Nano* **2011**, *5* (9), 6916–6924.

(54) Li, X.; Magnuson, C. W.; Venugopal, A.; Tromp, R. M.; Hannon, J. B.; Vogel, E. M.; Colombo, L.; Ruoff, R. S. Large-Area Graphene Single Crystals Grown by Low-Pressure Chemical Vapor Deposition of Methane on Copper. *J. Am. Chem. Soc.* **2011**, *133* (9), 2816–2819.

(55) Gómez-Navarro, C.; Meyer, J. C.; Sundaram, R. S.; Chuvilin, A.; Kurasch, S.; Burghard, M.; Kern, K.; Kaiser, U. Atomic Structure of Reduced Graphene Oxide. *Nano Lett.* **2010**, *10* (4), 1144–1148.

(56) Ferrari, a. C.; Meyer, J. C.; Scardaci, V.; Casiraghi, C.; Lazzeri, M.; Mauri, F.; Piscanec, S.; Jiang, D.; Novoselov, K. S.; Roth, S.; et al. Raman Spectrum of Graphene and Graphene Layers. *Phys. Rev. Lett.* **2006**, *97* (18), 1–4.

(57) Coleman, J. N. Liquid-Phase Exfoliation of Nanotubes and Graphene. *Adv. Funct. Mater.* **2009**, *19* (23), 3680–3695.

(58) Wang, S.; Zhang, Y.; Abidi, N.; Cabrales, L. Wettability and Surface Free Energy of Graphene Films. *Langmuir* **2009**, *25* (18), 11078–11081.

(59) Coleman, J. N.; Lotya, M.; O'Neill, A.; Bergin, S. D.; King, P. J.; Khan, U.; Young, K.; Gaucher, A.; De, S.; Smith, R. J.; et al. Two-Dimensional Nanosheets Produced by Liquid Exfoliation of Layered Materials. *Science (80-.).* **2011**, *331* (6017), 568–571.

(60) Israelachvili, J. *Intermolecular and Surface Forces*; Academic Press, 2002.

(61) de Gennes, P.-G., Brochard-Wyart, F. & Quere, D. *Capillarity and Wetting Phenomena. Drops, Bubbles, Pearls, Waves.*; Springer, 2003.

(62) Tölle, F. J.; Fabritius, M.; Mülhaupt, R. Emulsifier-Free Graphene Dispersions with

High Graphene Content for Printed Electronics and Freestanding Graphene Films. *Adv. Funct. Mater.* **2012**, *22* (6), 1136–1144.

(63) Lee, S. H.; Kim, H. W.; Hwang, J. O.; Lee, W. J.; Kwon, J.; Bielawski, C. W.; Ruoff, R. S.; Kim, S. O. Three-Dimensional Self-Assembly of Graphene Oxide Platelets into Mechanically Flexible Macroporous Carbon Films. *Angew. Chemie Int. Ed.* **2010**, *49* (52), 10084–10088.

(64) Kim, J.; Cote, L. J.; Kim, F.; Yuan, W.; Shull, K. R.; Huang, J. Graphene Oxide Sheets at Interfaces. *J. Am. Chem. Soc.* **2010**, *132* (23), 8180–8186.

(65) Franklin Kim, Laura J., and J. H. Graphene Oxide: Surface Activity and Two-Dimensional Assembly. *Adv. Mater.* **2010**, *22*, 1954–1958.

(66) Biswas, S.; Drzal, L. T. A Novel Approach to Create a Highly Ordered Monolayer Film of Graphene Nanosheets at the Liquid-Liquid Interface. *Nano Lett.* **2009**, *9* (1), 167–172.

(67) Ruoff, R. Graphene: Calling All Chemists. *Nat. Nanotechnol.* **2008**, *3* (1), 10–11.

(68) Li, D.; Müller, M. B.; Gilje, S.; Kaner, R. B.; Wallace, G. G. Processable Aqueous Dispersions of Graphene Nanosheets. *Nat. Nanotechnol.* **2008**, *3* (2), 101–105.

(69) Bagri, A.; Mattevi, C.; Acik, M.; Chabal, Y. J.; Chhowalla, M.; Shenoy, V. B. Structural Evolution during the Reduction of Chemically Derived Graphene Oxide. *Nat. Chem.* **2010**, *2* (7), 581–587.

(70) Nair, R. R.; Blake, P.; Grigorenko, a N.; Novoselov, K. S.; Booth, T. J.; Stauber, T.; Peres, N. M. R.; Geim, a K. Fine Structure Constant Defines Visual Transparency of Graphene Supporting Materials. *Science* **2008**, *320* (5881), 1308.

(71) Lee, J.; Subramanian, V. Weave Patterned Organic Transistors on Fiber for E-Textiles. *Electron Devices, IEEE Trans. …* **2005**, *52* (2), 269–275.

(72) Post, E. R.; Orth, M.; Russo, P. R.; Gershenfeld, N. E-Broidery: Design and Fabrication of Textile-Based Computing. *IBM Syst. J.* **2000**, *39* (3.4), 840–860.

(73) Cherenack, K.; Zysset, C.; Kinkeldei, T.; Münzenrieder, N.; Tröster, G. Woven Electronic Fibers with Sensing and Display Functions for Smart Textiles. *Adv. Mater.* **2010**, *22* (45), 5178–5182.

(74) Shim, B. S.; Chen, W.; Doty, C.; Xu, C.; Kotov, N. a. Smart Electronic Yarns and Wearable Fabrics for Human Biomonitoring Made by Carbon Nanotube Coating with Polyelectrolytes. *Nano Lett.* **2008**, *8* (12), 4151–4157.

(75) Lee, X.; Yang, T.; Li, X.; Zhang, R.; Zhu, M.; Zhang, H.; Xie, D.; Wei, J.; Zhong, M.; Wang, K.; et al. Flexible Graphene Woven Fabrics for Touch Sensing. *Appl. Phys. Lett.* **2013**, *102* (16), 163117.

(76) Voyer, J. Flexible and Conducting Metal-Fabric Composites Using the Flame Spray Process for the Production of Li-Ion Batteries. *J. Therm. Spray Technol.* **2012**, *22* (5), 699–709.

(77) Little, B. K.; Li, Y.; Cammarata, V.; Broughton, R.; Mills, G. Metallization of Kevlar Fibers with Gold. *ACS Appl. Mater. Interfaces* **2011**, *3* (6), 1965–1973.

(78) Xue, C.-H.; Chen, J.; Yin, W.; Jia, S.-T.; Ma, J.-Z. Superhydrophobic Conductive Textiles with Antibacterial Property by Coating Fibers with Silver Nanoparticles. *Appl. Surf. Sci.* **2012**, *258* (7), 2468–2472.

(79) Yamashita, T.; Takamatsu, S.; Miyake, K.; Itoh, T. Fabrication and Evaluation of a Conductive Polymer Coated Elastomer Contact Structure for Woven Electronic

Textile. *Sensors Actuators A Phys.* **2013**, *195*, 213–218.

(80) Collins, G. E.; Buckley, L. J. Conductive Polymer-Coated Fabrics for Chemical Sensing. *Synth. Met.* **1996**, *78* (2), 93–101.

(81) Negru, D.; Buda, C.-T.; Avram, D. Electrical Conductivity of Woven Fabrics Coated with Carbon Black Particles. *Fibers Text.* **2012**, *20* (1(90)), 53–56.

(82) Tu, Y.; Lv, M.; Xiu, P.; Huynh, T.; Zhang, M.; Castelli, M.; Liu, Z.; Huang, Q.; Fan, C.; Fang, H.; et al. Destructive Extraction of Phospholipids from Escherichia Coli Membranes by Graphene Nanosheets. *Nat. Nanotechnol.* **2013**, No. July, 1–8.

(83) Dong, Z.; Jiang, C.; Cheng, H.; Zhao, Y.; Shi, G.; Jiang, L.; Qu, L. Facile Fabrication of Light, Flexible and Multifunctional Graphene Fibers. *Adv. Mater.* **2012**, *24* (14), 1856–1861.

(84) Cong, H.-P.; Ren, X.-C.; Wang, P.; Yu, S.-H. Wet-Spinning Assembly of Continuous, Neat, and Macroscopic Graphene Fibers. *Sci. Rep.* **2012**, *2*, 613.

(85) Jalili, R.; Aboutalebi, S. H.; Esrafilzadeh, D.; Shepherd, R. L.; Chen, J.; Aminorroaya-Yamini, S.; Konstantinov, K.; Minett, A. I.; Razal, J. M.; Wallace, G. G. Scalable One-Step Wet-Spinning of Graphene Fibers and Yarns from Liquid Crystalline Dispersions of Graphene Oxide: Towards Multifunctional Textiles. *Adv. Funct. Mater.* **2013**, n/a – n/a.

(86) Yu, G.; Hu, L.; Vosgueritchian, M.; Wang, H.; Xie, X.; McDonough, J. R.; Cui, X.; Cui, Y.; Bao, Z. Solution-Processed graphene/MnO2 Nanostructured Textiles for High-Performance Electrochemical Capacitors. *Nano Lett.* **2011**, *11* (7), 2905–2911.

(87) Woltornist, S. J.; Oyer, A. J.; Carrillo, J.-M. Y.; Dobrynin, A. V; Adamson, D. H.

Conductive Thin Films of Pristine Graphene by Solvent Interface Trapping. *ACS Nano* **2013**, *7* (8), 7062–7066.

(88) Oyer, A. J.; Carrillo, J.-M. Y.; Hire, C. C.; Schniepp, H. C.; Asandei, A. D.; Dobrynin, A. V; Adamson, D. H. Stabilization of Graphene Sheets by a Structured Benzene/hexafluorobenzene Mixed Solvent. *J. Am. Chem. Soc.* **2012**, *134* (11), 5018–5021.

(89) Molina, J.; Fernández, J.; Inés, J. C.; del Río, a. I.; Bonastre, J.; Cases, F. Electrochemical Characterization of Reduced Graphene Oxide-Coated Polyester Fabrics. *Electrochim. Acta* **2013**, *93*, 44–52.

(90) Novoselov, K. S.; Geim, a K.; Morozov, S. V; Jiang, D.; Katsnelson, M. I.; Grigorieva, I. V; Dubonos, S. V; Firsov, a a. Two-Dimensional Gas of Massless Dirac Fermions in Graphene. *Nature* **2005**, *438* (7065), 197–200.

(91) Zhang, Y.; Tan, Y.-W.; Stormer, H. L.; Kim, P. Experimental Observation of the Quantum Hall Effect and Berry's Phase in Graphene. *Nature* **2005**, *438* (7065), 201–204.

(92) Chatterjee, S.; Wang, J. W.; Kuo, W. S.; Tai, N. H.; Salzmann, C.; Li, W. L.; Hollertz, R.; Nüesch, F. a.; Chu, B. T. T. Mechanical Reinforcement and Thermal Conductivity in Expanded Graphene Nanoplatelets Reinforced Epoxy Composites. *Chem. Phys. Lett.* **2012**, *531*, 6–10.

(93) Lee, J.-U.; Yoon, D.; Cheong, H. Estimation of Young's Modulus of Graphene by Raman Spectroscopy. *Nano Lett.* **2012**, *12* (9), 4444–4448.

(94) Boukhvalov, D. W.; Katsnelson, M. I. Modeling of Graphite Oxide. *J. Am. Chem. Soc.* **2008**, *130* (32), 10697–10701.

(95) Becerril, H. a; Mao, J.; Liu, Z.; Stoltenberg, R. M.; Bao, Z.; Chen, Y. Evaluation of Solution-Processed Reduced Graphene Oxide Films as Transparent Conductors. *ACS Nano* **2008**, *2* (3), 463–470.

(96) Liu, H.; Zhang, L.; Guo, Y.; Cheng, C.; Yang, L.; Jiang, L.; Yu, G.; Hu, W.; Liu, Y.; Zhu, D. Reduction of Graphene Oxide to Highly Conductive Graphene by Lawesson's Reagent and Its Electrical Applications. *J. Mater. Chem. C* **2013**, *1* (18), 3104.

(97) Pei, S.; Cheng, H.-M. The Reduction of Graphene Oxide. *Carbon N. Y.* **2012**, *50* (9), 3210–3228.

(98) Galpaya, D.; Wang, M.; Liu, M.; Motta, N.; Waclawik, E.; Yan, C. Recent Advances in Fabrication and Characterization of Graphene-Polymer Nanocomposites. *Graphene* **2012**, *2012* (October), 30–49.

(99) Verdejo, R.; Bernal, M. M.; Romasanta, L. J.; Lopez-Manchado, M. a. Graphene Filled Polymer Nanocomposites. *J. Mater. Chem.* **2011**, *21* (10), 3301.

(100) Ansari, S.; Kelarakis, A.; Estevez, L.; Giannelis, E. P. Oriented Arrays of Graphene in a Polymer Matrix by in Situ Reduction of Graphite Oxide Nanosheets. *Small* **2010**, *6* (2), 205–209.

(101) Wei, T.; Luo, G.; Fan, Z.; Zheng, C.; Yan, J.; Yao, C.; Li, W.; Zhang, C. Preparation of Graphene Nanosheet/polymer Composites Using in Situ Reduction–extractive Dispersion. *Carbon N. Y.* **2009**, *47* (9), 2296–2299.

(102) Barroso-Bujans, F.; Fernandez-Alonso, F.; Pomposo, J. a.; Enciso, E.; Fierro, J. L. G.; Colmenero, J. Tunable Uptake of Poly(ethylene Oxide) by Graphite-Oxide-Based Materials. *Carbon N. Y.* **2012**, *50* (14), 5232–5241.

(103) An, X.; Simmons, T.; Shah, R.; Wolfe, C.; Lewis, K. M.; Washington, M.; Nayak, S. K.; Talapatra, S.; Kar, S. Stable Aqueous Dispersions of Noncovalently Functionalized Graphene from Graphite and Their Multifunctional High-Performance Applications. *Nano Lett.* **2010**, *10* (11), 4295–4301.

(104) Gudarzi, M. M.; Sharif, F. Self Assembly of Graphene Oxide at the Liquid–liquid Interface: A New Route to the Fabrication of Graphene Based Composites. *Soft Matter* **2011**, *7* (7), 3432.

(105) Dao, T. D.; Erdenedelger, G.; Jeong, H. M. Water-Dispersible Graphene Designed as a Pickering Stabilizer for the Suspension Polymerization of Poly(methyl Methacrylate)/graphene Core–shell Microsphere Exhibiting Ultra-Low Percolation Threshold of Electrical Conductivity. *Polymer (Guildf).* **2014**, *55* (18), 4709–4719.

(106) Zhang, L.; Shi, T.; Wu, S.; Zhou, H. Graphene/polystyrene Nanocomposites Synthesized via Pickering Emulsion Polymerization. *High Perform. Polym.* **2013**, *26* (2), 156–165.

(107) Yin, G.; Zheng, Z.; Wang, H.; Du, Q.; Zhang, H. Preparation of Graphene Oxide Coated Polystyrene Microspheres by Pickering Emulsion Polymerization. *J. Colloid Interface Sci.* **2013**, *394*, 192–198.

(108) He, Y.; Wu, F.; Sun, X.; Li, R.; Guo, Y.; Li, C.; Zhang, L.; Xing, F.; Wang, W.; Gao, J. Factors That Affect Pickering Emulsions Stabilized by Graphene Oxide. *ACS Appl. Mater. Interfaces* **2013**, *5* (11), 4843–4855.

(109) Vaia, R. A.; Wagner, D. H. Framework for Nanocomposites. *Mater. Today* **2004**, No. November, 32–37.

(110) Liang, J.; Wang, Y.; Huang, Y.; Ma, Y.; Liu, Z.; Cai, J.; Zhang, C.; Gao, H.; Chen, Y. Electromagnetic Interference Shielding of Graphene/epoxy Composites. *Carbon N. Y.* **2009**, *47* (3), 922–925.

(111) Traina, M.; Pegoretti, a. In Situ Reduction of Graphene Oxide Dispersed in a Polymer Matrix. *J. Nanoparticle Res.* **2012**, *14* (4), 801.

(112) Singh, V.; Joung, D.; Zhai, L.; Das, S.; Khondaker, S. I.; Seal, S. Graphene Based Materials: Past, Present and Future. *Prog. Mater. Sci.* **2011**, *56* (8), 1178–1271.

(113) Dukhin, A. S.; Goetz, P. J. *Characterization of Liquids, Nano- and Microparticulates, and Porous Bodies Using Ultrasound*; Elsevier: Oxford, UK, 2010.

(114) Aveyard, R.; Binks, B. P.; Clint, J. H. Emulsions Stabilised Solely by Colloidal Particles. *Adv. Colloid Interface Sci.* **2003**, *100-102*, 503–546.

(115) Wang, J.; Wolf, R. M.; Caldwell, J. W.; Kollman, P.; Case, D. Development and Testing of a General Amber Force Field. *J. Comput. Chem.* **2004**, *25* (9), 1157–1174.

(116) Frisch, M. J.; Trucks, G. W.; Schlegel, H. B.; Scuseria, G. E.; Robb, M. A.; Cheeseman, J. R.; Scalmani, G.; Barone, V.; Mennucci, B.; Petersson, G. A.; et al. Gaussian 09. Gaussian, Inc.: Wallingford, CT, USA 2009.

(117) Price, D. J.; Brooks, C. L. A Modified TIP3P Water Potential for Simulation with Ewald Summation. *J. Chem. Phys.* **2004**, *121* (20), 10096–10103.

(118) Kumar, S.; Rosenberg, J.; Bouzida, D.; Swendsen, R.; Kollman, P. Multidimensional Free-Energy Calculations Using the Weighted Histogram Analysis Method. *J. Comput. Chem.* **1995**, *16* (11), 1339–1350.

(119) Larson, R. *The Structure and Rheology of Complex Fluids*; Oxford University Press: New York, 1998.

(120) Carreira, D.; Chu, K. Stress-Strain Relationship for Plain Concrete in Compression. *ACI J. Proc.* **1985**, *82* (6), 797–804.

(121) BASF. BASF Neopor http://www.neopor.basf.us/about/product-certification.

(122) Lee, C.; Wei, X.; Kysar, J. W.; Hone, J. Measurement of the Elastic Properties and Intrinsic Strength of Monolayer Graphene. *Science (80-.).* **2008**, *321*, 385–388.

(123) Soldano, C.; Mahmood, A.; Dujardin, E. Production, Properties and Potential of Graphene. *Carbon N. Y.* **2010**, *48* (8), 2127–2150.

(124) Wang, X.; Xing, W.; Feng, X.; Yu, B.; Song, L.; Hu, Y. Functionalization of Graphene with Grafted Polyphosphamide for Flame Retardant Epoxy Composites: Synthesis, Flammability and Mechanism. *Polym. Chem.* **2014**, *5*, 1145–1154.

(125) Zheng, Z.; Zheng, X.; Wang, H.; Du, Q. Macroporous Graphene Oxide-Polymer Composite Prepared through Pickering High Internal Phase Emulsions. *ACS Appl. Mater. Interfaces* **2013**, *5* (16), 7974–7982.

(126) Zhang, W. L.; Choi, H. J. Silica-Graphene Oxide Hybrid Composite Particles and Their Electroresponsive Characteristics. *Langmuir* **2012**, *28* (17), 7055–7062.

(127) Woltornist, S. J.; Alamer, F. A.; McDannald, A.; Jain, M.; Sotzing, G. a.; Adamson, D. H. Preparation of Conductive Graphene/graphite Infused Fabrics Using an Interface Trapping Method. *Carbon N. Y.* **2015**, *81*, 38–42.

(128) Woltornist, S. J.; Carrillo, J.-M. Y.; Xu, T. O.; Dobrynin, A. V; Adamson, D. H.

Polymer/Pristine Graphene Based Composites: From Emulsions to Strong, Electrically Conducting Foams. *Macromolecules* **2015**, *48* (3), 687–693.

(129) ChemDrawBio3D. CambridgeSoft: Cambridge, MA 2007.

(130) Wang, J.; Wang, W.; Kollman, P. a; Case, D. a. Automatic Atom Type and Bond Type Perception in Molecular Mechanical Calculations. *J. Mol. Graph. Model.* **2006**, *25* (2), 247–260.

(131) Plimpton, S. Fast Parallel Algorithms for Short-Range Molecular Dynamics. *J. Comput. Phys.* **1995**, *117*, 1–19.

(132) Hockney, R. W.; Eastwood, J. W. *Computer Simulation Using Particles*; Taylor and Francis Group: New York, 1988.

(133) Frisch, M. J.; Trucks, G. W.; Schlegel, H. B.; Scuseria, G. E.; Robb, M. A.; Cheeseman, J. R.; Scalmani, G.; Barone, V.; Mennucci, B.; Petersson, G. A.; Nakatsuji, H.; Caricato, M.; Li, X.; Hratchian, H. P.; Izmaylov, A. F.; Bloino, J.; Zheng, G.; Sonnenb, J. Gaussian. Gaussian Inc.: Wallingford, CT. 2009.

(134) Brown, W. M.; Wang, P.; Plimpton, S. J.; Tharrington, A. N. Implementing Molecular Dynamics on Hybrid High Performance Computers – Short Range Forces. *Comput. Phys. Commun.* **2011**, *182* (4), 898–911.

(135) Schneider, S.; Gompper, G. Shapes of Crystalline Domains on Spherical Fluid Vesicles. *Europhys. Lett.* **2005**, *70* (1), 136–142.

(136) Majidi, C.; Fearing, R. S. Adhesion of an Elastic Plate to a Sphere. *Proc. R. Soc. A Math. Phys. Eng. Sci.* **2008**, *464* (2093), 1309–1317.

Chapter 23: Appendix

23.1 Simulation Details from Part I: Conductive Thin Films of Pristine Graphene by Solvent Interface Trapping

We performed molecular dynamics simulations of adsorption of graphene at water/heptane interface. The Generalized Amber Force Field (GAFF)[115] parameters were used for atomistic models of solvents (see Figure 23-1) and graphene. The partial charge distributions for heptane were obtained by performing *ab-initio* calculations using the Gaussian 09 (G09) simulation package[116] with 6-31G(d) basis set and B3LYP DFT method. For water we used TIP3P force field potentials.[117]

$$U_{TOTAL} = \sum_{BONDS} K_r\left(r - r_{eq}\right)^2 + \sum_{ANGLES} K_\theta\left(\theta - \theta_{eq}\right)^2 + \sum_{DIHEDRALS} \frac{V_n}{2}\left[1 + \cos\left(n\phi - \gamma\right)\right] + \sum_{IMPROPER} K_\chi\left(\chi - \chi_{eq}\right)^2 + \sum_{i<j}\left[\frac{A_{ij}}{R_{ij}^{12}} - \frac{B_{ij}}{R_{ij}^{6}} + \frac{q_i q_j}{\varepsilon R_{ij}}\right] \quad (3)$$

The total potential energy of the system consisted of the bonded, bond angle, dihedral angle, improper angle and non-bonded interaction potentials. The interaction parameters for the van der Waals potential between heterogeneous atomic pairs were calculated as the geometric mean of the interaction parameters for each atom. The default AMBER force field weighing coefficients for pair-wise energy and force contributions were used to account for contributions from the van der Waals and electrostatic interactions.

The simulation box was built by using Chem3D,[129] G09, Antechamber[130] and AMBER2LAMMPS python script that is included with LAMMPS.[131] The G09 input file for the heptane molecule was built in Chem3D, then G09 calculations were performed. The

Gaussian output from the calculation was used as an input for Antechamber to determine charges, atom type, bond type, angle and dihedral type assignments.

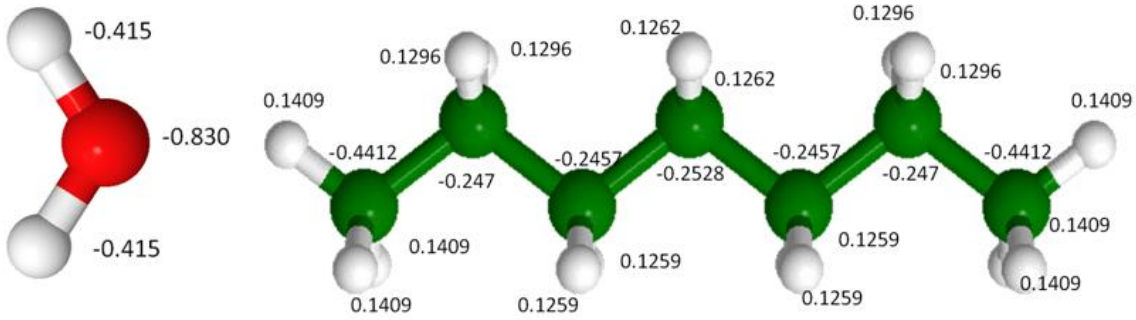

a) b)

Figure 23-1: Partial charge distributions used in simulations of water (a) and heptane (b). The water charges were obtained from Price and Brooks.(2) Charges for heptane were obtained by using Mulliken population analysis from ab initio calculations with 6-31G(d) basis set and B3LYP DFT method.

The AMBER topology file was created by using LEAP that was included in the Antechamber package. The AMBER topology file was converted into a LAMMPS data file using the python script AMBER2LAMMPS. Using output of the AMBER2LAMMPS script as a template, the solvent molecule was replicated and distributed in the simulation box using in-house code.

Table 23-1: Studied Systems

System	L_x(**Å**)	L_y(**Å**)	$\langle L_z \rangle$ (**Å**)	**#Carbon**	**#Water**	**#Heptane**	**Total**
Solvent	92.1	85.08	80.97	0	10000	1280	59440
1-Sheet	92.1	85.08	81.27	348	10000	1280	59872
2- Sheets	92.1	85.08	81.71	768	10000	1280	60304
4- Sheets	92.1	85.08	82.58	1536	10000	1280	61168
8- Sheets	92.1	85.08	84.20	3072	10000	1280	62896

9- Sheets	128.94	122.3	121.29	3420	41184	2576	186688

Graphene flakes were modeled by G8 coronene-like molecules consisting of eight generations of carbon rings and terminated by the hydrogen (see Figure 23-2). The partial charges of the coronene molecule were obtained from the Mulliken population analysis from *ab initio* calculations using G09 with 6-31G(d) basis set and B3LYP DFT method without geometry optimization.

The NPT ensemble simulations were performed using GPU accelerated LAMMPS code[6-7]. The equations of motion were integrated by using the velocity Verlet algorithm with a time step 1.0 fs. The system was periodic in x, y and z directions.

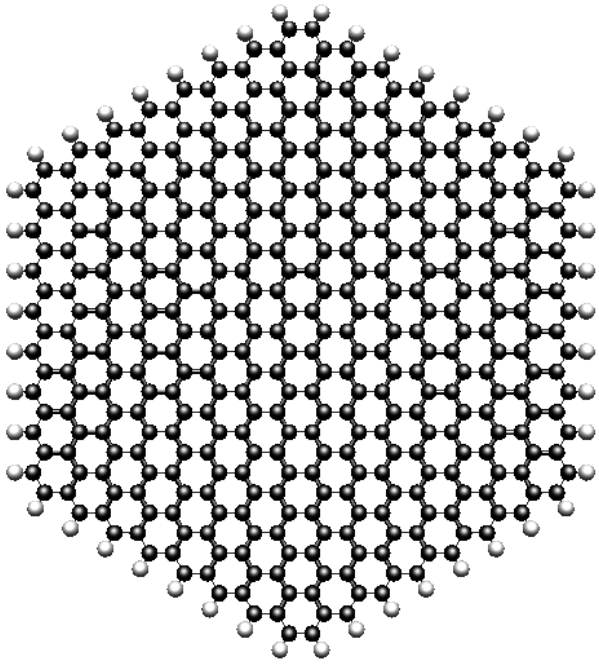

Figure 23-2: Generation eight (G8) coronene-like molecule $C_{384}H_{48}$. Carbon atoms are shown in black and hydrogen atoms are colored in light grey

The standard PPPM[132] method with accuracy 1.0×10^{-5} and the near-field cutoff set to 10.0 Å was used to account for contributions from the long-range electrostatic interactions. The graphene flakes were placed at the interface between two solvents.

Solvent molecules were distributed over the volume of the simulations box. The simulation box sizes and the number of atoms in a system are given in Table 23-1. The system was equilibrated for 3.25 ns to achieve the equilibrium box volume, average system pressure (1 atm) and temperature 300K. A Nose-Hoover thermostat and barostat with relaxation time 0.1 ps and 1.0 ps respectively were used to maintain temperature and pressure in the system. The Nose-Hoover barostat was applied along the z-direction only. During the first 0.25 ns of the equilibration run the location of the atoms belonging to graphene flakes were fixed, and the simulation box was allowed to stabilize, then all constraints were removed. Then NPT simulations were run for 3 ns allowing the system to equilibrate with no constraints. NPT simulations were followed by NVT simulations with a Nose-Hoover thermostat. These simulations lasted 3 ns during which the data were collected (production run). For the 9-sheet system the NPT simulation was run for 6.25 ns and data was collected over the final three ns, no NVT steps were used.

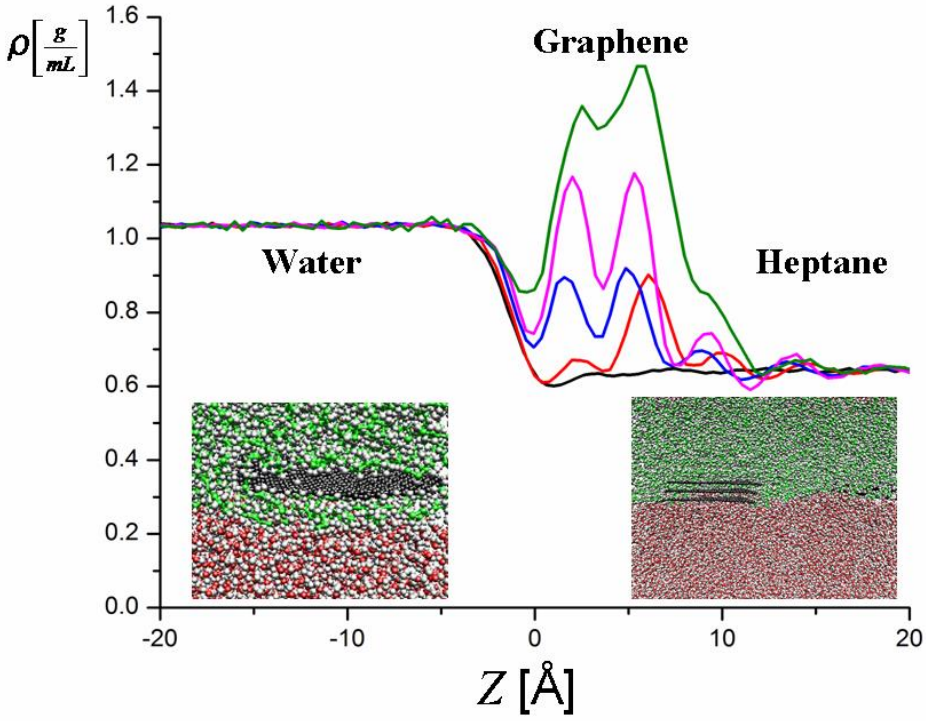

Figure 23-3: Density distribution in simulation box along z-axis for water/heptane (black line), water/heptane/graphene flake (red line), water/heptane/2 graphene flakes (blue line), water/heptane/4 graphene flakes (pink line), and water/heptane/8 graphene flakes (green line) systems. Insets show snapshots of the typical system configurations. In all figures hydrogen atoms are shown in light gray, oxygen atoms are colored in red, carbon atoms belonging to graphene and heptane are shown in black and green respectively.

Number fraction distribution in different water/heptane systems is shown in Figure 23-3. In our simulations, the number fraction is obtained by binning the system in the z-axis, with a height of 0.1 Å , and assigning any atoms within this box to their molecule. The number fraction was then calculated by averaging the number of atoms corresponding to water, heptane and graphene to the total number of atoms within the box. It follows from this figure that graphene flakes are preferentially located in the heptane phase. For a single flake system there is a heptane layer covering the flake. For multi flake systems we see two well-developed peaks close to the water/heptane

interface with the first peak located closer to the interface than the main peak in the single flake system. These peaks correspond to location of the graphene flake carbon atoms in two flake graphene aggregates. The magnitude of these peaks increases with increasing the number of flakes, which should not be surprising since number of carbon atoms belonging to aggregates increases as well.

We used Weighted Histogram Analysis Method[118] to calculate the potential of the Mean Force between a graphene flake and water/heptane interface. These simulations were performed at constant temperature and volume (system sizes are listed in Table 23-2). The constant temperature was maintained by coupling a system to the Nose-Hoover thermostat with relaxation time 0.1 ps. Initially a graphene flake was located at interface between water and heptane and had configuration taken from our NVT simulations.

Table 23-2: Systems used in PMF simulations

System	L_x(Å)	L_y(Å)	L_z (Å)	**#Carbon**	**#Water**	**#Heptane**	**Total**
1-Sheet	92.1	85.08	81.27	348	10000	1280	59872
9-Sheets	128.94	122.3	121.29	3420	41184	2576	186688

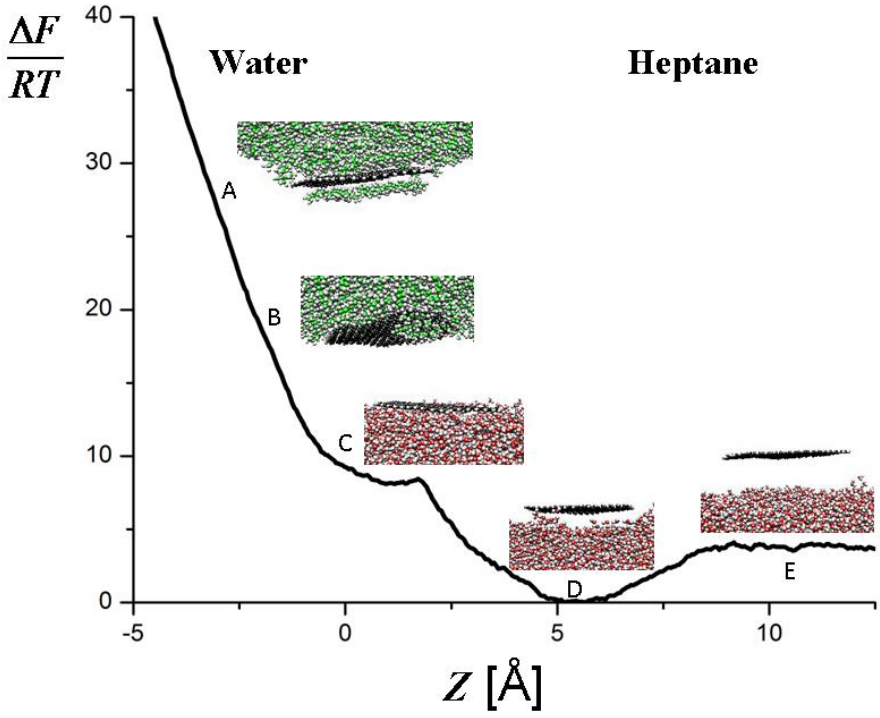

Figure 23-4: Potential of the mean force for single graphene flake system. Insets show typical configuration of the graphene flakes. The solvent in which graphene flake is pulled in is transparent.

In WHAM simulations the z-coordinate of the center of mass of the graphene flake or multi flake aggregate with z-coordinate of the center of mass z^{gr} was tethered to z* by harmonic springs,

$$U_{spring} = \frac{K_{spring}^{(1)}}{2}\left(z_{cm}^{gr} - z*\right)^2 \qquad (4)$$

where the value of the spring constant is $K_{spring}^{(1)}$ =250*Kcal/mole/Å*^{2} . To prevent the solvent interface from moving with the graphene we have tethered the z-coordinate of the center of mass of water molecules z^w at its initial location z_0. The value of the tethering spring constant was set to $K_{spring}^{(w)} = 750 Kcal/mole/\mathring{A}^2$. During these simulation

runs we varied location of the tethering point z* of the graphene flake or multi flake aggregate with increment $\Delta z^* = \pm 0.1$ Å until $z^* = \pm 12$Å is reached in water and heptane phases. For each location of the tethered point the system was equilibrated for a 0.1 ns. The equilibration step was followed by the production run lasting 0.3 ns during which we calculated the distribution of the center of mass location of graphene flake for WHAM calculations of the potential of the mean force.

Figure SI4 shows the potential of the mean-force for single flake system. There is a shallow local minimum at water/heptane. The main minimum is located at about 5.5 Å. The potential saturates when the graphene flake is covered by approximately two layers of the heptane molecules on both sides. Note that the potential of the mean force increases faster with moving a flake into the water phase than into the heptane phase. Therefore the graphene has higher affinity to heptane than to the water. Furthermore graphene flake moves its solvation heptane layer into a water phase deforming the water/heptane interface (see Inset in Figure 23-4).

23.2 Simulation Details from Part III: Pristine Graphene / Polystyrene Foams Templated by Graphene Sheet Stabilized Emulsions

We use molecular dynamics simulations to model the affinity of a graphene flake to a water/styrene interface. In our simulations we used the Generalized Amber Force Field (GAFF)[115] parameters for atomistic models of solvents (see Figure 23-5) and graphene. The partial charge distributions for styrene were obtained by performing *ab-*

initio calculations using the Gaussian 09 (G09) simulation package[133] with 6-31G(d) basis set and B3LYP DFT method. For water we used TIP3P force field potentials.[117]

$$U_{TOTAL} = \sum_{BONDS} K_r \left(r - r_{eq}\right)^2 + \sum_{ANGLES} K_\theta \left(\theta - \theta_{eq}\right)^2 + \sum_{DIHEDRALS} \frac{V_n}{2}\left[1 + \cos\left(n\phi - \gamma\right)\right] + \sum_{IMPROPER} K_\chi \left(\chi - \chi_{eq}\right)^2 + \sum_{i<j}\left[\frac{A_{ij}}{R_{ij}^{12}} - \frac{B_{ij}}{R_{ij}^{6}} + \frac{q_i q_j}{\varepsilon R_{ij}}\right] \quad (5)$$

The total potential energy of the system consisted of the bonded, bond angle, dihedral angle, improper angle and non-bonded interaction potentials. The interaction parameters for the van der Waals potential between heterogeneous atomic pairs were calculated by using the geometric mean approximation for interaction parameters between each atom. The default AMBER force field weighing coefficients for pair-wise energy and force contributions were used to account for contributions from the van der Waals and electrostatic interactions.

The simulation box was built by using Chem3D,[129] G09, Antechamber[130] and AMBER2LAMMPS python script that is included with LAMMPS.[131] The G09 input file for heptane molecule was built in Chem3D, then G09 calculations were performed. The Gaussian output from the calculation was used as an input for Antechamber to determine charges, atom type, bond type, angle and dihedral type assignments.

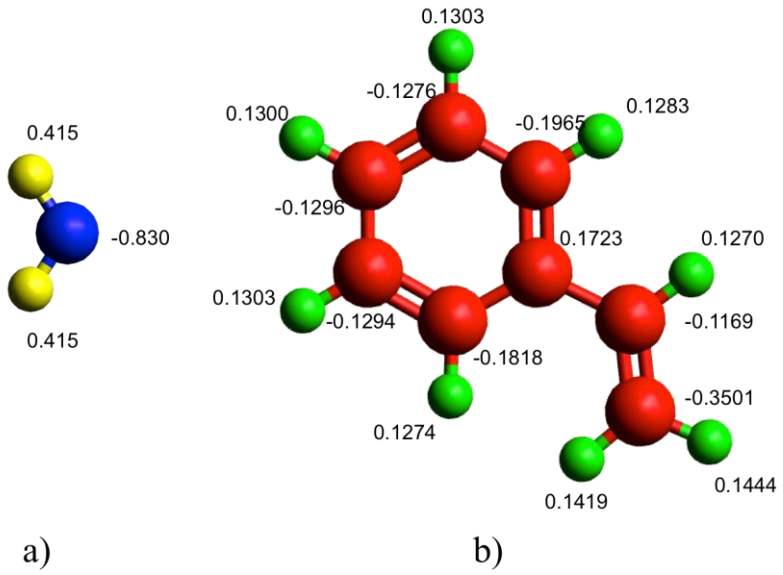

Figure 23-5: Partial charge distributions used in simulations of water (A) and styrene (B). The water charges were obtained from Price and Brooks.[117] Charges for styrene were obtained by using Mulliken population analysis from *ab initio* calculations with 6-31G(d) basis set and B3LYP DFT method.

The AMBER topology file was created by using LEAP that was included in the Antechamber package. The AMBER topology file was converted into a LAMMPS data file using the python script AMBER2LAMMPS. Using output of the AMBER2LAMMPS script as a template, the solvent molecule was replicated and distributed in the simulation box using in-house code.

Graphene flake was modeled by G8 coronene-like molecule consisting of the eight generation of carbon rings and terminated by the hydrogen (see Figure 23-6). The partial charges of the coronene molecule were obtained from the Mulliken population analysis from *ab initio* calculations using G09 with 6-31G(d) basis set and B3LYP DFT method without geometry optimization.

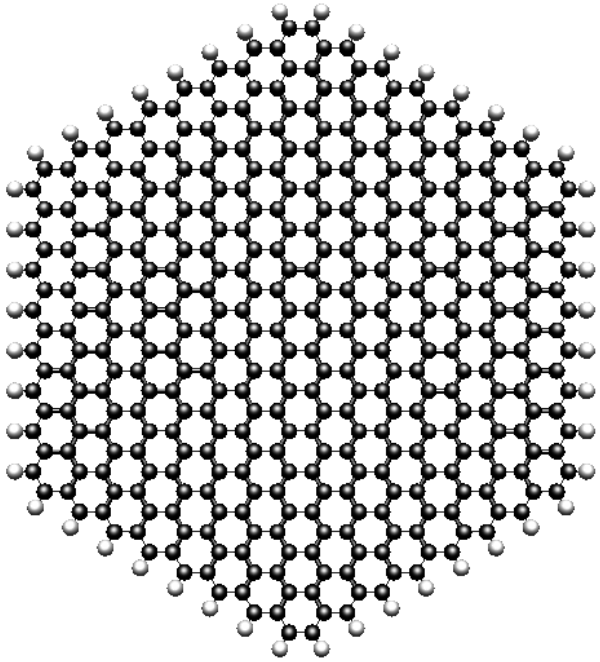

Figure 23-6: Generation eight (G8) coronene-like molecule $C_{384}H_{48}$. Carbon atoms are shown in black and hydrogen atoms are colored in light grey.

The NPT ensemble simulations were performed using GPU accelerated LAMMPS code.[131,134] The equations of motion were integrated by using the velocity Verlet algorithm with a time step 1.0 fs. The system was periodic in x, y and z directions. The standard PPPM[132] method with accuracy 1.0×10^{-5} and the near-field cutoff set to 10.0 Å was used to account for contributions from the long-range electrostatic interactions. The graphene flake was placed at the interface between two solvents. Solvent molecules were distributed over the volume of the simulations box. The simulation box size and the number of atoms in a system are given in Table 23-3. The system was equilibrated for 3.25 ns to achieve the equilibrium box volume, average system pressure (1 atm) and temperature 300K. A Nose-Hoover thermostat and barostat with relaxation time 0.1 ps and 1.0 ps respectively were used to maintain temperature and pressure in the system. The Nose-Hoover barostat was applied along

the z-direction only. During the first 0.25 ns of the equilibration run the location of the atoms belonging to graphene flake was fixed, and the simulation box was allowed to stabilize, then all constraints were removed. Then NPT simulations were run for 3 ns allowing the system to equilibrate with no constraints. NPT simulations were followed by NVT simulations with a Nose-Hoover thermostat. These simulations lasted 3 ns during which the data were collected (production run).

We have used the Weighted Histogram Analysis Method[118] to calculate the potential of the Mean Force between a graphene flake and water/styrene interface. These simulations were performed at constant temperature and volume. The constant temperature was maintained by coupling a system to the Nose-Hoover thermostat with relaxation time 0.1 ps. Initially a graphene flake was located at interface between water and heptane and had configuration taken from our NVT simulations.

Table 23-3: System sizes used in PMF simulations

System	L_x(Å)	L_y(Å)	L_z (Å)	#Carbon	#Water	#Styrene	Total
1-Sheet	88.3	86.7	73.2	384	9360	1360	50272

In WHAM simulations the z-coordinate of the center of mass of the graphene flake or multi flake aggregate with z-coordinate of the center of mass z_{cm}^{gr} was tethered to z* by harmonic springs

$$U_{spring} = \frac{K_{spring}^{(1)}}{2}\left(z_{cm}^{gr} - z^*\right)^2 \qquad (6)$$

where the value of the spring constant is $K_{spring}^{(1)} = 250\,Kcal/mole/\mathring{A}^2$. To prevent the solvent interface from moving with the graphene we have tethered the z-coordinate of the center of mass of water molecules z_{cm}^{w} at its initial location z_0. The value of the tethering spring constant was set to $K_{spring}^{(w)} = 250 Kcal/mole/\mathring{A}^2$. During these simulation runs we varied location of the tethering point z* of the graphene flake or multi flake aggregate with increment $\Delta z^* = \pm$ 0.1 Å until z*= $\pm$ 12Å is reached in water and heptane phases. For each location of the tethered point the system was equilibrated for 0.1 ns. Equilibration step followed by the production run lasting 0.3 ns during which we have calculated the distribution of the center of mass location of graphene flake for WHAM calculations of the potential of the mean force.

23.3 Stabilization of Emulsions by Graphitic Skin

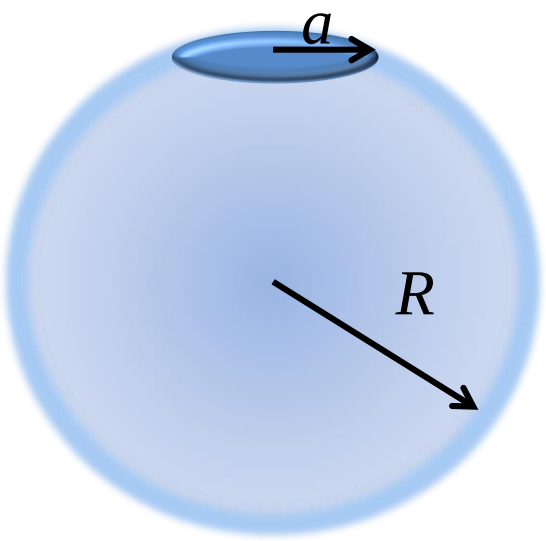

Figure 23-7: A water droplet with size *R* covered with graphitic skin formed by sheets of size *a*.

In our approach we assume that the emulsion consists of monodisperse water droplets with size *R* (see Figure SI2.1). The oil forms a continuous phase. The graphene sheets with a size *a* adsorb at water/oil interface. Graphene sheets form a skin layer of thickness *h* at the interface between oil and water. Due to curvature of the water droplets each graphene sheet should deform to remain at the interface between two immiscible liquids and form a skin layer. This results in the elastic energy penalty per sheet with radius *a* to be equal to[135,136]

$$U_{elast} \approx \frac{\pi}{384}\frac{Ed_0 a^6}{R^4} \qquad (7)$$

where *E* is the Young modulus of the graphene sheet with thickness d_0. The thickness of the skin layer, *h*, can be related to the weight fraction of the graphene in the emulsion, ϕ_g. The total mass of the graphene forming a skin layer covering a droplet with size *R* is equal to

$$m_g = 4\pi R^2 h\rho_g \qquad (8)$$

The weight fraction of the graphene with respect to water content m_w in the emulsion is equal to

$$\phi_g = \frac{m_g}{m_w} = \frac{4\pi R^2 h\rho_g}{\frac{4}{3}\pi R^3 \rho_w} = \frac{3h\rho_g}{R\rho_w} \qquad (9)$$

where ρ_w = 1.0 g/cm^3 and ρ_g =2.66 g/cm^3 are mass densities of water and graphene respectively. Solving the last equation for the layer thickness *h* one obtains

$$h = \frac{R}{3}\frac{\phi_g \rho_w}{\rho_g} = \frac{\beta R}{3} \qquad (10)$$

It is important to point out that there is a low bound for the layer thickness *h* which corresponds to coverage of the droplet by a single graphene layer with thickness

d_0. Thus for each mixture composition the size R of the droplet for full graphene coverage should be larger than $R_{\min} \approx 3d_0/\beta$.

The total elastic energy stored in all water droplets in the emulsion occupying volume V is equal to the number of droplets in a system V/V_0 times the elastic energy stored by deforming graphene sheets covering a droplet surface

$$U_{elast}^{tot} = \frac{V}{V_0}\frac{4\pi R^2 h}{\pi a^2 d_0}U_{elast} \qquad (11)$$

where V_0 is the volume per water droplet and the factor $4\pi R^2 h/\pi a^2 d_0$ accounts for number of graphene sheets within thickness h at the droplet interface. Here we assume additivity of the net elastic energy contribution from deformation of individual sheets. The volume per water droplet V_0 can be related to mass ratio, $\phi_{w/o}$, of water to oil and size of the water droplet, R, as follows

$$\phi_{w/o} = \frac{m_w}{m_o} = \frac{\frac{4}{3}\pi R^3 \rho_w}{\rho_o\left(V_0 - \frac{4}{3}\pi R^3\right)} \qquad (12)$$

where ρ_o is the oil mass density. Solving the last equation for V_0 one has

$$V_0 = \frac{4}{3}\pi R^3\left(1+\frac{\rho_w}{\phi_{w/o}\rho_o}\right) = \frac{4}{3}\pi R^3\alpha \qquad (13)$$

Now we can write the total elastic energy of the emulsion per unit volume as a function of the droplet size R and emulsion composition

$$\frac{U_{elast}^{tot}}{V} \approx \frac{\pi}{384}\frac{Eha^6}{R^4}\frac{4\pi R^2}{\pi a^2}\frac{1}{V_0} \approx \frac{E}{384}\frac{\beta}{\alpha}\frac{a^4}{R^4} \qquad (14)$$

Placement of the graphitic skin layer at the interface between water and oil also changes the interaction part of the system free energy. In the general case one can use a thin film approximation to account for the change of the system free energy with the formation of the skin layer. This evaluation requires knowledge of the surface tension for

water/oil, water/graphene, graphene/oil interface and Hamaker constants to account for interactions across the graphene skin layer covering a surface of a droplet and solubilized graphene sheet in an oil phase.[60,61] However, we can use results of the computer simulations of the water/graphene/heptane system to estimate the characteristic size of the droplets covered by graphene layer. In particular we will use a value of the change in the system free energy Δg for moving a graphene flake or flake aggregate from water/oil interface to the oil phase obtained from WHAM calculations. In our simulations we did not see a significant change for this quantity for pulling a single sheet or three flake aggregate. In both cases the energy change was about 4.5 *RT* for graphene sheets with area 848 Å^2.[87] Thus the adsorption free energy of the graphene layer at the interface can be estimated as $\Delta g \approx -2.2 mN/m$. The negative sign indicates affinity of the graphene to the water/oil interface. Taking this into account, the total free energy change of the water/oil/graphene system with total surface area of water droplets $A = 4\pi R^2 V / V_0$ is equal to

$$\Delta U_{surf} = \Delta g A = -|\Delta g| \frac{3V}{\alpha R} \qquad (15)$$

Combining elastic and surface energy terms together we finally arrive at the energy of the emulsion consisting of droplets covered by a graphitic skin

$$\frac{\Delta F_{total}}{V} \approx \frac{E}{384} \frac{\beta}{\alpha} \frac{a^4}{R^4} - \frac{3|\Delta g|}{\alpha R} \qquad (16)$$

Analysis of eq (16) shows that the surface energy term promotes formation of the smaller droplets to increase the area of the water/graphene/oil interface while the elastic energy term tends to decrease the interface curvature. The equilibrium size of the droplets is obtained by optimizing the system free energy change ΔF_{total} with respect to droplet size *R*

$$R^* \approx \left(\frac{E\beta a^4}{288|\Delta g|} \right)^{1/3} \quad (17)$$

Using this expression we can estimate a size of droplets formed in the emulsion with the weight fraction of graphene at 1% ($\beta \approx 0.01 \times 2.66 \approx 0.03$) sonicated into flakes with size 0.1μm. For the Young modulus *E* we use 1.0 TPa.[5,93] This results in size of droplets to be on the order of 1.7μm.

It is important to point out that eq SI2.11 can only be used for evaluation of the graphene stabilized droplets if there is enough graphene sheets to cover the water/oil interface. This is true as long as $R^* \geq 3d_0 / \beta$. This results in the following condition for the critical composition of the emulsion

$$\beta^* \approx 9.4 \left(\frac{|\Delta g| d_0^3}{Ea^4} \right)^{1/4} \quad (18)$$

For mixtures with composition such that $\beta < \beta^*$, the growth of the coalescing droplets will continue until their surface is covered by a monolayer of graphene sheets. Such droplets will have size

$$R \approx 3d_0 / \beta \quad (19)$$